Structure and fluctuations of smectic membranes

Wim H. de Jeu

FOM-Institute for Atomic and Molecular Physics, Kruislaan 407, 1098 SJ Amsterdam, The Netherlands

Boris I. Ostrovskii

Institute of Crystallography, Russian Academy of Sciences, 117333 Moscow, Russia

Arcadi N. Shalaginov

Department of Physics and Guelph-Waterloo Physics Institute, University of Guelph, Guelph, Ontario N1G 2W1, Canada

(Published 5 February 2003)

Smectic membranes are perfect model systems for studying low-dimensional phase transitions and the associated fluctuations. During the last two decades we have seen important progress in the understanding of the structure and fluctuation behavior of these systems, driven by both new experimental techniques and theoretical developments. Phase transitions are reviewed involving liquid, hexatic, and crystalline layers, which provide several types of model system for low-dimensional melting. The authors discuss the influence of the surfaces on the physical properties of the membranes as well as the crossover from three- to two-dimensional behavior. The layer-displacement fluctuations in smectic membranes have been investigated by specular and diffuse x-ray reflectivity. Theoretical and experimental aspects of the displacement-displacement correlation function are discussed. Of special interest is the quenching or enhancement of fluctuations at surfaces, which is directly related to the phenomenon of surface ordering. The authors consider the conditions under which fluctuations are conformal throughout a membrane, and then the dynamic aspects of the layer-displacement correlation function, which include the effects of finite size, surface tension, and viscous dissipation. This leads in smectic membranes to a discrete spectrum of elastic and viscous relaxation modes, which have been studied experimentally with coherent x rays at third-generation synchrotron sources. The fluctuating character of crystalline-B membranes is also considered. Finally, the article looks briefly at thinning transitions, smectic membranes of chiral molecules, smectic films on substrates, and applications to biologically relevant systems. Open questions and future trends in the field are discussed.

CONTENTS

I. MOTIVATION AND SCOPE

Although liquid crystals have been known since the end of the 19th century, they continue to provide us with scientific surprises due to their variety of low-dimensional phases and phase transitions. Interest in the field seems undiminished and experimental work over the past 50 years has produced a vast literature (see, for example, Vertogen and de Jeu, 1988; de Gennes and Prost, 1993). An important stimulus to research is the application of liquid crystals in displays. However, liquid crystals are also of considerable interest for more fundamental reasons. They have been studied extensively as model systems of specific types of ordering, as they provide a variety of different phases and phase transitions (see, for example, Pershan, 1988). The simplest type of smectic phase is smectic-A (Sm-A), in which the elongated molecules are organized in stacks of liquid layers in which the long molecular axes are, on average, parallel to the layer normal. Hence a periodic structure exists in one dimension: the rodlike molecules form a density wave along the layer normal, while the system remains fluid in the other two directions. Higher-ordered smectic phases are characterized by an additional degree of ordering within the smectic planes.

In this review we discuss the structural aspects and the fluctuation behavior of smectic membranes (freely suspended smectic films). There are several good reasons for the interest in these systems. In the first place, smectic phases are systems at their lower marginal dimensionality, which means that the ordering of the layers is not truly long range. This can be contrasted with three-dimensional solids, which exhibit full long-range order. Second, the availability of films of variable thickness allows us to study the crossover from three- to two-dimensional behavior as well as the influence of the surfaces on the morphology and the phase behavior. The experimental study of such effects has been strongly stimulated by the availability of powerful light sources, such as lasers and synchrotron radiation facilities. Both experiments and theory have reached a level of maturity that makes a review timely.

In a three-dimensional crystal the particles vibrate around well-defined lattice positions with an amplitude that is small compared to the lattice spacing. As the dimensionality is decreased, fluctuations become increasingly important. As a result long-range translational order cannot exist in either one or two dimensions; it would be destroyed by thermal fluctuations (Landau *et al.*, 1980). The spatial dimension at which thermal fluctuations just prevent the existence of long-range order is called the lower marginal dimensionality, which for solids has the value 2. In this case, the positional correlation decays algebraically as a function of distance. Sm-A liquid crystals are an example of a three-dimensional system that exists at its lower marginal dimensionality. The correlation function describing the periodicity of the smectic layers decays algebraically as $r^{-\eta}$, where the exponent η is small and positive. It can be studied by x-ray scattering. Instead of delta-function-type Bragg peaks with diffuse tails characteristic of three-dimensional crystal periodicity, power-law singularities corresponding to the smectic layering have been observed (Als-Nielsen *et al.*, 1980; Safinya *et al.*, 1986). The thermal fluctuation modes in smectics correspond to bending and compression of the layers as shown in Fig. 1, characterized by elastic constants K and B, respectively. Defining $u(\mathbf{r})$ as the layer displacement from its equilibrium position, $\langle u^2(\mathbf{r})\rangle$ is found to diverge logarithmically with the sample size (Landau-Peierls instability), as will be discussed in detail in Sec. II.A:

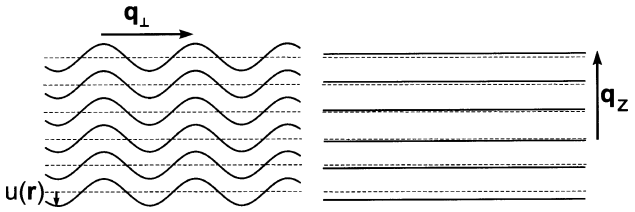

FIG. 1. Undulation and compression of smectic layers with corresponding wave vector.

$$\langle u^2(\mathbf{r})\rangle = \frac{k_B T}{8\pi\sqrt{KB}} \ln\left(\frac{L}{d}\right). \tag{1}$$

Here L is the thickness of the system, d the smectic layer periodicity, and $k_B T$ the thermal energy. A similar divergence due to long-wavelength modes makes two-dimensional crystals unstable. The long-range order is destroyed by the thermal fluctuations of the system: although the algebraic decay is slow, the mean-square layer displacement diverges with the sample size.

A unique property of smectic liquid crystals is their ability, due to the layered structure, to form films that are freely suspended or free-standing over an aperture in a frame. This property has been known since the beginning of the last century. Friedel (1922) used it in his monograph on liquid crystals as an argument in favor of the existence of layers in the smectic phase. However, it was not until the 1970s that smectic membranes found extensive usage in experimental studies (Young *et al.*, 1978; Moncton and Pindak, 1979; Rosenblatt *et al.*, 1979). In such films the smectic layers align parallel to the two air-film surfaces, which are flat because the surface tension minimizes the surface area of the film. Apart from the edges such films can be considered as substrate-free. Thus in essence they can be seen as membranes consisting of stacks of smectic layers, and in this review we shall consistently use the term *smectic membranes*. They have a high degree of uniformity: the alignment of the smectic layers is almost perfect, allowing us to study single-domain samples of various thicknesses. The surface area can be as large as a thousand mm^2, while the thickness can be easily varied from thousands of layers (tens of μm) down to two layers (about 5 nm). Membranes thicker than several hundred layers can be considered as bulk systems. Thin membranes approach two-dimensional behavior. In addition, in liquid crystals (and thus in smectic membranes) a free surface may stabilize a higher-ordered phase that is only observed at

lower temperatures in the bulk or not observed in the bulk at all. This is in contrast to solids, which exhibit surface-induced disorder that can lead to surface melting (see, for example, Dosch, 1992). In the case of liquid crystals, surface freezing occurs instead. Outside the field of liquid crystals surface freezing is a rare phenomenon found only in some long-chain alkanes and alcohols (Gang *et al.*, 1998).

When a Sm-A phase is cooled a hexatic smectic-B phase (Sm-B) may occur. In this case the molecules in the smectic planes are locally positioned on a triangular "lattice," but the positional order decays over distances not larger than a few tens of nm. From the positional point of view each layer is still a two-dimensional liquid. In addition bond-orientational order exists (see, for example, Vertogen and de Jeu, 1988; de Gennes and Prost, 1993): the orientations of the local clusters are correlated over a large scale. The three-dimensional hexatic structure consists of stacks of such layers leading to long-range three-dimensional bond-orientational order. Finally, at lower temperatures a crystalline-B (Cr-B) phase can be found possessing long-range three-dimensional positional order. The in-plane triangular lattices in each of the layers are locked together. They are true crystals even though it is relatively easy to impose elastic deformations along the layers. The transformation from Cr-B to Sm-A provides an interesting example of low-dimensional melting, including the occurrence of an intermediate hexatic phase with bond-orientational order.

Smectic membranes can be controlled to an extent that is rare for physical systems. In combination with the properties mentioned this makes them ideal model systems for studying low-dimensional fluctuation behavior and phase transitions, which have almost no equivalent in any other type of system. This review concentrates on studies using x rays, which are the main tool for this type of investigation. Results from other methods will be mentioned where appropriate. Emphasis will be on the orthogonal phases with hexatic and crystalline ordering, and we shall touch only in passing on transitions between phases with liquid in-plane order. These points make this review complementary to some existing reviews of smectic membranes (Pieranski *et al.*, 1993; Bahr, 1994; Demikhov 1995; Stoebe and Huang, 1995; Sonin, 1998; Oswald and Pieranski, 2002). We restrict ourselves to "classical" liquid-crystalline systems and do not consider related systems like phases of non-rod-shaped and amphiphilic molecules, modulated smectic phases (Ostrovskii, 1999), or Langmuir monolayers (Als-Nielsen *et al.*, 1994; Kaganer, Möwald, and Dutta, 1999).

Following this introductory section, Sec. II discusses smectic phases in some detail, including the main features of the x-ray patterns, regarding both the layering and the in-plane structure within the layers. The section ends with a discussion of the experimental realization and stability of smectic membranes. The main focus of Sec. III will be theoretical and experimental aspects of phase transitions in smectic membranes. In combination with the difference in phase behavior between the bulk layers and the surface layers in smectic membranes, this allows us to investigate in some detail low-dimensional melting transitions. Hence special attention will be given to phase transitions Sm-A–Sm-B–Cr-B, both in the bulk of the films and at the surfaces.

Section IV concentrates on layer-displacement fluctuations in smectic membranes. The tools used are specular and diffuse x-ray reflectivity. Knowledge of the resolution function is of crucial importance to interpret experimental results quantitatively. The main body of this section is devoted to a theoretical and experimental discussion of the displacement-displacement correlation function, which is intimately connected with the Landau-Peierls instability. Of special interest is the quenching or enhancement of the fluctuations at the surfaces of smectic membranes. Furthermore we consider the conditions under which the fluctuations are conformal throughout the membrane. In this field diffuse x-ray-scattering experiments provide information on scales from macroscopic to molecular dimensions. At small wave-vector transfer the (elastic) material parameters can be determined; at large wave-vector transfer the hydrodynamic theory breaks down and in principle information on the form factor of the layers is obtained.

Section V can be considered as the dynamic equivalent of Sec. IV. It concerns fundamental questions regarding the behavior of the dynamic layer-displacement correlation function and the effects of finite sizes in smectic membranes, including nonzero surface tension and viscous dissipation. The finite size of smectic membranes leads to a discrete spectrum of elastic and viscous relaxation modes. Their study has been triggered by new experimental possibilities using coherent x rays at third-generation high-brilliance synchrotron sources. Finally, the last section considers thinning transitions, smectic membranes of tilted chiral molecules, thin smectic films on a substrate, and applications to biologially relevant systems.

II. SMECTIC MEMBRANES

A. Smectic liquid-crystal phases

Liquid crystals are composed of relatively large organic molecules that possess a strongly anisometric shape (in this review of the rod type). A list of the liquid-crystalline (mesogenic) molecules that occur more than once in this review is given in the Appendix. On melting, liquid-crystalline compounds do not pass from the crystalline state directly into an isotropic liquid, but form one or several intermediate phases possessing different degrees of orientational (nematic) or translational (smectic) order. In the nematic phase long-range orientational order of the long molecular axes persists, while the positional order is short range as in an isotropic liquid. The local preferred direction of the long molecular axes is given by a unit vector $\mathbf{n}$ referred to as the *director*; $\mathbf{n}$ and $-\mathbf{n}$ are equivalent. Smectic liquid-crystal phases possess, in addition to the nematiclike orientational order, some degree of translational order.

Smectic-A and smectic-C phases are characterized by translational order in one dimension and liquidlike positional order in the other two directions. In the Sm-A phase the director is oriented orthogonal to the layers, whereas in the Sm-C phase **n** is tilted with respect to the layer normal. The density distribution along the normal to the smectic layers (the z direction) can be developed in a Fourier series:

$$\rho(z)=\rho_0+\sum_{n=1}^{\infty}\rho_n\cos\{q_n[z+u(\mathbf{r})]\}, \tag{2}$$

where $q_n=2\pi n/d=nq_0$, d is the layer spacing, and $u(\mathbf{r})=u_z(\mathbf{r})$ is the layer displacement from the equilibrium position $z=nd$ with the origin chosen at $z=0$. This density profile can be considered as a convolution of the form factor of a single layer and the molecular distribution function of the centers of gravity (see, for example, Vertogen and de Jeu, 1988). The form factor depends on the average conformation and orientation of the molecules. The distribution function depends on both the collective (hydrodynamic) displacement of the layers and the individual motion of molecules, as will be discussed in Sec. IV.C.3. The distribution function can generally be written as a Fourier series,

$$f(z)=\frac{2}{d}\sum_{n=1}^{\infty}\tau_n\cos(nq_0z), \tag{3}$$

where $\tau_n=\langle\cos(nq_0z)\rangle$ are the translational order parameters. The lowest order parameter τ_1 is related to the amplitude of the sinusoidal harmonic of the density modulation. In a more phenomenological approach the smectic order parameter is defined as (see, for example, de Gennes and Prost, 1993)

$$\Psi(z)=\psi(z)\exp[-\imath\phi(z)], \tag{4}$$

where $\psi(z)$ is the amplitude and $\phi(z)=q_0u(z)$ is a phase proportional to the layer displacement $u(z)$. Comparing with Eq. (2) one notes that $\rho_1\cos\{q_0[z+u(\mathbf{r})]\}=\mathrm{Re}[\psi\exp(\imath q_0z)]$. Though both ψ and ϕ fluctuate, the latter fluctuations are much stronger. This is easily understood by realizing that a uniform shift of the layers does not require any energy. As a consequence, long-wavelength fluctuations of layer displacements are well developed. In the following we shall concentrate on these types of fluctuation, but one should keep in mind that, close to a phase transition to a more symmetric nematic or isotropic phase, fluctuations of ψ must also be taken into account.

The deformational free energy of the stacked two-dimensional fluid layers is described by the displacement field $u(\mathbf{r})=u(\mathbf{r}_\perp,z)$. Terms entering the free energy must be invariant to operations that leave the system unchanged. Thus the free energy can only depend on derivatives of $u(\mathbf{r})$. In the harmonic approximation the layers are neither much tilted from the x,y plane nor strongly compressed. Symmetry considerations lead to the so-called Landau–de Gennes free energy F (see, for example, de Gennes and Prost, 1993; Chaikin and Lubensky, 1995):

$$F_B=\frac{1}{2}\int d^3r\left\{B\left(\frac{\partial u(\mathbf{r})}{\partial z}\right)^2+K\left[\frac{\partial^2u(\mathbf{r})}{\partial x^2}+\frac{\partial^2u(\mathbf{r})}{\partial y^2}\right]^2\right\}, \tag{5}$$

where B and K are elastic constants. The integration is carried out over the volume of the system. F_B can be rewritten as a sum of contributions from fluctuations with different wave vectors,

$$F_B=\frac{1}{2(2\pi)^3}\int d^3q[Bq_z^2+Kq_\perp^4]|u(\mathbf{q})|^2, \tag{6}$$

which allows the use of the equipartition theorem. Accordingly each independent quadratic term in the free energy has on average $\frac{1}{2}k_BT$ of energy and therefore

$$\langle u^2(\mathbf{r})\rangle=\frac{k_BT}{(2\pi)^3}\int\frac{d^3q}{Bq_z^2+Kq_\perp^4}. \tag{7}$$

Wavelengths larger than the sample size L normal to the layers and W in the plane of the layers are not possible. Similarly, modes with wavelengths shorter than the layer spacing d or lateral molecular spacing a_0 are not allowed. Hence the integration boundaries are $2\pi/W\leqslant q_\perp\leqslant 2\pi/a_0$ and $2\pi/L\leqslant q_z\leqslant 2\pi/d$. As $W\gg L$ and $a_0<d$, the limits of integration can be expanded: $W\to\infty$ and $a_0\to 0$. Consequently,

$$\begin{aligned}\langle u^2(\mathbf{r})\rangle&=\frac{k_BT}{4\pi^2}\int\int dq_z dq_\perp\frac{q_\perp}{Bq_z^2+Kq_\perp^4}\\&=\frac{k_BT}{8\pi\sqrt{KB}}\ln\left(\frac{L}{d}\right).\end{aligned} \tag{8}$$

A similar expression but with cutting by W and a_0 can be obtained by first integrating over q_z (without cutting) and then over $\mathbf{q}_\perp$. We see that $\langle u^2(\mathbf{r})\rangle$ diverges logarithmically with L, which is called the Landau-Peierls instability (Peierls, 1934; Landau, 1937). As a result, for sufficiently large L, the fluctuations become of the order of the layer spacing, which means that the layer structure would be wiped out. However, in all practical circumstances the layer-displacement amplitude is significantly smaller than the layer spacing: the smectic layers are still well defined.

The quasi-long-range order in Sm-A systems is to be distinguished from true long-range order by the pair-correlation function:

$$\langle\rho(\mathbf{r})\rho(0)\rangle-\langle\rho(\mathbf{r})\rangle\langle\rho(0)\rangle\propto\langle\exp\{\imath q_0[u(\mathbf{r})-u(0)]\}\rangle. \tag{9}$$

In the harmonic approximation this can be written as

$$G(\mathbf{r})=\langle\exp\{\imath q_0[u(\mathbf{r})-u(0)]\}\rangle=\exp\left[-\frac{1}{2}q_0^2g(\mathbf{r})\right], \tag{10}$$

where

$$g(\mathbf{r})=\langle[u(\mathbf{r})-u(0)]^2\rangle. \tag{11}$$

In the case of true long-range order $G(\mathbf{r})$ approaches a constant value for $r\to\infty$. If $G(\mathbf{r})$ shows an algebraic decay with r, we speak of quasi-long-range order. The

smectic pair-correlation function has been calculated to be (Caillé, 1972; Als-Nielsen, 1980)

$$G(\mathbf{r}) = G(r_\perp, z) \propto \exp(-2\eta\gamma_E)\left(\frac{2d}{r_\perp}\right)^{2\eta} \times \exp\left[-\eta E_1\left(\frac{r_\perp^2}{4\lambda z}\right)\right]. \quad (12)$$

The exponent η is given by

$$\eta = \frac{q_0^2 k_B T}{8\pi\sqrt{KB}}, \quad (13)$$

while $\gamma_E = 0.5772$ is Euler's constant, $E_1(x)$ the exponential integral, and $\lambda = \sqrt{K/B}$ is the so-called penetration depth, which is of the order of the layer spacing d. Using the asymptotic expressions for the exponential integral, Eq. (12), leads to

$$G(r_\perp, z) \propto z^{-\eta} \quad \text{for } r_\perp \ll \sqrt{\lambda z},$$
$$G(r_\perp, z) \propto r_\perp^{-2\eta} \quad \text{for } r_\perp \gg \sqrt{\lambda z}. \quad (14)$$

Within the layers of the Sm-A and Sm-C phase the positional order is short range. Thus the positional correlations decay exponentially: $G(\mathbf{r}_\perp) \propto \exp(-kr_\perp)$, where k is an inverse correlation length. The other known smectic phases all possess so-called bond-orientational (hexatic) order. In that situation correlations of the orientations of local hexagons persist over large distances, even in the absence of positional order. For smectic layers this leads to a sixfold rotational symmetry and the orientational correlations are described in terms of the two-component bond-orientational ordering field:

$$\Psi_6(\mathbf{r}_\perp) = \psi_6 \exp[\imath 6\theta_6(\mathbf{r}_\perp)]. \quad (15)$$

The phase is given by the angle θ_6 of the intermolecular direction with respect to a reference axis. Such an anisotropic two-dimensional liquid has been called a *hexatic phase* (Halperin and Nelson, 1978). The bond-orientational correlation function decays at large distances algebraically as

$$G_6(\mathbf{r}_\perp) = \langle \Psi_6(\mathbf{r}_\perp)\Psi_6(0)\rangle = \psi_6^2 \langle \exp\{\imath 6[\theta_6(\mathbf{r}_\perp) - \theta_6(0)]\}\rangle \propto r_\perp^{-\eta_6}, \quad (16)$$

with an exponent $\eta_6 = 18k_B T/(\pi K_A)$, where K_A is the effective stiffness of the bond-orientational field. The hexatic phase is characterized by quasi-long-range bond-orientational order, while the positional order is still short range. Similarly to the displacement of the smectic layers, the algebraic decay of the bond-orientational correlations leads to a long-wavelength divergence of the mean-square amplitude $\langle \delta\theta_6^2 \rangle$ of the fluctuations in the bond angles:

$$\langle \delta\theta_6^2 \rangle = \frac{k_B T}{(2\pi)^2 K_A} \int \frac{d^2 q_\perp}{q_\perp^2} = \frac{k_B T}{2\pi K_A} \ln\left(\frac{W}{a}\right). \quad (17)$$

The Sm-B phase is the hexatic counterpart of the orthogonal Sm-A phase. The Sm-I and Sm-F phases are hexatic similar to the Sm-B phase, but, as in the Sm-C phase, **n** makes a nonzero tilt angle with the layer normal. In the Sm-I phase the projection of **n** onto the smectic plane (the so-called **c** director) points towards a nearest neighbor in a local hexagon, while for the Sm-F phase **c** points to the next-nearest neighbor. In addition a Sm-L phase also exists in which the tilt azimuth is intermediate between these two situations (Chao *et al.*, 1997).

The scenario outlined so far applies to two-dimensional systems. Birgeneau and Litster (1978) suggested that some of the more ordered smectic phases might actually be the three-dimensional analog of the bond-ordered hexatic phase of Halperin and Nelson. Then each smectic layer is a two-dimensional hexatic system with additional angular correlations from layer to layer. In such a three-dimensional case the mean-square fluctuations of the bond angles remain finite (Prost, 1984), in contrast to the situation in two dimensions. Thus a three-dimensional (or stacked) hexatic phase exhibits true long-range bond-orientational order. At the same time the in-plane positional correlations remain short range and decay exponentially with distance.

An increase in the positional order leads to phases with a hexagonal in-plane lattice. These Cr-B, Cr-J, and Cr-G phases are crystalline versions of the orthogonal Sm-B and tilted Sm-I and Sm-F phases, respectively. Two-dimensional crystals are at their lower critical dimensionality of two and therefore are unstable relative to long-wavelength phonons (see, for example, Chaikin and Lubensky, 1995). Consequently, the positional correlations should decay algebraically with distance $G(\mathbf{r}_\perp) \sim r_\perp^{-\eta_{cr}}$ with a power-law exponent η_{cr}. The bond-orientational correlations are long range: $G_6(\mathbf{r}_\perp)$ remains constant in the limit $r_\perp \to \infty$. When the two-dimensional crystal planes are locked together into a three-dimensional structure, true long-range positional as well as bond-orientational order is found. Finally, further crystalline phases, Cr-E, Cr-K, and Cr-H, result from a distortion of the hexagonal in-plane lattice. This is due to the ordering of the backbone planes of the molecules in a herringbone packing. These phases possess a centered rectangular in-plane lattice. Cr-E is orthorhombic while Cr-K and Cr-H are monoclinic with a tilt direction corresponding to the Sm-I and Sm-F phases, respectively. Table I summarizes the different smectic and related lamellar crystalline phases. More details are presented in the books by Gray and Goodby (1984) and Pershan (1988).

B. Main features of x-ray patterns

In this section we shall summarize the basic x-ray features of smectics in general and smectic membranes in particular. Complementary information has been obtained by optical measurements (microscopy, reflectivity, ellipsometry, light scattering) (Pindak, 1992; Pieranski *et al.*, 1993; Bahr, 1994), heat-capacity studies (Stoebe and Huang, 1995), and mechanical measurements (Pindak and Moncton, 1982). In general an x-ray experiment determines the Fourier image of the density-density cor-

TABLE I. Structure and symmetry properties of three-dimensional smectic and crystalline phases. (Note that a two-dimensional hexatic phase has QLR bond-orientational order; two-dimensional crystals possess QLR positional order.) LRO, QLRO, and SRO refer to long-range, quasi-long-range and short-range order, respectively. NN and NNN indicate tilt in the direction of the nearest neighbor and next-nearest neighbor of the local hexagon.

Type of positional and bond-orientational order	Phase			
	Orthogonal	Tilted to NN	Tilted to NNN	Tilted between NN and NNN
Interlayer positions QLRO In-plane positions SRO	Sm-A		Sm-C (random tilt)	
Interlayer positions QLRO In-plane positions SRO Bond orientations LRO	Sm-B	Sm-I	Sm-F	Sm-L
Hexagonal in-plane lattice All ordering LRO	Cr-B	Cr-J	Cr-G	Cr-M
Rectangular in-plane lattice (Herringbone order)	Cr-E	Cr-K	Cr-H	Cr-N

relation function $G(\mathbf{r})$. This is expressed as the structure factor $S(\mathbf{q})$, which is given by

$$S(\mathbf{q})=\int d^3r\, G(\mathbf{r})\exp(i\mathbf{q}\cdot\mathbf{r}). \tag{18}$$

Hence a reconstruction of $G(\mathbf{r})$ from $S(\mathbf{q})$ yields information on the character of the translational order. Three types of positional order can be distinguished (Fig. 2). Long-range translational order in an ideal three-dimensional crystal results in delta-function-type diffraction peaks. In systems with reduced dimensionality thermal fluctuations destroy the long-range translational order and cause power-law singularities instead of delta-function peaks. In a conventional liquid the positional correlations decay exponentially with distance, giving a Lorentzian scattering profile. A similar type of short-range positional order is observed within smectic and hexatic layers.

Any diffraction experiment is defined by a specific variation of the wave-vector transfer $\mathbf{q}=\mathbf{q}_{\rm out}-\mathbf{q}_{\rm in}$ with $q=|\mathbf{q}|=(4\pi/\lambda)\sin\theta$, where θ and λ are the scattering angle and the wavelength of the radiation, respectively. The general feature of all smectic phases is a set of sharp $(00n)$ quasi-Bragg peaks in the direction along the layer normal at wave-vector transfer $q=q_n=2\pi n/d$. The in-plane order is short range and can be determined from the width of the in-plane $(hk0)$ peaks. This type of diffraction pattern represents the rare situation in which quasi-Bragg peaks in one direction of reciprocal space (along the layer normal) are combined with liquidlike in-plane peaks.

1. X-ray diffraction normal to the layers

To study smectic layering, one must set the wave-vector transfer along the layer normal. For bulk samples this is accomplished by an incident x-ray beam approximately perpendicular to a magnetic field that aligns the director. In the case of smectic membranes a reflectivity setup can be used (see Sec. IV.A.1). The algebraic decay of the positional correlations in the smectic layers given by Eq. (14) implies that the x-ray structure factor has a

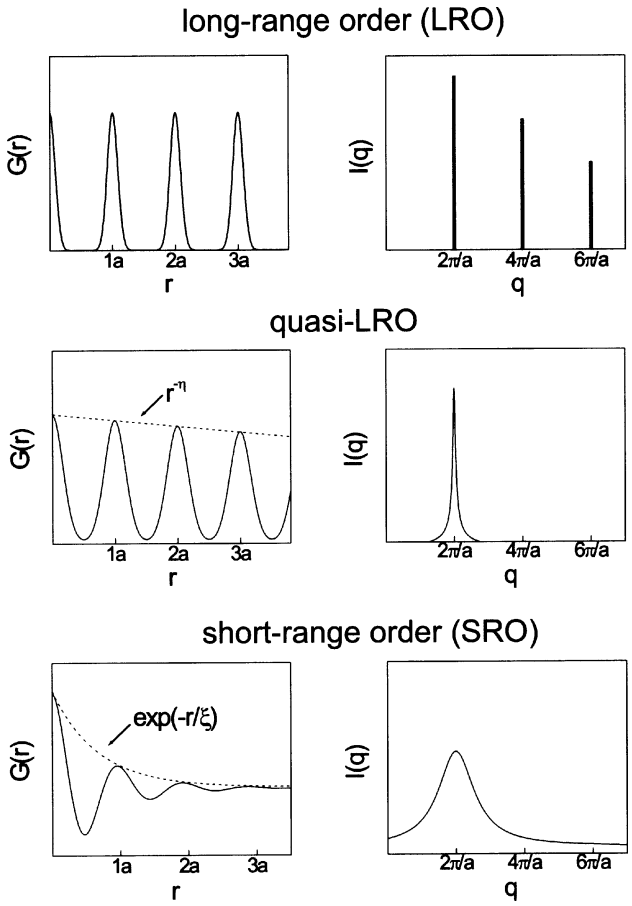

FIG. 2. Correlation function and resulting diffraction pattern for various types of positional order.

power-law rather than a delta-function singularity (Caillé, 1972; Gunther *et al.*, 1980):

$$S(q_\perp=0,q_z)\propto(q_z-q_n)^{-2+\eta_n},$$
$$S(q_\perp,q_z=q_n)\propto q_\perp^{-4+2\eta_n}, \tag{19}$$

where $\eta_n=n^2\eta$ with η given by Eq. (13). This type of anisotropic line shape was first observed in smectics by Als-Nielsen *et al.* (1980) and then confirmed for various thermotropic (Zisman *et al.*, 1987; Kaganer *et al.*, 1991; Nachaliel *et al.*, 1991) and lyotropic lamellar phases (Safinya *et al.*, 1986; Roux and Safinya, 1988; Wack and Webb, 1989). There are a finite number of power-law singularities of the type of Eq. (19); when $\eta_n>2$ they are replaced for large q_n by cusplike peaks. This singular behavior of the structure factor in smectics can be contrasted to the Bragg peaks with diffuse tails found in three-dimensional crystals. Thermal vibrations in three-dimensional crystals reduce the intensities of the Bragg peaks by a Debye-Waller factor $\exp(-2M)$, but introduce no line broadening. In the limit of infinite-size smectic samples, the Bragg peaks are absent due to the divergence of the Debye-Waller factor:

$$\exp(-2M_n)=\exp[-q_n^2\langle u^2(\mathbf{r})\rangle]\propto\left(\frac{L}{d}\right)^{-\eta_n}. \tag{20}$$

Now all scattering is concentrated in the power-law wings, Eq. (19), and is due to the layer fluctuations. For samples of finite thickness the situation is different. In this case the Debye-Waller factor is not divergent and the x-ray intensity consists of thermal diffuse scattering given by Eq. (19) with a true, albeit weakened, Bragg peak on top (Gunther *et al.*, 1980). The form factor of a domain of thickness L leads to a Bragg peak of width $\sim L^{-1}$ and height $\sim LW^{2-2\eta_n}$, W being the lateral size. This peak is accompanied by wings decreasing (on average) as q^{-2} (Gunther *et al.*, 1980; Kaganer *et al.*, 1991). Note that according to Eq. (20) the maximum intensity of the finite-size Bragg peak decreases rapidly with n, leading to a drastically diminishing intensity of the higher-order harmonics. For typical values $\eta\simeq0.1$ and $L\simeq20$ μm the contribution $\sim(L/d)^{-\eta_n}$ of the Bragg peak to the total intensity is ~0.4 for the first diffraction maximum (001) and ~0.01 for the next reciprocal-lattice point (002).

In most thermotropic low-molecular-mass smectics only the first quasi-Bragg peak is clearly present, the intensity of the others being orders of magnitude less. The only exceptions are mesogens with perfluorinated or siloxane terminal groups (Ostrovskii, 1999). Polymeric smectics (Nachaliel *et al.*, 1991; Davidson and Levelut, 1992) and lyotropic smectics (Smith *et al.*, 1987; Roux and Safinya, 1988) are less compressible (the elastic modulus B is larger) and thus higher-order harmonics are more pronounced. The intensity of the successive harmonics is also modified by the wave-vector dependence of the molecular form factor $F(\mathbf{q})$. The latter has a maximum value at $q=0$ and decays nonmonotonically as q increases. For example, the molecular form factor favors more intense higher harmonics for lyotropic smectics with a bilayer structure as well as for polymeric smectics with side chains.

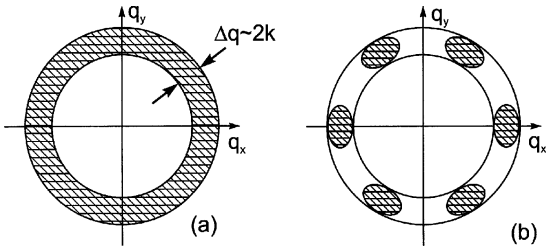

FIG. 3. Schematic illustration of the in-plane scattering of a smectic membrane: (a) isotropic smectic layers; (b) bond-orientational (hexatic) ordering. After Brock *et al.*, 1989.

2. In-plane x-ray diffraction

Using diffraction in a transmission geometry $\mathbf{q}$ lies in the plane of smectic layers. Thus any positional ordering that satisfies the condition $\mathbf{q}=\mathbf{q}_{\perp0}$, where $\mathbf{q}_{\perp0}$ is an in-plane reciprocal-lattice vector, gives rise to a peak of scattered intensity. Transmission electron diffraction is a very appropriate method for studying bond-orientational order in thin hexatic membranes (Cheng *et al.*, 1987, 1988; Chou, Ho, and Hui, 1997). Positional correlations can be advantageously obtained using transmission and grazing-incidence x-ray diffraction. The latter technique also allows us to probe surface-induced ordering (Dosch, 1992; Als-Nielsen *et al.*, 1994).

In the Sm-A phase the in-plane structure is liquidlike due to the short-range positional order. The structure factor of a two-dimensional liquid has the form of a broad cylindrical tube with its axis parallel to the layer normal. It has a width $\sim2k$, where $\xi=k^{-1}$ is a characteristic length over which positional correlations between the molecules decay exponentially. The form factor of rodlike molecules is large only in a plane normal to the long axis, which is called the *reciprocal disc* of the molecule. The intersection of the cylindrical tube with the reciprocal disc gives rise to a diffuse ring of scattering in the $\mathbf{q}_\perp$ plane (see Fig. 3). The radius of the ring corresponds to $q_{\perp0}\simeq4\pi/(a\sqrt{3})$, where a is the average molecular separation.

The structure factor of a simple liquid can be obtained on the basis of the phenomenological Ornstein-Zernike model (Stanley, 1971; Landau *et al.*, 1980) and can be expressed as

$$S(q_\perp)=\langle|\rho(\mathbf{q}_\perp)|^2\rangle\sim[(q_\perp-q_{\perp0})^2+k^2]^{-1}. \tag{21}$$

The scattering profile is a Lorentzian with a full width at half maximum (FWHM) of $2k$ centered at the preferred wave vector $q_{\perp0}$. The Fourier transform of Eq. (21) in three dimensions gives the well-known result for the asymptotic behavior of the pair-correlation function (Landau *et al.*, 1980),

$$G(r_\perp)\sim r_\perp^{-1}\exp(-kr_\perp). \tag{22}$$

The short-range positional order described by this equation is typical for conventional three-dimensional liquids and many other disordered systems. However, *a priori* it is not obvious that the same type of correlation function also applies to stacks of two-dimensional liquids. The Fourier transform of the Lorentzian structure factor, Eq. (21), in two dimensions results in a correlation function that decays with distance as

$$G(r_\perp) \sim K_0(k r_\perp), \tag{23}$$

where K_0 is the modified Bessel function of zero order. For positional correlations in a two-dimensional liquid this latter function seems to be a better approximation. Note that if Eq. (22) is back-Fourier-transformed in two dimensions, we obtain a line shape $[(q_\perp - q_{\perp 0})^2 + k^2]^{-1/2}$ that is hardly comparable with experimental data for the Sm-A phase. Thus the interpretation of the diffuse liquidlike peak in Sm-A is somewhat ambiguous: a different correlation function is found depending on whether a three-dimensional or a two-dimensional Fourier transformation is preferred.

In the hexatic Sm-B phase the presence of bond-orientational order breaks the angular isotropy of the structure factor. This leads to a sixfold modulation of the scattering in the $\mathbf{q}_\perp$ plane (see Fig. 3). A Fourier expansion of the azimuthal scattering profile gives

$$S(\chi) = \sum_n C_{6n} \cos(6n\chi), \tag{24}$$

where χ is the rotation angle of the sample. The coefficients C_{6n} can be considered as order parameters that measure the amount of $6n$-fold bond ordering in the film. In combination with this orientational anisotropy, hexatics display a diffuse scattering profile in the radial direction, corresponding to short-range positional order. When the temperature is decreased, the width of the radial peak diminishes simultaneously with the further development of the bond-orientational order. This indicates a coupling between the positional correlations and the bond-orientational order.

A line-shape analysis in the hexatic Sm-B phase is complex due to the coupling between the liquid density and the bond-orientational order parameter (Bruinsma and Nelson, 1981). The evolution of the liquid structure factor in the vicinity of the hexatic-isotropic transition was studied in the framework of the phenomenological XY model. In this approach the radial line shape takes the form (Aeppli and Bruinsma, 1984; Brock *et al.*, 1989)

$$S(\mathbf{q}_\perp) \sim \int_{-\pi/6}^{\pi/6} d\theta_6 \frac{\exp\left(-\frac{1}{2}\theta_6^2/\langle \delta\theta_6^2\rangle\right)}{k^2 + q_\perp^2 + q_{\perp 0}^2 - 2q_\perp q_{\perp 0}\cos(\phi - \theta_6)}, \tag{25}$$

where ϕ is the angle between the in-plane components of $\mathbf{q}_\perp$ and $\mathbf{q}_{\perp 0}$. The bond-orientational fluctuations $\langle \delta\theta_6^2\rangle$ cause a broadening of the azimuthal intensity distribution producing a mosaic averaging of the initial Lorentzian-like profile. As a result, the radial line shape can be approximated by

$$S(q_\perp) \sim [(q_\perp - q_{\perp 0})^2 + k^2]^{-1/2}. \tag{26}$$

Because the bond-orientational order is quasi-long-range in two-dimensional hexatics [see Eq. (17)], the x-ray-diffraction pattern from an infinite hexatic sample should consist of an isotropic ring. However, finite-size effects modify this pattern, so that a sixfold modulation is observed in experiments on thin monodomain hexatic membranes (Brock *et al.*, 1986; Cheng *et al.*, 1988). Since thermodynamic stability requires $K_A/k_B T \geqslant 72/\pi$ (see Sec. III.A.2), according to Eq. (17), the bond-angle fluctuations can be as large as $\langle \delta\theta_6^2\rangle^{1/2} \simeq 16°$ ($W = 50$ μm, $a = 0.5$ nm). This causes significant azimuthal broadening of the diffraction pattern in the vicinity of the Sm-A–Sm-B transition. Alternatively, a uniform diffuse ring of the type of Eq. (26) can also be due to averaging over multiple domains with different orientations within the illuminated area.

Experimentally square-root Lorentzian line shapes fit in-plane hexatic radial scans quite well over a broad interval of temperatures and thicknesses (Davey *et al.*, 1984; Brock *et al.*, 1986). However, in the case of thick monodomain hexatic Sm-B films ($\gtrsim 10$ μm) of the compounds RFL6 and PIR5, the radial line shape was reported to be closer to a simple Lorentzian (Górecka *et al.*, 1994). The in-plane reflections exhibit an almost perfect sixfold symmetry, which points to strong interlayer bond-orientational correlations. Similar observations have been made with electron diffraction in hexatic membranes of various compositions and thicknesses. Clearly the hexatic phase, originally expected to exist in two-dimensional systems (Halperin and Nelson, 1978), could be a three-dimensional phase with true long-range bond-orientational order.

At lower temperatures the hexatic phase crystallizes, as signaled by condensation of the modulated ring of scattering into sharp $(hk0)$ reflections from the two-dimensional hexagonal lattice. As two-dimensional crystals are characterized by quasi-long-range positional order with a pair-correlation function $G(\mathbf{r}_\perp) \sim r_\perp^{-\eta_{cr}}$, their structure factor has the form

$$S(q_\perp) \propto |q_\perp - q_{hk0}|^{-2+\eta_{cr}}. \tag{27}$$

The exponent $\eta_{cr} = (k_B T/4\pi\mu)[(\lambda + 3\mu)/(\lambda + 2\mu)]q_{hk0}^2$ depends on the elastic Lamé coefficients λ and μ. For a finite lattice with size W the singular behavior of Eq. (27) is valid only for $q_\perp \gg W^{-1}$, while the central part of the diffraction profile is dominated by a Bragg peak with a width $\sim W^{-1}$ (Imry and Gunther, 1971). Both the lattice fluctuations and the molecular form factor cause the peak intensities to decay rapidly with increasing $q_\perp$. Thus only the first-order (020) and (110) peaks of the hexagonal lattice are visible. Power-law singularities of the type of Eq. (27) have been observed in a two-layer Cr-B film of the compound 14S5 (Moncton *et al.*, 1982) and in a five-layer membrane of the compound 8OSI in the Cr-J phase (Noh *et al.*, 1991).

Three-dimensional crystals are characterized by delta-function-type Bragg peaks, accompanied by diffuse tails of the form $|q_\perp - q_{hk0}|^{-2}$ resulting from nondivergent

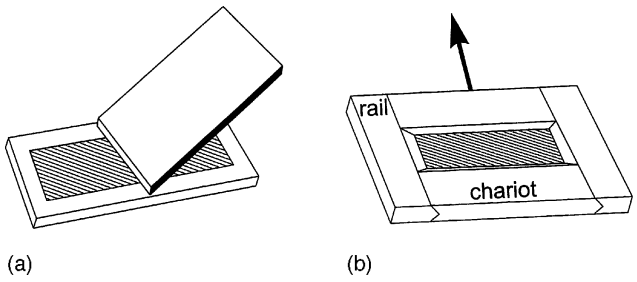

FIG. 4. Spreading a smectic membrane: (a) using a fixed frame and a separate wiper; (b) by means of a frame of variable size.

phonon excitations. This type of behavior was observed in relatively thick Cr-B films of the compound 4O.8 (Moncton and Pindak, 1979; Pershan *et al.*, 1981) and in some other compounds (Leadbetter *et al.*, 1979). Thus the Cr-B phase in thick films has three-dimensional positional order. This is in agreement with bulk samples that show sharp in-plane diffraction peaks, indicating long-range periodicity within the layers. Combined Bragg reflections of the type (hkn) are also found, indicating that the layers are locked together in a three-dimensional periodic structure. Scans along q_z taken at the positions of the in-plane reciprocal-lattice vectors $\mathbf{q}_{\perp 0}$ reveal different types of layer stacking AAA…, ABAB…, or ABCABC… (Pershan, 1988).

The tilted phases are more complex as, due to the tilt of molecules, the reciprocal disc is tilted with respect to the plane of the smectic layers. As a result the diffuse ring in the Sm-C, Sm-I, and Sm-F phase is also inclined. In this situation the reciprocal disc of the molecules intersects the modulated tube of the hexatic structure factor at points lying outside the plane of the layers. As a result, the diffuse peaks move out of the $\mathbf{q}_\perp$ plane (Smith *et al.*, 1990; Kaganer *et al.*, 1995). Smectic-I and Sm-F hexatic phases were first observed by x-ray diffraction of bulk smectic samples (Benattar *et al.*, 1979) and later studied systematically in smectic membranes of variable thickness (Collett *et al.*, 1984; Sirota *et al.*, 1987b). If the tilt azimuth is intermediate between the nearest neighbors and the next-nearest neighbors, in lowest order three distinct diffraction peaks exist (Kaganer *et al.*, 1995). This type of tilted smectic phase has been observed both in lyotropic (Smith *et al.*, 1988) and in thermotropic (so-called Sm-L phase) smectic membranes (Chao *et al.*, 1997).

C. Stability of smectic membranes

Smectic membranes can be drawn manually by wetting the edges of an opening in a glass or metal holder with the mesogenic compound in the smectic phase and then moving a spreader across the hole (Young *et al.*, 1978; see Fig. 4). By varying the amount of smectic material, the temperature and the speed of drawing, one can produce membranes ranging from 5 nm (two layers) to tens of μm (thousands of layers). Alternatively a frame with a variable area can be used (Pieranski *et al.*, 1993; Bahr, 1994). Such a rectangular frame possesses one or two movable parts with sharp edges, the distance of which can be changed by a micrometer screw. The advantage of the latter technique is that a series of membranes with progressively decreasing thickness can be produced upon increasing the area of the frame. Directly after preparation a film usually consists of regions of different thickness, from which it equilibrates to a uniform situation. The equilibration time varies from minutes to days depending on the specific compound, the temperature, and the type of frame. Usually the thinnest region grows at the expense of the thicker ones.

Since the early work of Pieranski *et al.* (1993), the (meta)stability of smectic membranes has been discussed by several authors (Geminard *et al.*, 1997; Picano *et al.*, 2000, 2001). A review has been given by Oswald and Pieranski (2002). As is well known, across a flat liquid interface in equilibrium no pressure difference can exist (see, for example, Rowlinson and Widom, 1982). This is no longer true for a smectic surface because the layers are elastic and can support a normal stress that will equilibrate any small pressure difference $\Delta p = p_{\rm air} - p_{\rm sm}$. In addition to the surface tension γ, this pressure difference contributes to the tension Γ along the smectic membrane:

$$\Gamma = 2\gamma + \Delta p L. \tag{28}$$

The contribution of the stress to Δp depends on the shape of the meniscus between the membrane and its support. The pressure in the meniscus can be influenced by the amount of material near the edges or by the speed with which the film is stretched during the preparation. Geminard *et al.* (1997) studied the meniscus surrounding a needle in a smectic film by observing the fringes in monochromatic light. The results show that a smectic meniscus is composed of a collection of steps due to edge dislocations repelled from the free surfaces. Further experiments indicate that the smectic meniscus contains a thick part with a large density of dislocations, and a thinner part adjacent to the membrane in which dislocations remain elementary (Picano *et al.*, 2000, 2001). The latter has a circular profile with radius of curvature R, which for thick films matches tangentially the free surface of the membrane. The value of R fixes the pressure difference inside both the meniscus and the film via $\Delta p = \gamma/R$, which is of the order of 0.1–1 N/m^2. For membranes less than about 50 layers this behavior changes and an apparent "contact" angle appears.

For optical and x-ray measurements in a transmission geometry the film area can be restricted to a few mm^2. For x-ray reflectivity studies a large footprint of the incident x-ray beam must be accommodated. Therefore membranes are typically spanned over a 10×25 mm^2 rectangular hole in a polished plate with sharp top edges. This brings the membrane as close to the top of the holder as possible and reduces shadowing of the beam. The two surfaces of a membrane induce an almost perfect alignment of the smectic layers: the residual curvature of the film is due mainly to the nonplanarity of the edges of the holder. The resulting mosaicity, expressed as the angular spread of the surface normal,

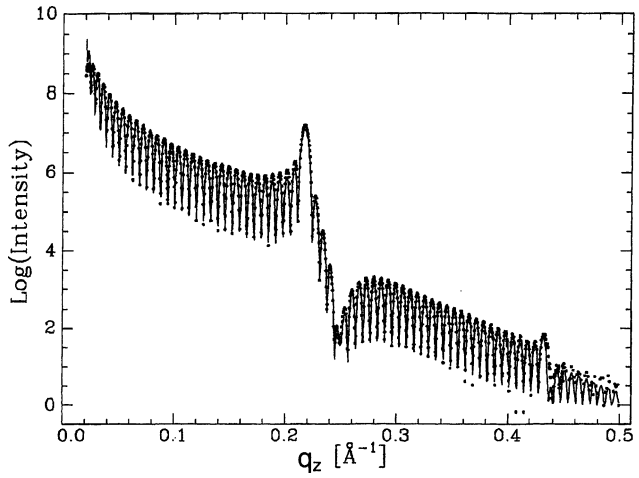

FIG. 5. X-ray reflectivity of a 33-layer smectic membrane of 7AB.

can be as small as 0.002° at a footprint of about 3 $\times 3$ mm^2 (Mol *et al.*, 1996). The membrane thickness can be easily determined by optical reflectivity, which for sufficiently thin films scales as the square of the thickness (Rosenblat and Amer, 1980; Pieranski *et al.*, 1993). The number of smectic layers in a film can be precisely determined from specular x-ray reflectivity. Reflection occurs at both the front and the back interface, leading to constructive or destructive interference depending on the incoming angle (Kiessig or interference fringes; see Fig. 5). The period of the fringes is inversely proportional to the film thickness L. In addition the internal periodic structure generates finite-size Bragg-like peaks centered at q_n. Thus the number of smectic layers $N = L/d$ can be determined unambiguously. Smectic membranes are stable over many days or even months despite the fact that they are homogeneously compressed over their surface. Their thickness can be modified by variation of the tension Γ, for example, by changing the surface area using the variable area frame. The thickness variation usually proceeds via nucleation of edge-dislocation loops (Geminard *et al.*, 1997; Picano *et al.*, 2000; Oswald *et al.*, 2002) and the final state depends on the way the film has been created. Though the basic features of the meniscus and the role of the tension are now established, several other aspects still remain to be explored.

III. STRUCTURE AND PHASE TRANSFORMATIONS

A. Theoretical aspects of phase transitions

The in-plane structure of smectic membranes can vary as a function of temperature, film thickness, etc., from liquid (Sm-A) to hexatic (Sm-B) and crystalline (Cr-B). In addition surface-induced phases may occur. This multiplicity of crystallization (melting) transitions in smectic films differing in composition and thickness makes their theoretical description rather complicated. The defect-unbinding theory (Kosterlitz and Thouless, 1973; Halperin and Nelson, 1978) predicts that the melting of a two-dimensional crystal involves two continuous transitions separated by an intermediate hexatic phase. Alternatively, the melting transition might be of the usual first-order type observed in three-dimensional crystals. The observation of hexatic phases in smectic liquid crystals is compatible with the defect-mediated melting scenario. However, the mere existence of a hexatic phase does not by itself necessarily provide proof of a specific melting mechanism. In other cases the hexatic phase is preempted by a direct first-order Cr-B–Sm-A phase transition (Moncton *et al.*, 1982).

Bulk hexatic smectic phases can be considered as three-dimensional systems of stacked hexatic layers. The coupling between the layers leads—even in the absence of interlayer positional correlations—to true long-range bond-orientational order, and changes the nature of the corresponding transitions (Aharony *et al.*, 1986). Because the two-dimensional limit can be approached in sufficiently thin films, smectic membranes are perfect model systems for studying the true nature of the Kosterlitz-Thouless transition. Additional theoretical predictions indicate that the hexatic order is reduced by out-of-plane layer-displacement fluctuations. As the fluctuations are often quenched at the surfaces, the stability of the hexatic phase is enhanced at these positions compared to the interior of a film (Selinger, 1988; Hołyst, 1992). Hence surface-induced crystallization in the top layers of smectic membranes can occur, which provides another way to probe the two-dimensional melting sequence. The theory of two-dimensional melting and the effects of bond-orientational order on the phase sequences in low-dimensional systems have been reviewed by Nelson (1983), Strandburg (1988), and Glaser and Clark (1993). In the following sections we restrict ourselves to a description of the basic ideas and the attendant results as relevant to smectic membranes.

1. Landau approach

In discussing the development of translational and bond-orientational order in smectic membranes, we start from a Landau theory of crystallization. Crystallization of a liquid leads to the appearance of a spatial density modulation $\rho(\mathbf{r}) = \langle\rho\rangle + \delta\rho(\mathbf{r})$, which can be expanded in a Fourier series: $\delta\rho(\mathbf{r}) = \Sigma_{\mathbf{k}}\rho_{\mathbf{k}}\exp(\imath\mathbf{k}\cdot\mathbf{r})$. Let us consider first the common case in which the amplitudes of the density waves alone represent the ordering field of the liquid-to-crystal transition (Landau, 1937). The free energy can be expanded in powers of $\rho_{\mathbf{k}}$, each term containing wave vectors forming a closed polygon $\Sigma_i\mathbf{k}_i = 0$ to ensure translational invariance. The expansion starts with the term $\Sigma_{\mathbf{k}}a_\rho\rho_{\mathbf{k}}\rho_{-\mathbf{k}}$, in which the coefficient a_ρ depends on temperature, pressure, and the length of the vector $\mathbf{k}$. The crystallization transition is driven by a change of sign of a_ρ at the transition point T_c. The actual wave vector of the crystallization is the one that realizes this condition first. The next term is $\sim\Sigma_{\mathbf{k}}\rho_{\mathbf{k}_1}\rho_{\mathbf{k}_2}\rho_{\mathbf{k}_3}$, and the condition $\mathbf{k}_1+\mathbf{k}_2+\mathbf{k}_3=0$ selects equilateral triangles of wave vectors. The crystallization transition is first order due to the presence of this cubic

term in the free-energy expansion. The free energy is minimized by maximizing the number of equilateral triangles of wave vectors. In three dimensions this is achieved by the formation of a tetrahedron, which gives rise to crystallization into a body-centered-cubic structure (Alexander and McTague, 1978). Other structures arise depending on the angular contribution from the fourth-order term (Kats *et al.*, 1993a). It should be noted that the amplitude of the density wave is not the only possible crystallization order parameter in the Landau theory. In the case of nonspherical organic molecules of the liquid-crystal type, long-chain amphiphilics, and *n*-alkanes, the crystallization scenario also depends on the ordering of the short axes of the molecules (the "backbone plane") with respect to the bond directions (Kaganer and Loginov, 1995).

In two dimensions only one equilateral triangle can be formed, giving rise to a transition into a two-dimensional hexagonal crystal. In such a crystal the bond-orientational ordering field is determined by the two-component order parameter Ψ_6. Its contribution to the free energy of the system can be described by powers of $|\Psi_6|$ with leading term $\sim a_6^2|\Psi_6|^2$. Inclusion of a coupling term $\sim\Sigma_{\mathbf{k}}|\rho_{\mathbf{k}}|^2[\Psi_6\exp(-\iota\theta_{\mathbf{k}})+\Psi_6^*\exp(\iota\theta_{\mathbf{k}})]$ ensures that the bond-orientational order parameter Ψ_6 is phase locked to $\mathbf{k}$ (the asterisk denotes complex conjugation). If a_6 is large and positive when a_ρ changes sign, one expects a direct transition into a crystal. If a_6 changes sign before a_ρ does, the Landau theory describes a continuous transition into an orientationally ordered hexatic phase. Unlike the crystalline phase, ordering in Ψ_6 does not require any of the $\rho_{\mathbf{k}}$ to become finite. Thus the hexatic phase remains positionally disordered. Since Ψ_6 is a complex order parameter, this transition belongs to the universality class of the two-dimensional XY model. A more sophisticated Landau theory is required to describe the hexatic-crystal transition (Nelson, 1983). The presence of a third-order term in the free-energy expansion again implies that the transition is first order.

Two-dimensional crystals at their lower marginal dimensionality exhibit an algebraic decay of the density correlation function. The fluctuations in the phase of the translational order parameter $\rho_{\mathbf{k}}=|\rho_{\mathbf{k}}|\exp(\iota\mathbf{k}\cdot\mathbf{u})$, where $\mathbf{u}(\mathbf{r})$ represents the displacement field, are strong enough to destroy the long-range positional order. A renormalization-group analysis performed within the framework of the Kosterlitz-Thouless theory indicates that fluctuations depress the transition temperatures well below their Landau values and change the character of the melting transition (Nelson and Halperin, 1979). In particular, the hexatic-crystal transition need not be first order in two dimensions. The hexatic phase is characterized by quasi-long-range orientational order and melts into the liquid phase via a mechanism of disclination unbinding. Hence the transition from crystal to liquid can occur either directly via a first-order transition or through a two-step process with an intermediate hexatic phase. The latter approach will be discussed in some detail in the next section.

2. Defect-mediated phase transitions

Berezinskii (1972) and Kosterlitz and Thouless (1973) proposed a theory for transitions in XY models, based on topological defects called vortices. Typical examples are two-dimensional superfluids and superconductors. The mechanism for the Berezinskii-Kosterlitz-Thouless (BKT) transition is the unbinding of a dilute gas of vortex pairs. The theory predicts a continuous transition from the low-temperature phase, characterized by quasi-long-range order, to the high-temperature disordered phase. Two-dimensional crystals belong to the same universality class as the XY model, and the relevant topological point defects responsible for the order-disorder transitions are dislocations and disclinations. The theory of defect-mediated melting of two-dimensional crystals was generalized by Halperin and Nelson (1978), Nelson and Halperin (1979), and Young (1979). The extended BKT mechanism assumes that in a two-dimensional crystal below the melting temperature T_m, in addition to conventional thermal phonon excitations, a finite concentration of dislocation pairs also exists. These pairs have equal and opposite Burgers vectors and are thermally generated even at low temperatures. The elastic energy of a bound pair of dislocations with a characteristic size R can be estimated as

$$\frac{F_d}{k_{\mathrm{B}}T}=K\ln\left(\frac{R}{a_c}\right)+E_c, \tag{29}$$

in which E_c is the energy of the dislocation core with radius a_c, and the dimensionless dislocation coupling coefficient K is related to the Lamé elastic constants by $K=4\mu(\lambda+\mu)a^2/(\lambda+2\mu)k_{\mathrm{B}}T$. As a consequence of the reduced dimensionality of the system the pair interaction of Eq. (29) varies logarithmically with the core separation. The average size of a pair of dislocations is given by

$$\langle R^2\rangle\sim\int R^2\exp\left(-\frac{F_d(R)}{k_{\mathrm{B}}T}\right)d\Omega, \tag{30}$$

in which the integration is performed over all orientations. Thus the average size of a pair is determined by $F_d(R)$, while the concentration is governed mainly by the core energy E_c. The melting transition corresponds to the unbinding of dislocation pairs into free dislocations once their size increases sufficiently to screen the interaction between dislocations of opposite sign.

A renormalization-group analysis of the BKT mechanism leads to a single continuous transition from a crystal to a liquid phase with a correlation length that diverges as T approaches T_m from above: $\ln\xi\propto(T-T_m)^{-\nu}$ with $\nu=0.369$. This is very different from the power-law divergence of the correlation length associated with a conventional second-order transition. The specific heat exhibits at T_m an unobservable essential singularity: $C_p\propto\xi^{-2}$. However, there is a small bump in the specific heat above T_m due to the gradual unbinding of dislocation pairs. Throughout the crystal phase, there will be an algebraic decay of spatial correlations which leads to the power-law singularities in the structure fac-

tor equation (27). Due to the universal value of the renormalized coupling constant K at the melting point, the exponent η_{cr} attains for a hexagonal lattice a maximum value $\eta_{\mathrm{cr}}^{\max}=1/3$ at T_m (Nelson and Halperin, 1979).

The above results are similar to the BKT predictions for vortex-unbinding transitions in two dimensions. Halperin and Nelson found, however, that the dissociation of dislocation pairs, which destroys the quasi-long-range translational order, does not necessarily produce an isotropic liquid. In such an anisotropic (hexatic) liquid the bond-orientational correlation function decays algebraically $G_6(\mathbf{r})\sim r^{-\eta_6}$ with the exponent given below Eq. (16). The hexatic phase is characterized by quasi-long-range bond-orientational order, while the positional order is short range and the shear modulus zero. The reason for the bond-orientational ordering being retained while the positional correlations are destroyed is that free dislocations are less disruptive of the bond directions. A free dislocation in a hexagonal lattice is composed of a tightly bound pair of sevenfold and fivefold disclinations. The subsequent unbinding of the disclination pairs has a profound influence on the decay of the bond-orientational order. A renormalization-group analysis of this mechanism predicts a continuous disclination-unbinding transition at a temperature $T_i > T_m$ into an isotropic liquid. The renormalized stiffness of the bond-orientational field $K_A/k_{\mathrm{B}}T$ has a universal discontinuity at T_i from a value $72/\pi$ to zero above the transition. As T approaches T_m from above, K_A diverges proportional to the square of the positional correlation length. As in the dislocation-unbinding transition, the specific heat should exhibit a peak above T_i due to the gradual unbinding of disclination pairs. Above T_i a conventional isotropic liquid exists: all correlation functions decay exponentially.

Several computer simulations have been performed to determine the nature of the melting of two-dimensional crystals. Early studies are reviewed by Strandburg (1988, 1992) and Glaser and Clark (1993). For more recent results see, for example, Jaster (1999) and Bates and Frenkel (2000). Even for the case of hard discs, the most simple two-dimensional model system, the situation is not at all clear. Simulations provide inconsistent results, claiming either a weakly first-order or a continuous crystal-isotropic transition. This discrepancy may be a natural result of the limited size of the system as well as the running time in simulation experiments. A recent study by Jaster (1999) using extremely large systems (up to 65 536 hard discs) contradicts a one-stage continuous crystal-isotropic transition. In addition it is not possible to rule out either a one-step weakly first-order crystal-isotropic liquid transition or a two-step continuous crystal-hexatic-isotropic pathway. The behavior of the susceptibility and the bond-orientational correlation length in the isotropic phase coincides with the predictions of the BKT theory. Additionally, a finite-size scaling analysis in the transition region allowed Jaster to locate a disclination-unbinding transition point compatible with the BKT scenario. Similar results have been obtained for a two-dimensional system of classical point particles interacting via an r^{-12} repulsive potential (Bagchi *et al.*, 1996). The important conclusion from computer simulations is that small differences in the potential can drastically change the phase behavior. This suggests that the melting scenario in two dimensions is not universal but depends on the specific properties of the system, such as the energy of the dislocation core E_c and the interparticle potential.

Compelling evidence for the BKT theory in systems with long-range interparticle potentials stems from work on electrons on the surface of helium (Glattli *et al.*, 1988), on charged polymer colloids confined between glass plates (Murray and van Winkle, 1987), and on a confined monolayer of colloidal particles with dipole interactions (Kusner *et al.*, 1994). For a long time the melting of xenon adsorbed on graphite was considered to be a true example of a BKT transition. Precision heat-capacity and vapor-pressure isotherm measurements (Jin *et al.*, 1989), however, indicate that there is a weakly first-order crystal-liquid transition with no intermediate hexatic phase. There is strong evidence for the existence of a hexatic phase in some other two-dimensional systems, for example, hard-core discs with very narrow attractive potentials (Bladon and Frenkel, 1995; Chou and Nelson, 1996), although in these cases it does not necessarily occur as part of the melting process. A hexatic phase showing first-order liquid-hexatic and hexatic-crystal transitions has also been observed for sterically stabilized uncharged colloidal spheres (Marcus and Rice, 1996).

3. Weak-crystallization theory

The transition sequence crystal-hexatic-isotropic can be preempted by a first-order melting transition of a different origin. An example of this was given by Glaser and Clark (1990). In their model the melting transition is due to condensation of localized thermally generated geometrical defects (polygons having four or more sides) into grain-boundary-like structures. We note that, according to Eqs. (29) and (30), the dislocation-unbinding melting mechanism will be inefficient if, due to specific properties of the material, the nucleation energy of dislocation pairs is large ($F_d \gg k_{\mathrm{B}}T$). In this case the amplitudes of the density waves $\rho_{\mathbf{k}}$, which are the signature of a crystal, become zero before the dissociation of dislocation pairs starts. If this transition is weakly first order it can be described within the framework of the fluctuation theory of weak crystallization, which we shall now discuss briefly.

The fluctuation theory of weak crystallization is based on the assumption that the free energy can be expanded in powers of the order parameter $\phi(\mathbf{r})=\delta\rho/\langle\rho\rangle$, the ratio of the density modulation to the average density (Kats *et al.*, 1993a), at least for $\phi \ll 1$. To take into account the effects of fluctuations, a gradient term $(\alpha/8q_0^2)[(\nabla^2+q_0^2)\phi]^2$ is added to the expansion, α being a phenomenological coefficient. The structure of the gradient term reflects the fact that crystallization occurs

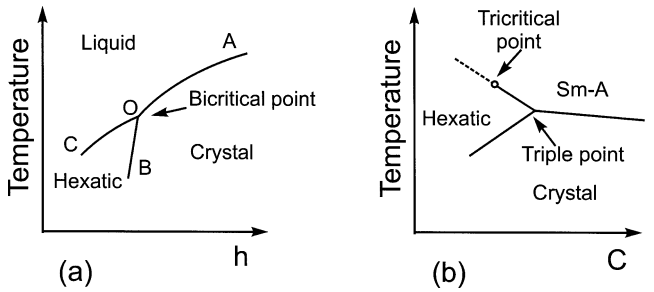

FIG. 6. Generic phase diagram near the Sm-A–Sm-B–Cr-B triple point: (a) two-dimensional case (Kats and Lajzerowicz, 1996); (b) three-dimensional case (Aharony *et al.*, 1986).

from a liquid and therefore the condensation of the order parameter (which is a precursor of crystallization) occurs in reciprocal space on the sphere $|\mathbf{q}|=q_0$. In this case the phase space occupied by fluctuations is large, which leads to a renormalization of the correlation function (Kats *et al.*, 1993a),

$$\langle \phi(\mathbf{q})\phi(-\mathbf{q})\rangle = \frac{k_B T}{\Delta+\alpha(q-q_0)^2}. \tag{31}$$

Here Δ is the so-called gap in the correlation function, which plays the role of controlling parameter for the weak-crystallization transition: the gap is small near the phase-transition point and possesses complex behavior. Self-consistency of the theory requires $\Delta \ll \alpha q_0^2$. The predictions of the weak-crystallization theory differ in many aspects from the dislocation-unbinding concept. For example, the specific heat shows a finite jump and a power-law singularity of the form $C_p(T)=a+b/\Delta^{3/2}$, where a and b can be considered as constant near T_m. Furthermore the shear modulus is proportional to Δ. Finally there is no definite maximum value for the exponent η of the power-law singularity in the structure factor.

Using the weak-crystallization approach, we can estimate the elastic energy of a dislocation pair in a two-dimensional crystal as

$$\frac{E_d}{k_B T} \simeq q_0 \sqrt{\frac{\alpha}{\Delta}} \ln\left(\frac{R}{a_c}\right), \tag{32}$$

which is much larger than unity. Thus dislocation pairs remain bounded and the BKT mechanism does not work. Schematically one can draw the phase diagram of the system in two dimensions as shown in Fig. 6(a) (Kats and Lajzerowicz, 1996). Along OA there is a first-order weak-crystallization transition, while at OB and OC we find continuous transitions that may be driven by a defect-unbinding mechanism. O is the so-called bicritical point. The BKT theory does not work at OA, while the mechanism of weak crystallization is inefficient at OC and OB, since due to the hexatic ordering the order parameter softens not at a circle but only near six points in reciprocal space.

4. Smectic-hexatic phases

The ordering field of the Sm-A–Sm-B transition is a two-component bond-orientational order parameter. This places this transition in the XY universality class and allows it to be continuous in three dimensions. However the Sm-A–Sm-B transition is strongly influenced by fluctuations, since the energy of the fluctuations does not depend on the orientation of $\mathbf{q}$ and the phase space occupied by the fluctuations is large. As a result, fluctuations can cause the transition to be first order, even in the absence of a cubic term in the free-energy expansion (Brazovskii, 1975). The Sm-A–Cr-B transition in three dimensions is always first-order due to long-range positional order and the presence of a cubic term in the free-energy expansion. The same cubic term is present for a Sm-B–Cr-B transition and gives rise to a first-order transition in three dimensions. These two first-order lines meet at a triple point with different slopes, since the coupling between Ψ_6 and $\rho_{\mathbf{k}}$ ($\sim \rho_{\mathbf{k}}^2 \Psi_6$) shifts the transition Sm-B–Cr-B relative to the continuation of the Sm-A–Cr-B line [see Fig. 6(b)]. This discontinuity in the slope at the triple point causes the Sm-A–Sm-B transition to become first order in its vicinity (Aharony *et al.*, 1986). As in the nematic–Sm-A transition (de Gennes and Prost, 1993), this introduces a tricritical point on the Sm-A–Sm-B line [see Fig. 6(b)].

Two- and three-dimensional hexatic behavior in smectic membranes of finite thickness can be distinguished by the scaling behavior of the higher harmonics of the bond-orientational order parameter C_{6n} defined in Eq. (24). In agreement with the experiments mentioned in Sec. II.B, the scaling argument predicts that the coefficients C_{6n} behave as $C_{6n}=C_6^{\sigma_n}$ with $\sigma_n=n+\lambda n(n-1)$, where $\lambda=0.3$ in the three-dimensional case and $\lambda \simeq 1$ in two dimensions (Aharony *et al.*, 1986; Aharony and Kardar, 1988; Paczuski and Kardar, 1988).

For the tilted hexatic phases (Sm-I and Sm-F), the ordering field associated with the tilt corresponds to the two-component order parameter $\Phi=\theta \exp(\iota\varphi)$, where θ is a tilt magnitude and φ is the azimuthal angle of the director. As both the bond angle θ_6 and the azimuthal angle φ break the in-plane symmetry, the model Hamiltonian describing the tilted hexatic phase contains a sixfold periodic coupling term: $-h\cos(6\theta_6-6\varphi)$ (Nelson and Halperin, 1980; Bruinsma and Nelson, 1981). Hence the hexatic phase transition occurs in the presence of an ordering (tilt) field, and the coupling induces a finite hexatic order in a Sm-C phase, unless the coupling constant h is negligibly small. Thus the Sm-C phase is not a thermodynamically distinct phase. It differs from the tilted hexatic phase only by the strength of the bond-orientational order. This situation is similar to, for example, the paramagnetic-ferromagnetic transition in the presence of a small magnetic field. The twofold symmetry of the tilt field also breaks the sixfold symmetry of the hexatic axes, but this effect is rather weak (Brock *et al.*, 1989). The various two- and three-dimensional melting transitions are summarized in Table II.

Still another mechanism can modify the hexatic ordering in smectic membranes and, more generally, affect the whole melting (crystallization) scenario. The crucial point is that the hexatic ordering takes place in a system of strongly fluctuating layers. Nelson and Peliti (1987)

TABLE II. Summary of order-parameter correlations in the various phases at large distances. Abbreviations are the same as in Table I.

		Hexatic ($T_m<T<T_i$)		Crystal ($T<T_m$)	
Correlations	Liquid ($T>T_i$)	2D	3D	2D	3D
$G(r)$	$\sim\exp(-r/\xi)$	$\sim\exp(-r/\xi)$		$\sim r^{-\eta}$	constant
Positions	SRO	SRO		QLRO	LRO
$G_6(r)$	$\sim\exp(-r/\xi)$	$\sim r^{-\eta_6}$	constant	constant	
Bond orientations	SRO	QLRO	LRO	LRO	

showed that the Hamiltonian of a single curved hexatic membrane must involve the covariant derivative of the bond-angle field $\theta_6(\mathbf{r}_\perp)$ to account for the frustration due to the membrane curvature. This approach was generalized by Selinger (1988) for stacked hexatic layers with layer fluctuations described by the displacement field $u(\mathbf{r}_\perp)$. The corresponding elastic Hamiltonian includes a coupling term between hexatic order and layer fluctuations that may turn the Sm-A–Sm-B transition first order. This is similar to the coupling between the smectic order parameter and the nematic director fluctuations that drive the Sm-A–N transition to be weakly first order (Halperin *et al.*, 1974).

The effects of the coupling of the bond-angle and smectic layer curvature were later considered in a somewhat different way. Using the disclination-unbinding theory of Nelson and Halperin (1979), Hołyst (1992) has shown that out-of-plane layer fluctuations decrease the disclination core energy and thus decrease the transition temperature. Consequently, due to the layer fluctuation profile over the film, the disclination core energy changes accordingly. If the fluctuations are quenched at the surface its value is larger at the surface than in the bulk. Therefore the Sm-A–Sm-B transition temperature will also be larger at the surface than in the interior of the film. This situation applies if the ratio of hydrodynamic parameters determining the layer fluctuation profile fulfills $\gamma>\sqrt{KB}$ (see Sec. IV.B.1). For typical values of the smectic elastic constants and the hexatic stiffness modulus K_A, the temperature difference between the hexatic transitions in the first and second layers is a few degrees; between the second and third layers it is an order of magnitude smaller. This corresponds to the order of magnitude found experimentally in certain cases (see Sec. III.B.3). This analysis indicates that the quenching of the smectic layer fluctuations at the surface provides a mechanism for surface ordering.

5. Surface-induced ordering

In liquid crystals a free surface usually stabilizes a higher-ordered phase. Naively one would expect a free surface to be more disordered than the bulk material, due to the breaking of molecular binding at the interface (the "missing neighbor" effect). However, microscopic interactions close to the surface may be quite different from those deeper in the bulk. As a result, the surface may order before the bulk, or may even exhibit ordering phenomena of a different type than in the bulk material. Examples can be found in many liquid crystals. At temperatures somewhat above a nematic–Sm-A transition, smectic layers are usually formed at a free surface (Als-Nielsen *et al.*, 1982; Gramsbergen *et al.*, 1986; Pershan *et al.*, 1987). Approaching the Sm-A phase from above in the isotropic phase, either a finite number of successive layering transitions is observed (Ocko *et al.*, 1986) or a continuous growth of the surface Sm-A phase occurs (Lucht and Bahr, 1997b; Lucht *et al.*, 2001). In the case of a Sm-A–Sm-C transition a free surface usually induces a tilt, causing the Sm-C phase to grow continuously from the surface into the Sm-A interior of the film as the bulk transition temperature is approached from above (Heinekamp *et al.*, 1984; Amador and Pershan, 1990; Bahr *et al.*, 1996).

Two effects can be distinguished when discussing surfaces of smectic membranes. The first one is purely geometrical and reflects the breaking of the translational and rotational invariance of the medium at an interface. As a consequence, near the surface the thermodynamic averages of local order parameters will be different from their bulk values. In the case of relatively thin smectic films the influence of the long-range van der Waals forces can be important too. Second, the conjunction of "missing neighbor" effects with the anisotropy of the liquid-crystal intermolecular forces leads to an effective surface field, which can induce surface ordering (Thurtell *et al.*, 1985; Tjipto-Margo *et al.*, 1989). The surface interactions can either suppress or enhance the bulk ordering. Alternatively the surface can experience an intrinsic critical behavior. In the absence of a microscopic theory of surface ordering in smectic films, surface transitions can be treated phenomenologically by a Landau theory. This type of theory has proved its feasibility in applications to magnetic systems, metal alloys, superconductors, and several other systems (Binder, 1986). In this approach the free energy contains a bulk contribution of the order parameter $m(\mathbf{r})$ up to some essential power, together with a gradient term $\frac{1}{2}C[\nabla m(\mathbf{r})]^2$ and surface contributions $-H_s m(\mathbf{r})$ and $[C/(2\lambda_{ex})]m^2(\mathbf{r})$. Here H_s is the surface field acting on the order parameter in the surface planes only, and λ_{ex} is the so-called extrapolation length, which was originally introduced in the context of superconductivity (de Gennes, 1966). The ratio C/λ_{ex} determines the energy scale for the surface contribution to the free energy. In the case of a negative

surface energy (i.e., $\lambda_{ex}<0$), the surface enhances the ordering. For a smectic membrane the free energy is integrated over the thickness L and the surface free-energy contribution is determined by the boundary value at $m_s=m(z=0;\ z=L)$. For $T>T_c$, where T_c is the bulk transition temperature, and a small enough surface field, nonharmonic terms in $m(\mathbf{r})$ can be neglected. Minimization of the free energy leads to an order-parameter profile of a rather simple form,

$$m(z)=m_s\frac{\cosh[(2z-L)/2\xi_b]}{\cosh(L/2\xi_b)}, \tag{33}$$

where ξ_b is the bulk correlation length, and

$$m_s=\frac{H_s\lambda_{ex}/C}{1+(\lambda_{ex}/\xi_b)\tanh(L/2\xi_b)}. \tag{34}$$

A surface transition occurs at a temperature $T_{cs}>T_c$ given by $T_{cs}/T_c=1+(C/T_c)\lambda_{ex}^{-2}$. In the temperature interval $T_{cs}>T>T_c$ the interior of the film is disordered. The surface-induced order occurs only near the interfaces and penetrates exponentially into the interior to a depth determined by $\xi_b<L$. For sufficiently thin membranes the exponential decay from both interfaces will overlap, giving a nonzero value of the order parameter in the middle of the film. At $T=T_c$ one finds a nonexponential decay of the ordering induced by the surface field. For $T<T_c$ the bulk order parameter retains a nonzero value m_b. In this case the order parameter decays exponentially from the value m_s at the surface to the value m_b in the bulk.

The Landau approach can successfully describe surface ordering that penetrates continuously into the interior. When the order parameter refers to smectic layering—the de Gennes (1990) theory of presmectic ordering—these results have been applied to smectic membranes to explain thinning transitions (see Sec. VI.A). Another relevant example is found above the Sm-A–Sm-C transition. In that case the order parameter is the tilt-angle magnitude θ. Tilt-angle profiles have been determined using ellipsometry (Bahr and Fliegner, 1993), optically (Andreeva *et al.*, 1999), and using x-ray reflectivity (Tweet *et al.*, 1990; Fera, Opitiz, *et al.*, 2001), and fit well to Eqs. (33) and (34). A similar approach has been used to describe the dependence of the Sm-A–Sm-C transition temperature on the film thickness (Heinekamp *et al.*, 1984). However, the Landau theory presented cannot describe the situation when the surface ordering develops via a series of successive layering transitions. Such a scenario is quite common for transitions in smectic membranes involving hexatic and crystalline phases.

An alternative description of surface ordering takes the range of interactions between the molecules into account. The surface ordering is predicted to have universal critical behavior, which depends only on this range and on the roughness of the interface between the surface-ordered region and the interior (Dietrich, 1988; Schick, 1990). If the dominant interactions are due to the long-range van der Waals forces, the thickness L of the ordered surface domain is predicted to grow according to a power law $L\sim t^{-1/3}$, in which $t=|T-T_c|/T_c$ is the reduced temperature. For systems dominated by short-range exponential interactions, the predicted divergence is logarithmic, $L\sim\ln(1/t)$. If the interface between the surface phase and the interior is smooth, the growth of the ordered surface region is predicted to occur in a layer-by-layer sequence. For rough interfaces the power-law or logarithmic growth is predicted to proceed continuously into the interior.

Surface ordering in liquid crystals can also be considered as a special case of interfacial wetting (Swanson *et al.*, 1989; Lucht and Bahr, 1997b). It occurs when a more-ordered surface phase wets the less-ordered interior phase-vapor interface. A surface-ordering scenario thus follows the corresponding wetting behavior, which includes nonwetting, incomplete wetting, and complete wetting. Crystallization transitions in smectic membranes usually fall in the nonwetting category: the entire interior of the film crystallizes abruptly. However, in several cases smectic membranes exhibit incomplete wetting. In that case two or more surface layers order above the bulk transition, and the thickness of the ordered surface domain remains finite until the rest of the film interior orders abruptly at the bulk transition temperature. In the case of a second-order transition the thickness of the ordered surface domain cannot stay finite at the bulk transition temperature and the complete wetting scenario is realized. In this case the growth of the ordered surface area is determined by the growth of the bulk correlation length, which diverges at the second-order transition. From the Landau theory of wetting (Schick, 1990) one can expect either a continuous or a layer-by-layer type of ordering.

B. Experimental studies of in-plane ordering

In this section we restrict ourselves to transitions in smectic membranes involving hexatic and crystal phases. The theoretical predictions for phase transitions in two dimensions have strongly inspired experimental studies in this field. In two dimensions for sufficiently thin films the large-scale thermally excited positional fluctuations tend to destabilize the more ordered phases. In contrast, surface-enhanced ordering competes with the effects of reduced dimensionality. As a result a rich variation of smectic phase diagrams appear, depending on temperature, composition, and membrane thickness. Examples include surface freezing, accompanied by either a continuous layer-by-layer development of hexatic or crystalline order, or by abrupt crystallization of the remaining part of the film. Additionally, the director of the surface layers of a membrane in an orthogonal smectic phase may be tilted. A common characteristic of all these cases is the simultaneous presence of at least two distinct phases, one at the surface and one in the interior of the film.

1. Hexatic and crystalline ordering

X-ray diffraction of a number of bulk liquid-crystal materials by Leadbetter *et al.* (1979) indicated as early

as 1979 the existence of different types of Sm-B phases. However, it was not until 1981 that Pindak *et al.* (1981) identified in the compound 65OBC the hexatic Sm-B phase from its characteristic diffraction pattern of six diffuse arcs. Subsequent transmission electron diffraction (Cheng *et al.*, 1988) allowed the bond-orientational order parameter C_{6n} to be determined. Heat-capacity studies (Huang *et al.*, 1981) of the Sm-A–Sm-B transition in 65OBC indicated the transition to be continuous with a divergent nearly symmetric peak. Such behavior implies large hexatic fluctuations that couple to density fluctuations, causing the sixfold symmetric x-ray scattering to become singular at $T=T_i$ (Aeppli and Bruinsma, 1984). This critical behavior in the x-ray structure factor has also been observed at the same transition in a similar compound, 46OBC (Davey *et al.*, 1984). The position and width of the diffuse x-ray peaks exhibit $(T-T_i)^{1-\alpha}$ singularities in the vicinity of T_i in agreement with the heat-capacity results (Pitchford *et al.*, 1985). Here $\alpha \simeq 0.5$ is the critical exponent for the specific heat C_p. Measurements on two-layer films of 46OBC show a continuous two-dimensional Sm-A–Sm-B transition, even though the corresponding transition in the bulk (three dimensional) was found to be weakly first order. The phase behaviors of 65OBC and 46OBC have much in common. However, they differ in one essential point: mechanical measurements of 65OBC provide evidence for freezing of the surface layers in the film well above the bulk transition to the crystalline phase, later identified as a Cr-E phase. In contrast to 65OBC, in 46OBC no indications of a crystalline surface-ordering transition were found. However, in thin films the range of stability of the hexatic phase is considerably enhanced. These early measurements clearly indicate that in thin membranes surface-enhanced ordering can drastically modify the phase sequences and their range of stability.

Beginning in the late 1970s the tilted Sm-I and Sm-F phases were extensively studied by x-ray diffraction in bulk (Benattar *et al.*, 1979; Diele *et al.*, 1980; Gane *et al.*, 1981). These phases can be considered as the tilted analogs of the orthogonal hexatic Sm-B phase (see Table I). The hexatic nature of the Sm-I phase was unambiguously demonstrated by x-ray diffraction on magnetically oriented samples (Brock *et al.*, 1986). The diffraction pattern exhibited the characteristic sixfold arrangement of diffuse arcs, from which the higher-order harmonics of the hexatic order parameter C_{6n} $(n=1-7)$ were calculated. From measurements in Sm-I films of variable thickness a crossover from three- to two-dimensional behavior could be established (Brock *et al.*, 1989). Additionally, in the limit of thin films, the "disappearance" of the higher harmonics of the hexatic order parameter, predicted by harmonic scaling theory, was observed. Similar results were obtained for orthogonal hexatic Sm-B films. For one-layer (Chou, Ho, and Hui, 1997) and two-layer (Chou *et al.*, 1996) membranes of 54COOBC and for a two-layer film of a hexatic mixture on the basis of 65OBC (Cheng *et al.*, 1988), transmission electron diffraction yields $C_{6n}=C_6^{n^2}$ in agreement with the predictions of scaling theory of the two-dimensional XY model (Aharony and Kardar, 1988; Paczuski and Kardar, 1988). These results imply that two-layer films indeed approach the two-dimensional limit.

Pioneering ac heat-capacity experiments have been performed by Huang and co-workers on various compounds exhibiting an intermediate hexatic phase. The results show that upon crystallization most of the entropy is released by the system as it cools through the liquid-hexatic phase transition, rather than at the lower temperature hexatic-crystal transition (Stoebe and Huang, 1995). This corresponds to a heat-capacity anomaly showing divergent behavior at the upper transition. Fits to a power-law singularity typically give a heat-capacity critical exponent $\alpha \simeq 0.3-0.6$. These calorimetric observations are very different from the predictions of defect-mediated theory, which indicate a broad bump at the high-temperature side of the transition. This discrepancy remains unresolved.

The three-dimensional orthogonal Cr-B phase with true long-range positional order was first identified in membranes of the compound 4O.8 (Moncton and Pindak, 1979). This interpretation was confirmed by the solidlike shear response of a low-frequency torsional oscillator in contact with the film (Pindak *et al.*, 1980; Tarczon and Miyano, 1981). These crystalline films are in the two-dimensional limit characterized by an algebraic decay of the positional order that leads to a power-law singularity in the structure factor [see Eq. (27)]. For this power-law line-shape behavior of the diffuse scattering, an exponent $\eta_{\rm cr} \simeq 0.13$ was determined for a two-layer Cr-B film of the compound 14S5 (Moncton *et al.*, 1982). Further experiments using the compound 8OSI in the Cr-J phase (Noh *et al.*, 1991) have been performed on films from about 1000 to 5 layers at two degrees below the transition to the hexatic Sm-I phase. This transition was found to be abrupt, suggesting first-order character in agreement with earlier studies (Brock *et al.*, 1989). Analysis of the scattering profiles (see Fig. 7) provides evidence of a dimensional crossover: the thinnest film (five layers) shows an effective two-dimensional power-law exponent $\eta_{\rm eff} \simeq 0.18$. With an increasing number of layers the in-plane line shape changes from $(q-q_{\perp 0})^{-2+\eta_{\rm eff}}$ to $(q-q_{\perp 0})^{-2}$. The value of $\eta_{\rm eff}$ approaching zero indicates a crossover from two- to three-dimensional long-range positional order. The measured exponents are within the limit $\eta_{\rm cr} < \eta_{\rm max} = 1/3$, predicted by the dislocation-unbinding theory for a two-dimensional hexagonal crystal (see Sec. III.A.2). However, the two-dimensional limit corresponding to a two-layer film was not reached.

The above results can be compared with the power-law behavior of the structure factor in other two-dimensional molecular crystalline systems. Data are available for crystalline alcohol monolayers on the surface of water (Zakri *et al.*, 1997) and for crystalline monolayers of Xe (Heiney *et al.*, 1983) and Ar (Nielsen *et al.*, 1987) adsorbed on graphite. Interestingly, in both cases the exponent varies from $\eta \simeq 0.3$ deep in the crystal phase up to about 0.4–0.6 at T_m, which is beyond the

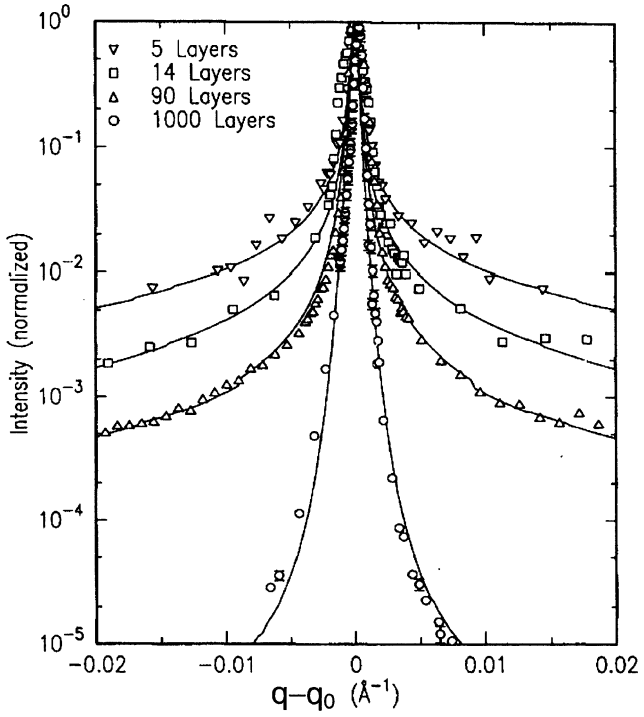

FIG. 7. In-plane scans for 8OSI membranes of various thicknesses in the Cr-B phase. From Noh *et al.*, 1991.

limit $\eta_{\max}=1/3$. The large values might be due to the high nucleation energy of dislocation pairs, making the dislocation-mediated melting scenario irrelevant (Kats and Lajzerowicz, 1996). The exponent $\eta_{\rm cr}$ can also be larger than $\eta_{\max}$ if in addition to the long-wavelength thermal phonons other sources of positional disorder are present. An example is provided by thermal elastic excitations driven by a distortion of the unit cell from hexagonal to rectangular (so-called herringbone distortions), which have been observed for Langmuir monolayers of octadecanol (Kaganer, Brezesinski, *et al.*, 1999). More recently power-law behavior has been observed for the scattering profiles of stacks of two-dimensional crystalline arrays of the membrane protein bacteriorhodopsin (Koltover *et al.*, 1999). The exponent η_{cr} was found to increase as a function of temperature and to approach $\eta_{cr}\simeq 0.15$ at T_m. The melting of the crystalline membrane occurs by a first-order transition, which is manifested by a large hysteresis in the spacing of the two-dimensional protein lattice.

2. Thickness dependence of phase diagrams

Drastic changes can be observed in the phase diagrams of liquid crystals when the film thickness is decreased. We shall discuss this topic by treating in some detail the compound 7O.7. For further examples we refer the reader to Pershan (1988). In the bulk 7O.7 does not possess a hexatic phase, but in films a rich variety of hexatic behavior is found (Collett *et al.*, 1985; Sirota *et al.*, 1987b). The bulk phase sequence in 7O.7 is on cooling: isotropic–N–Sm-A–Sm-C–Cr-B–Cr-G. With decreasing film thickness, first restacking transitions occur in the Cr-B phase. In films thinner than about 175 layers a tilted hexatic Sm-F phase appears between the Cr-B and Cr-G phases. The Sm-F phase transforms at higher temperatures to the Sm-I phase in films thinner than about 25 layers. All the stacking modifications of the orthogonal Cr-B phase vanish completely below this thickness. Pershan and co-workers (Sirota *et al.*, 1987a; Amador *et al.*, 1989) studied thin 7O.7 membranes and found below six layers two distinct Sm-C–Sm-I transitions. Upon cooling from Sm-C the first Sm-I top layers occur while the interior layers remain Sm-C, and only about eight degrees lower the film changes fully to Sm-I. In the intermediate temperature range the scattering consists of a coexisting broad liquidlike peak from the interior Sm-C phases and a sharper peak due to the positionally more correlated Sm-I top layers. Electron diffraction of films of eight layers and less confirm this coexistence (Chao *et al.*, 1997). Thicker films up to 25 layers reveal a pair of short bright arcs and a pair of longer arcs in the presence of a uniform diffuse ring. The latter is indicative of a Sm-A interior, while the twofold symmetry of the short and long arcs indicates the presence of both Sm-I and Sm-C ordering. Thus 7O.7 films in the thickness range between eight and 25 layers show, as a function of distance from the surface, three coexisting phases: an outermost hexatic Sm-I layer, several Sm-C-like layers, and a Sm-A interior.

At first sight the suppression of the Cr-B phase in thin 7O.7 films might be considered as the expected destabilization of a more ordered phase by the reduced dimensionality of the system. However, the presence of tilted surface layers gives a hint that more probably surface interactions stabilize the tilted structures. The latter effect would, however, not be restricted to thin films only. Moreover, in other compounds of the same series (for example, 4O.8) surface interactions stabilize the orthogonal Cr-B phase, which survives even in two-layer films (Chou, Jin, *et al.*, 1997). In the compound 5O.6 a hexatic Sm-F phase appears at temperatures below the Cr-B phase even in bulk samples. This all points to the possibility that the Cr-B phase in 7O.7 is intrinsically unstable with respect to tilted hexatic phases and that a relatively small decrease in the dimensionality of the sample is sufficient to drive a transition from Cr-B to Sm-F or Sm-I.

In certain cases the effects of reduced dimensionality and enhanced surface ordering can be separated. For example, the Sm-A–Sm-B transition temperatures of the interior layers in membranes of the compound 75OBC show nonmonotonic dependence on the film thickness, as indicated by specific-heat measurements (Geer *et al.*, 1992). For membranes between about 70 and 15 layers, a small decrease of the transition temperatures occurs as anticipated from the reduced dimensionality. However, for films with fewer than 15 layers, surface ordering leads to a pronounced increase in the transition temperatures. This observation confirms the general trend in smectic membranes that the effect of surface interactions on the phase stability dominates in the limit of thin films.

3. Surface-ordering effects

The development of hexatic and/or crystalline order in smectic membranes of various thicknesses upon cooling from the Sm-A phase has been well documented by combining information from x-ray scattering, electron diffraction, optical reflectivity, and heat-capacity measurements. To demonstrate the essential physics we shall concentrate on surface transitions involving orthogonal hexatic (crystalline) phases. This can be illustrated by the phase behavior of the compounds 3(10)OBC and 7SOBC. Upon cooling 3(10)OBC membranes from the Sm-A phase, hexatic order is first established at the outermost layers and then proceeds into the film in a layer-by-layer fashion for at least four outer layers (Stoebe *et al.*, 1992). Even three- and four-layer films show two well-separated transitions, corresponding to transformations to hexatic ordering in the top layers and in the interior layers, respectively. This suggests very weak interlayer coupling. Two-layer membranes possess two-dimensional behavior. Precise calorimetry measurements indicate that the Sm-A–Sm-B transitions in the nm-OBC series are continuous, both in bulk and in thin membranes (Stoebe and Huang, 1995). A similar layer-by-layer development of surface hexatic order has been detected for the Sm-A–Sm-B transition in the compound 54COOBC (Jin *et al.*, 1996) and for the Sm-A–Sm-I transition in 9O.4 (Swanson *et al.*, 1989). The sequence of transition temperatures corresponding to layer-by-layer penetration of the surface hexatic order into the film interior can be described by the power law

$$L = L_0 \left[\frac{T_c(L) - T_c}{T_c} \right]^{-\nu}, \tag{35}$$

with an exponent $\nu \simeq 1/3$. Now L is the thickness of the surface-ordered domain, determined by a number of hexatic layer steps, and $T_c(L)$ is the liquid-hexatic transition temperature corresponding to the last layer in question (Swanson *et al.*, 1989; Stoebe *et al.*, 1992; Jin *et al.*, 1996). The value of the critical exponent $\nu \simeq 1/3$ indicates that simple van der Waals forces are responsible for the interlayer angular interactions.

The layer-by-layer ordering at the Sm-A–Sm-B transition in thin films of 7SOBC (Geer *et al.*, 1993) is accompanied by additional distinct surface transitions of Sm-B to Cr-E. The Sm-B–Cr-E transition in surface layers occurs very close to the Sm-A–Sm-B transition in the interior layers. This surface transition is first order and shows a pronounced thermal hysteresis. This allows us to study the continuous Sm-A–Sm-B transition in the film interior with and without Cr-E surface layers, by carrying out the measurements during heating or cooling, respectively. The presence of Cr-E surface layers strongly reduces the height of the interior Sm-A–Sm-B heat-capacity peak (Geer *et al.*, 1993). In films of fewer than nine layers it is completely suppressed. A possible explanation is that the surface crystal layers modify the in-plane structure of the neighboring Sm-A layers in such a way that the hexatic fluctuations (the main source of entropy at the Sm-A–Sm-B transition) are suppressed. Electron diffraction indicates that the Cr-E surface layers in 7SOBC exist in twin domains in which the orientation of the rectangular lattice is rotated by 2°–3° with respect to the underlying Sm-B bond-orientational axes (Cheng *et al.*, 1991). Such a rotation possibly releases the strain caused by the two incommensurate types of structures: the hexagonal hexatic "substrate" and the rectangular overlayer, and can be considered a special case of orientational epitaxy.

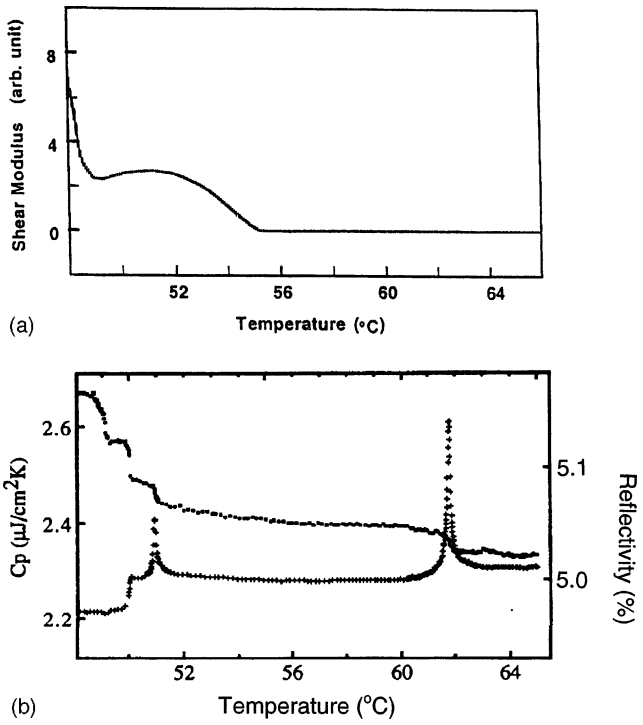

FIG. 8. Evidence for surface layer transitions in an eight-layer 4O.8 membrane: (a) shear response, after Pindak *et al.* (1980) and Tarczon and Miyano (1981); (b) heat capacity-(crosses) and optical reflectivity (solid squares) (Jin *et al.*, 1994).

The compound 4O.8 has long been considered a prototypical liquid-crystal material which possesses in the bulk a direct first-order transition from the Sm-A to the Cr-B phase at 48.5 °C (Moncton and Pindak, 1979; Pershan *et al.*, 1981). However, early mechanical measurements with a low-frequency torsional oscillator in contact with the film indicated two anomalies in the shear response: at the bulk Sm-A–Cr-B transition and about 6 °C above this temperature [Pindak *et al.*, 1980; Tarczon and Miyano, 1981; see Fig. 8(a)]. Later Jin *et al.* (1994) detected via heat-capacity and optical reflectivity measurements, a whole cascade of phase transitions, attributed to step-by-step surface crystallization [see Fig. 8(b)]. Subsequently transmission electron diffraction (Chao *et al.*, 1996) provided evidence of a novel crystallization scenario: the Cr-B phase proceeds into the Sm-A phase in a layer-by-layer fashion involving an intermediate hexatic Sm-B phase, which does not exist in the bulk.

Upon cooling 4O.8 membranes of six layers or more from the Sm-A phase, one finds the typical sequence of diffraction patterns shown in Fig. 9 (Chao *et al.*, 1996).

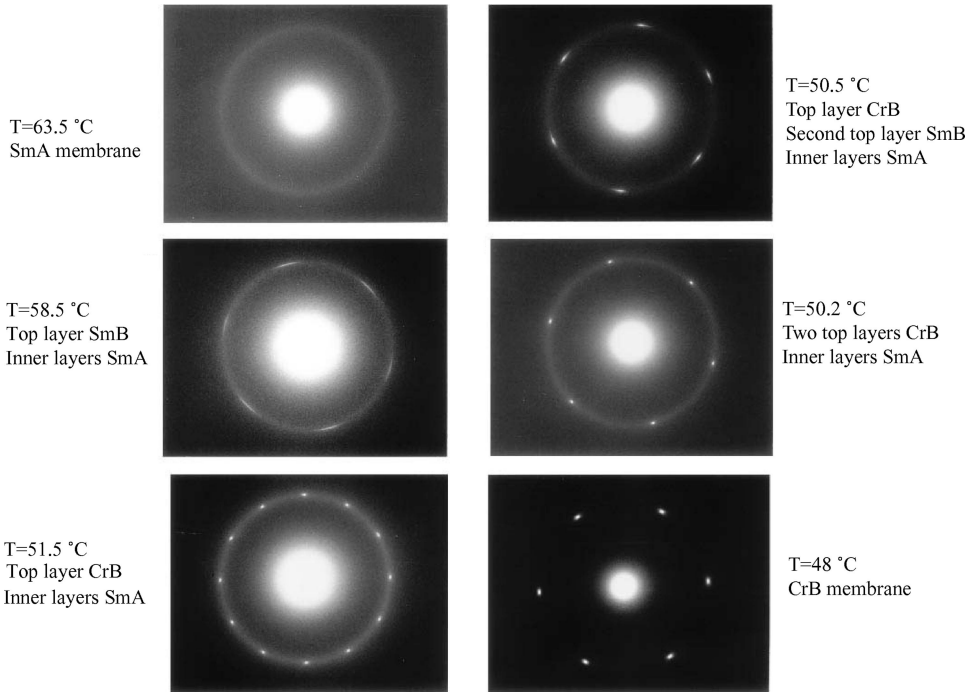

FIG. 9. Electron diffraction pattern of a ten-layer 4O.8 membrane (Chao *et al.*, 1996).

Above 62 °C the film is in the Sm-A phase and shows a diffuse ring. At about 62°C the surface layers undergo a transition to the Sm-B phase, while the interior layers remain in the Sm-A phase (six diffuse arcs on top of a diffuse ring). Interestingly, the directions of the hexatic axes in the top layers at both sides of the film appear to be correlated, though there are liquid Sm-A layers in between them. At about 55 °C the top layers freeze into the Cr-B phase and we note two sets of sixfold spots on top of a diffuse ring. The presence of two sets of Bragg spots with equal intensity but arbitrary relative orientation implies that the orientations of the crystalline axes in the top and bottom surface layers are not fully correlated. At about 51 °C the second set of exterior layers transforms into the Sm-B phase. The 12 diffraction spots have now collapsed into six, which suggests that the sub-top Sm-B layers serve to lock in the crystalline axes of the top and bottom surface layers. In addition we still observe six diffuse arcs from the Sm-B sub-top layers and a diffuse ring from the liquid interior. At 50.4 °C the second exterior layers also freeze into the Cr-B phase and we are left with six spots on top of a diffuse ring. This interpretation is confirmed by the fact that the integrated intensity of the diffraction spots now is about twice that of the crystalline pattern at $T>51$ °C. Finally, after additional layer-by-layer transitions, the entire film transforms into the Cr-B phase (six spots only).

The above interpretation fits very well with other measurements on 4O.8 films. First, at $T_i \simeq 62$ °C, the heat capacity shows a distinct phase transition, but there is no shear response [see Fig. 8(b)]. This is consistent with this phase transition's being a surface transition to a hexatic phase, which does not support a shear deformation. The divergent heat-capacity anomaly at the Sm-A–Sm-B transition in the surface layers is consistent with similar observations in other materials (Stoebe and Huang, 1995). Second, at about 55 °C, mechanical measurements detected the onset of a shear response of the film. This is consistent with the observation of a Sm-B–Cr-B transition in the surface layers. No detectable heat-capacity signal was observed at this transition (Jin *et al.*, 1994). The second anomaly observed in heat capacity at about $T=51$ °C corresponds to the Sm-A–Sm-B transition in the second set of exterior layers. Finally, below 49 °C the results are all consistent with the entire film's freezing into the Cr-B phase.

X-ray reflectivity studies of the layer-by-layer crystallization in 4O.8 films reveal clear changes in the layer-displacement fluctuation profile across the film (Fera *et al.*, 1999). The corresponding transition temperatures for an eight-layer film as displayed in Fig. 10(a) are in good agreement with the results from electron-diffraction and specific-heat measurements. The fluctuation profiles presented in Fig. 10(b) indicate in the Sm-A phase quenched fluctuations at the surfaces. Following the first Sm-A–Sm-B and Sm-B–Cr-B transitions in the top layers, a considerable damping of the layer-displacement fluctuations occurs. The new profile provides the basis for the second series of crystallization transitions in the next-nearest top layers. Once two layers are crystallized on each side, the fluctuations of the remaining four Sm-A layers are such that the total profile over the film is approximately flat. In agreement with this behavior the differences in transition temperatures between the "new" Sm-A surface layers and those in the center of the film converge rapidly. In this picture the cascade of successive Sm-A–Sm-B–Cr-B phase transitions is triggered off by the changing fluctuation profile in successive layers.

The fluctuation scenario in 4O.8 also helps us to understand another phenomenon. Electron diffraction of 4O.8 films indicates a coupling of the bond-order direc-

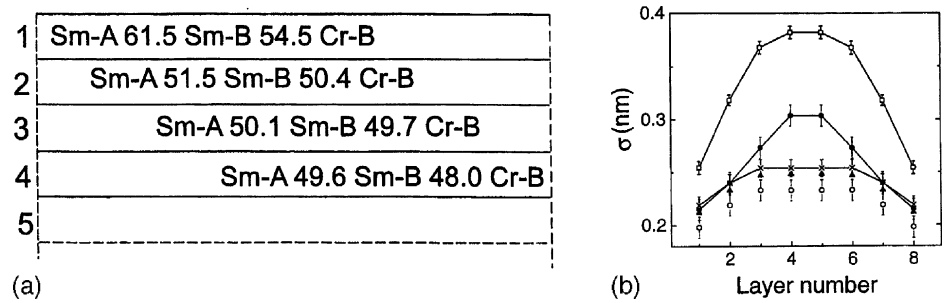

FIG. 10. Layer-by-layer crystallization in an eight-layer 4O.8 membrane (Fera *et al.*, 1999): (a) transition temperatures; the layer number is indicated at the left. (b) Fluctuation profiles: □, Sm-A phase at 62.5 °C; ●, one Cr-B top layer at 52.5 °C; ○, two Cr-B top layers at 50.3 °C; ▲, two Sm-A layers left in the middle at 49.7 °C; ×, Cr-B phase at 47.0 °C.

tions of the top and bottom layers (Chao *et al.*, 1996). This is rather counterintuitive, as the intermediate Sm-A layers still have a liquid in-plane structure. However, earlier x-ray reflectivity studies of smectic membranes (Mol *et al.*, 1997) indicate that for thin films the hydrodynamic fluctuations in the Sm-A phase are fully conformal (see also Sec. IV.C.2). As a consequence, any directional interaction between the fluctuation amplitude and the local hexatic lattice (Hołyst, 1992) will be the same on both sides of the film. Hence conformal fluctuations provide a natural mechanism for correlating the lattice directions in the surface hexatic layers at the top and bottom of a membrane.

The melting in 4O.8 films is unique in the sense that the two-stage melting process occurs successively in one smectic layer after another [Fig. 10(a)]. Such a melting behavior implies that the interaction between neighboring layers is very small. In the limit of a two-layer 4O.8 film, the whole film attains hexatic order and the Sm-B phase is stabilized in a temperature range of about 5 °C between the Sm-A and Cr-B phases (Chou, Jin, *et al.*, 1997). It is evident that the hexatic phase is an important component of the melting process, which supports the two-stage melting scenario predicted by defect-mediated melting theory in two dimensions. Besides the two-layer 4O.8 film mentioned, the surface top layers in thicker membranes may also serve as a model system for studying the liquid-hexatic-crystal sequence in two dimensions. For such studies of surface crystallization in 4O.8, see the next section.

A further interesting example of dimensional crossover by surface-enhanced order was observed in Cr-B films of another compound (14S5), studied by x-ray diffraction (Moncton *et al.*, 1982) and with a low-frequency torsional oscillator (Bishop *et al.*, 1982). In a two-layer film a single hysteretic transition from Cr-B to Sm-A was observed. Films of three layers and more present two first-order transitions: first to films with Cr-B top layers and Sm-A interior layers, and second, about ten degrees higher, to the Sm-A phase. In the three-layer film the single interior layer was originally thought to possess some hexatic type of order. However, later heat-capacity and electron-diffraction measurements rule out such a possibility (Chao *et al.*, 1996, 2001).

Another type of melting behavior associated with the Cr-B phase was observed in films of 54COOBC (Jin *et al.*, 1996). This compound differs from 4O.8 by the presence of an intermediate hexatic Sm-B phase in between Sm-A and Cr-B in the bulk. Similarly to 3(10)OBC and 75OBC, when cooled from Sm-A the hexatic order first appears in the top layers and then proceeds into the film's interior in a layer-by-layer fashion. However, the freezing into Cr-B occurs abruptly through a single first-order transition. The surface hexatic order exhibits a pronounced heat-capacity anomaly which can be seen in films down to two layers. At the same time a heat-capacity step is associated with the onset of the Cr-B order. This can be observed in thick membranes but not in those with fewer than seven layers, similar to the situation in 4O.8. The specific-heat measurements also indicate that the Sm-A–Sm-B transition in the top layers is weakly first order.

Finally we shall touch upon the surface ordering in smectic membranes of tilted phases that may also show multiple surface-freezing transitions. For example, the compound FTE1, studied with electron diffraction by Chao *et al.* (1997), exhibits a unique sequence of melting transitions involving novel hexatic (Sm-L) and crystal (Cr-N) phases (see Table I). First the surface layers undergo a transition to the Sm-I phase, while the interior layers remain in the Sm-C phases. Subsequently the Sm-L surface layers replace the Sm-I layers on top of the Sm-C interior. On further cooling a continuous change in the tilt direction of the Sm-L top layers in the direction of the Sm-F-like structure occurs, and the entire film transforms to the Sm-F phase. Such behavior was predicted theoretically by Selinger and Nelson (1989). Meanwhile, radial scans of the scattered intensity have indicated that the in-plane positional correlation length increases by a factor of 3. On further cooling the outermost layers of the Sm-F film freeze into a crystalline phase, which was identified as Cr-H (see Table I). The diffraction patterns show a single set of diffraction spots from the Cr-H layers, indicating perfect lattice epitaxy between the rectangular Cr-H surface lattice and the hexagonal Sm-F interior. Finally, the entire film changes its tilt direction to the Sm-L symmetry while the outermost layers transform into the Cr-N phase. Now the tilt direction of both the surface Cr-N and interior Sm-L phases are locked in at an intermediate azimuthal angle, which is independent of temperature. Compared to the surface ordering of the orthogonal phases, the

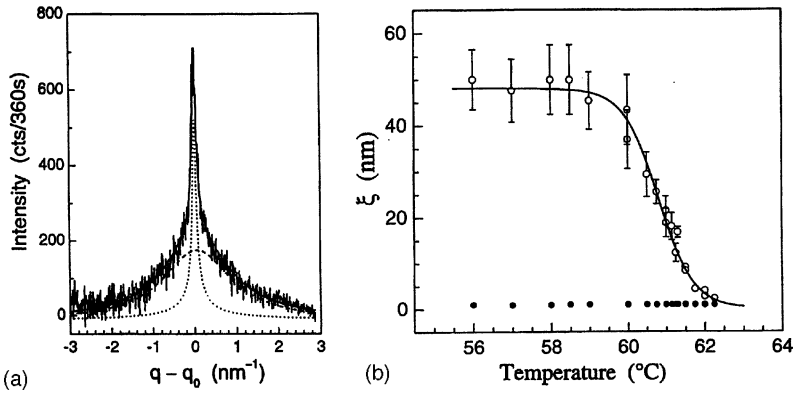

FIG. 11. In-plane ordering of the single hexatic Sm-B top layers in a seven-layer 4O.8 membrane: (a) x-ray scattering profile at 60.0 °C; solid line is a fit to the sum of a Lorentzian and a square-root Lorentzian; (b) temperature dependence of the in-plane positional correlation length; (●), five inner liquid layers; (○), two hexatic top layers.

presence of a molecular tilt clearly introduces further complications leading to multiple-phase behavior.

To finish this section we want to emphasize that the physical origin of the enhanced surface order in smectic membranes is not yet clear. Since many phases of different structures can be stabilized at the free surface, the microscopic details of surface interactions appear to be less important. What do the tilted Sm-C phase (with liquid in-plane order) and the orthogonal hexatic Sm-B phase, have in common that stabilizes them on a free Sm-A surface under appropriate conditions? A possible answer—that applies equally well to orthogonal and tilted phases—might be the quenching of the layer-displacement fluctuations at the Sm-A surface, which according to theoretical arguments (Selinger, 1988; Holyst, 1992) enhances hexatic order.

4. Crystallization of a single top layer

In membranes of the compound 4O.8 the outermost layers undergo separate Sm-A–Sm-B and Sm-B–Cr-B transitions before the second set of layers start their own freezing transitions [see Fig. 10(a)]. Neither positional nor angular (bond-orientational) correlations exist between the surface layers and the interior Sm-A layers that act as a substrate. Hence the top layer at each side of the membrane may serve as a perfect model system for studying crystallization of a liquid in two dimensions. When discussing this situation we disregard the subsequent further crystallization steps in the interior layers. Calorimetric measurements for an eight-layer film indicate that the top layer isotropic-hexatic transition is continuous with a divergent, nearly symmetric, specific-heat anomaly (Jin *et al.*, 1994; Chao *et al.*, 1996). At the Sm-B–Cr-B transition no anomaly was found. These results contradict defect-mediated theory, which predicts in both cases a broad bump on the high-temperature side of the transition, which results from the increased density of unbound defects.

de Jeu *et al.* (2003) performed grazing-incidence x-ray diffraction on the top layers of 4O.8 membranes with a thickness of 7 and 43 layers. The angle of incidence and the exit angle were symmetrically set at 0.6°. As this value is well above the critical angle of total reflection, the refracted wave penetrated through the whole film, and the in-plane structure of all layers was measured. Figure 11(a) shows for the seven-layer film the diffraction peak at $q_{\perp 0} \simeq 14.3\ \mathrm{nm}^{-1}$, corresponding to local in-plane hexagonal packing with $a = 4\pi q_{\perp 0}/\sqrt{3} \simeq 0.51$ nm. It consists of a relatively narrow diffraction peak originating from the outermost hexatic Sm-B layers fitted by a square-root Lorentzian on top of a broad Lorentzian liquid peak from the five Sm-A interior layers. The integrated intensity I_{surf} of the former part is essentially independent of the membrane thickness, which proves its origin in the two surface layers. In contrast, the I_{int} of the latter part scales linearly with the number of liquid interior layers. This leads to a constraint on $I_{\mathrm{int}}/I_{\mathrm{surf}}$, which equals 2.5 and 21.5 for the 7-layer and 43-layer membranes, respectively.

After deconvolution from the instrumental resolution, the fitting yields the temperature dependence of $\xi = k^{-1}$ shown in Fig. 11(b). The Lorentzian width of the interior Sm-A layers is independent of the temperature and corresponds to in-plane positional correlations of about 1 nm. Indeed any interaction between the freezing outermost layers and the liquid interior layers must be very small. With decreasing temperature the positional correlation length ξ of the hexatic top layers increases between 62.5 and 60 °C continuously from about 2.5 nm to more than 40 nm, and then saturates. Clearly a pretransitional growth of ξ is present above the hexatic-isotropic transition at $T_i = 61.5$ °C. This behavior implies large hexatic fluctuations that couple to the density fluctuations, causing the x-ray scattering to become singular at T_i (Aeppli and Bruinsma, 1984). Such critical behavior in the x-ray structure factor has also been observed in membranes of the compounds 65OBC (Pindak *et al.*, 1981) and 46OBC (Davey *et al.*, 1984), which exhibit a Sm-A–Sm-B transition through the whole film. We have not observed any thermal hysteresis in the hexatic linewidth, which indicates that the hexatic-isotropic transition in a 4O.8 surface layer is second order. These results are in agreement with the heat-capacity measurements in an eight-layer 4O.8 film. We conclude that the grazing-incidence x-ray-diffraction results for the isotropic-hexatic transition in a 4O.8 top layer are in qualitative agreement with the BKT theory.

Chao *et al.* (2000) performed transmission electron-diffraction studies of 4O.8 membranes between 3 and 12 layers. They report somewhat surprisingly an intermediate "phase" between isotropic and hexatic Sm-B, associ-

ated with the absence of a modulated ring of scattering between 62 and 59 °C. We speculate that this observation is due to the occurrence of multiple hexatic domains of random orientations over the area probed, whose size becomes larger with decreasing temperature. The enhanced two-dimensional hexatic bond-angle fluctuations also introduce a line broadening in the direction along the arc in the vicinity of T_i (see Sec. II.B.2).

Upon cooling the seven-layer 4O.8 membrane further, one observes at 55.5 °C another surface transition in the top layers. In the x-ray diffraction this is signaled by condensation of the diffuse hexatic peak into the sharp, resolution-limited peak of the Cr-B phase. Simultaneously, the rather uniform in-plane mosaic of the Sm-B phase becomes discrete. The well-defined order in the orientation of the lattice sites is revealed by narrow peaks with a mosaicity of about 1° (FWHM) as measured in χ scans. No thermal hysteresis was observed at the hexatic-crystal transition in a surface top layer. The evolution of the hexatic linewidth above the Sm-B–Cr-B transition indicates no pretransitional growth within the resolved temperature accuracy $\lesssim 0.05$ °C. This suggests that the hexatic-crystal transition in a 4O.8 top layer is abrupt and belongs to the class of weakly first-order transitions.

C. Conclusions and outlook

Experimentally it is clear that smectic liquid crystals provide definite examples of hexatic phases with bond-orientational order. The hexatic phase can be fully described on the basis of symmetry considerations, which does not imply any specific melting mechanism. In spite of extensive experimental work there is no conclusive evidence for the dislocation-unbinding mechanism proposed in the BKT theory. The defect-mediated theory predicts rather specific types of singularities, which have not been observed in smectic membranes. Instead a nearly symmetrical specific-heat anomaly showing divergent behavior has been found at the hexatic-isotropic transition. In many cases the crystal-hexatic phase transition in thin films is first order, which may preempt a continuous melting transition. In agreement with recent computer simulations, the melting scenario in two dimensions may not be universal but depends on specific properties of the system, such as the energy of the dislocation core and the interparticle potential.

Smectic membranes as thin as one or two layers represent true two-dimensional systems. More data are needed for the power-law singularities in the structure factor in these systems. Especially reliable measurements of the power-law exponent η_{cr} in the vicinity of the melting point would enhance our understanding of two-dimensional melting. An alternative way to study the structure factor of two-dimensional smectics is to exploit further grazing-incidence x-ray diffraction of surface crystalline ordering in smectic membranes.

Surface ordering in smectic phases is a common behavior and has been investigated in some detail. The basic features can be described in terms of the Landau theories of surface ordering and wetting. Nevertheless, no clear microscopic model exists for the enhanced ordering at surfaces and its influence in the surface phase behavior. The latter often involves two phases, one at the surface and one in the interior, that are simultaneously present. The quenching or enhancement of the fluctuations at a surface seems to play a crucial role in this behavior. However, it is not clear how this drives different ordering scenarios like continuous layer-by-layer or abrupt growth of the surface phase. X-ray reflectivity is the tool that can provide the necessary information on fluctuation profiles, which should be further explored.

IV. LAYER-DISPLACEMENT FLUCTUATIONS

A. X-ray reflectivity as a tool

In the last decade x-ray reflectivity has emerged as a powerful nondestructive technique for studying the properties of surfaces and interfaces. Experiments include solid-vapor interfaces (Zabel and Robinson, 1992), liquid interfaces (Als-Nielsen *et al.*, 1994; Daillant and Gibaud, 1999), polymer films (Russell, 1990; Tolan, 1998) and multilayer systems (Holý *et al.*, 1999). In the context of this review liquid-crystalline surfaces are of particular interest and have an extensive literature.[1] The first x-ray reflectivity applications to smectic membranes were those of Gierlotka *et al.* (1990) and Tweet *et al.* (1990). Since then this technique has evolved as a major tool for obtaining information on the fluctuation behavior of smectic systems. Extensions to soap films have also been made, both experimentally (Daillant and Bélorgey, 1992; Sentenac and Benattar, 1998) and theoretically (Kats *et al.*, 1993b). Moreover free-standing films of lyotropic systems (Smith *et al.*, 1988), of smectic polymers (Decher *et al.*, 1993; Reibel *et al.*, 1995), and of associating polyelectrolytes (Millet *et al.*, 1999) have been investigated.

X-ray reflectivity provides information on the thickness of a film, the electron-density gradients perpendicular to the interfaces, and the roughness (fluctuations) of the interfaces. During the last decade diffuse scattering from surfaces has also attracted much interest (Sinha *et al.*, 1988; Sinha, 1991; Daillant and Gibaud, 1999), including the study of fluctuations of smectic membranes (Shindler *et al.*, 1995; Mol *et al.*, 1996) and those associated with capillary waves on liquid surfaces (Sanyal *et al.*, 1991; Tidswell *et al.*, 1991; Ocko *et al.*, 1994; Doerr *et al.*, 1999; Fradin *et al.*, 2000). While specular scattering is sensitive to the laterally averaged electron-density profile, diffuse scattering provides information on the height-height correlations of an interface, i.e., on the in-

[1]Work on liquid-crystalline surfaces includes that of Als-Nielsen *et al.*, 1982; Pershan and Als-Nielsen, 1984; Als-Nielsen, 1986; Gramsbergen *et al.*, 1986; Ocko *et al.*, 1986, 1987; Pershan *et al.*, 1987; Pershan, 1988; Ocko, 1990; Olbrich *et al.*, 1993; Kellogg *et al.*, 1995; and Lucht *et al.*, 2001.

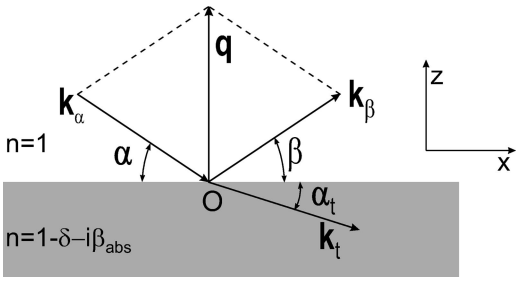

FIG. 12. Scattering geometry for x-ray reflectivity measurements; specular reflectivity is defined by $\beta=\alpha$.

plane correlations. As several excellent books on x-ray reflectivity have recently become available (Tolan, 1998; Daillant and Gibaud, 1999; Holý *et al.*, 1999), we shall restrict ourselves here to a short summary of the results needed in the remaining part of this review.

1. Specular reflectivity

Two major theoretical approaches exist to treating the scattering process. The *kinematical* or *first Born approximation* is based on the assumption that for a given x ray, the scattering process in the sample occurs at most once. This assumption is correct if the scattering represents a weak disturbance of the transmitted wave and if the probability of a scattered wave to be scattered again is low. The other theoretical approach, the *dynamic scattering theory*, takes multiple scattering processes into account. As we shall see, in the case of smectic membranes we can usually rely on the kinematical approximation (Als-Nielsen, 1986; Sinha *et al.*, 1988).

The scattering of a plane x-ray wave incident on a single flat interface can be described in terms of an index of refraction $n\simeq 1-\delta+i\beta_{\rm abs}$. Here $\delta=\rho_e r_e\lambda^2/2\pi$, in which ρ_e is the electron density and r_e the classical radius of the electron, and $\beta_{\rm abs}=\mu\lambda/4\pi$ with $1/\mu$ representing the absorption length of x rays in the medium. For x rays the index of refraction is usually slightly less than 1, with typical values for δ and $\beta_{\rm abs}$ of the order of 10^{-6} and 10^{-8}, respectively. Figure 12 pictures an interface in the xy plane separating air with $n=1$ and a liquid crystal with n. X rays with an incoming wave vector $\mathbf{k}_\alpha$ with $|\mathbf{k}|=k=2\pi/\lambda$ are incident at a glancing angle α. The x-ray beam is partly reflected at an angle β and partly transmitted at an angle α_t. The total scattering angle is given by $2\theta=\alpha+\beta$. Hence for specular reflectivity $\theta=\alpha=\beta$, and we shall use θ to denote this situation. The outgoing wave vector $\mathbf{k}_\beta$ of the reflected wave is in the plane of $\mathbf{k}_\alpha$ and the surface normal. For elastic scattering, $|\mathbf{k}_\alpha|=|\mathbf{k}_\beta|=k$ and the wave-vector transfer is given by $\mathbf{q}=\mathbf{k}_\beta-\mathbf{k}_\alpha$ with $q=2k\sin\theta$. For specular reflectivity, the wave-vector transfer is parallel to the surface normal (z axis) and $\mathbf{q}=(0,0,q_z=q)$.

As for x rays $n<1$, a critical angle of total reflection θ_c exists. For liquid-crystalline materials $\theta_c\simeq 0.15^\circ$ at $\lambda\simeq 0.1$ nm. When $\theta<\theta_c$, the incident wave is totally reflected from the interface and only an evanescent wave is traveling parallel to the surface. In this situation the $1/e$ penetration depth of the x rays is, neglecting absorption, $(2k\sqrt{\theta_c^2-\theta^2})^{-1}\simeq 5-40$ nm. For small angles and since $1\gg\delta\gg\beta_{\rm abs}$, according to Snell's law $\cos\theta_c=1-\delta$, which can be approximated by $\theta_c\simeq\sqrt{2\delta}=\lambda\sqrt{\rho_e r_e/\pi}$. The wave-vector transfer q' in the medium can be obtained using Snell's law and $\lambda'=\lambda/n$ and is given by $q'^2=q^2-q_c^2$, in which $q_c\simeq 2k\theta_c$.

The Fresnel reflectivity $R_{\rm F}$ is defined as the ratio of the intensities of the reflected and the incoming beam (Born and Wolf, 1959). In the limit $q\gg q_c$ refraction is negligible, $q'\simeq q$, and neglecting higher orders we get

$$R_{\rm F}\simeq\left(\frac{q_c}{2q}\right)^4=\frac{16\pi^2\rho_e^2 r_e^2}{q^4}. \tag{36}$$

At large angles the reflected intensity decays as q^{-4}. Owing to the rapid falloff in intensity with increasing angle, the range of q in reflectivity measurements is small, typically $q_{\rm max}\simeq 6\ {\rm nm}^{-1}$ [Fig. 13(a)]. In this situation corrections for polarization and absorption can be neglected.

The above considerations can be extended to the case of a flat film of thickness L and uniform density. The reflectivity can be calculated using the *recursive matrix method*, also known as the box or *slab model*, derived by Parrat using optical methods (Parrat, 1954). The reflectances at an interface between media j and $(j+1)$ are given by the Fresnel coefficients:

$$r_{j,j+1}=\frac{q_{j+1}-q_j}{q_{j+1}+q_j}, \tag{37}$$

where q_0 and q_1 can be identified with q and q' as defined above. For a single slab the ratio of reflected to incident intensity from the total film becomes $R_{\rm F}(q)=rr^*$ in which

$$r=\frac{r_{0,1}+r_{1,2}\exp(-\imath q_1 L)}{1+r_{0,1}r_{1,2}\exp(-\imath q_1 L)}. \tag{38}$$

The results are shown in Fig. 13(b). Now constructive and destructive interference of x rays reflected from the top and bottom of the film occurs with a period $2\pi/L$. As a result the reflectivity curve exhibits a series of oscillations, the so-called *Kiessig fringes*. The amplitude of these oscillations depends on the contrast in electron density between the film and the surrounding material. The next step is to include an internal structure in the membrane. Figure 13(c) shows a model calculation of the reflectivity of a smooth periodic film in a vacuum with thickness $L=Nd$, N being the number of layers. This figure can be compared with the experimental results shown in Fig. 5. The Kiessig fringes and the finite-size Bragg peaks determine L and d, respectively. Interference between Fresnel reflection and Bragg scattering enhances and extinguishes the scattered intensity at q values lower and higher than the Bragg positions, respectively. In fact this involves phase information about the layering, and the situation depicted describes a low-density termination at the interfaces (see further Sec. IV.C.3).

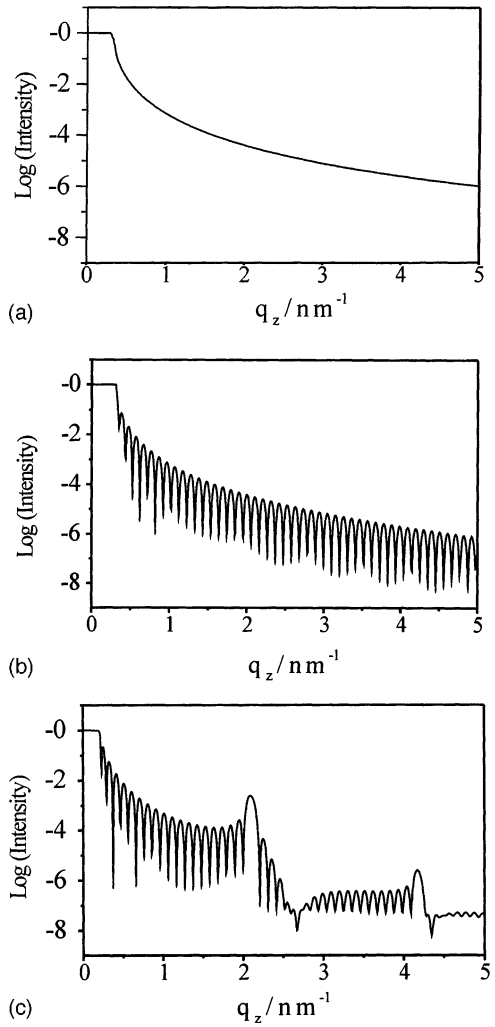

FIG. 13. Model x-ray reflectivity calculations: (a) Fresnel reflectivity of a single smooth interface; (b) reflectivity from a smooth structureless film with $L=90$ nm, $\delta=3\times10^{-6}$ and $\beta=1\times10^{-8}$; (c) as (b) with an internal structure of 30 layers with alternating between δ and $\delta'=2\times10^{-6}$.

More generally, an electron-density variation along the film normal can be described by a series of slabs of different constant density. Neglecting refraction and multiple scattering (first Born approximation) and taking the limit of an infinite number of infinitesimally thin slabs, one can derive the so-called master formula for the specular x-ray reflectivity:

$$I(q_z)=R_{\mathrm{F}}\left|\int_{-\infty}^{\infty}\frac{d\rho(z)}{dz}\exp(-\imath q_z z)dz\right|^2. \tag{39}$$

The first Born approximation is valid in the weakly interacting limit but diverges in the regime of total reflection. This can be corrected for by replacing q in the exponent of Eq. (39) by the average wave-vector transfer $q'=\sqrt{q^2-q_c^2}$ inside the membrane (Sinha *et al.*, 1988). Thus refraction corrections are still neglected for individual slabs, but the major refraction at the air/film interface is taken into account. This expression behaves well over the entire q range.

2. Diffuse scattering and roughness

So far we have assumed the interfaces to be perfectly smooth, while in all practical cases roughness is found over a range of in-plane length scales. This contributes lateral modulations to the electron-density profile of the sample and causes x rays to be scattered in nonspecular or diffuse directions. The refractive index profile $n(z)$, which so far has been treated as a sharp step, can be calculated by replacing the rough interface by a sequence of smooth interfaces along z, weighted by a probability density $P(z)$. A simple and convenient choice for $P(z)$ is a Gaussian function with a width σ corresponding to the mean-square roughness. This leads to an error function for the refractive index profile. Within this approximation roughness can be incorporated into the reflectance at an interface by multiplying the Fresnel coefficient Eq. (37) with a Gaussian factor, leading to

$$r_{i,j}=\frac{q_i-q_j}{q_i+q_j}\exp(-2q_iq_j\sigma_{i,j}^2). \tag{40}$$

This expression has been used in the literature both for $q_i=q_j=q$ and for $q_i=q$ and $q_j=q'$. Note that an expression similar to Eq. (40) is found for a flat graded interface. On the basis of specular reflectivity alone one cannot discriminate between these two cases. However, a rough surface also scatters diffusely while a graded interface does not.

Different lateral roughness profiles can give rise to the same mean-square value σ, and specular reflectivity cannot distinguish between these cases. The statistical properties of a rough interface are fully characterized by the height-height correlation function $H(r_\perp)=\langle z(0)z(r_\perp)\rangle$ (Sinha *et al.*, 1988; Tolan, 1998; Daillant and Gibaud, 1999). As the diffuse scattering originates from these lateral inhomogeneities, it can be used to retrieve the behavior of $H(r_\perp)$. The diffuse scattering averages over large lateral distances, which might extend to hundreds of microns depending on the diffraction geometry and coherent properties of the beam. The transverse coherence length ξ_t is defined as the maximum in-plane distance over which waves still interfere coherently at the detector. The resulting intensity can be seen as the incoherent sum of intensities that are scattered from various regions of the sample whose sizes coincide with the coherence domain. The variation of the off-specular component of the diffraction vector $q_\perp$ allows us to probe the scattering associated with different lateral length scales.

It should be realized that the situation in smectic membranes is fundamentally different from that of classical diffuse x-ray scattering from a solid surface. In the first place the roughness is not static, but arises from displacement-displacement correlations between the thermal fluctuations. This is similar to capillary waves on a liquid surface. However, the diffuse scattering is not only due to the surface, but originates from the whole film, in which all the smectic layers are subjected to thermal fluctuations (see Sec. IV.C.3). More importantly,

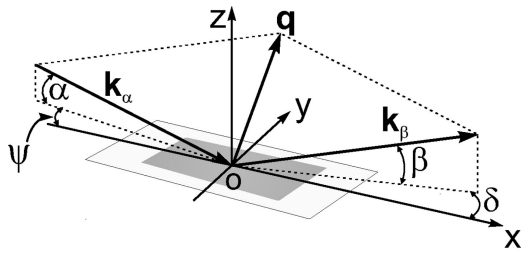

FIG. 14. General scattering geometry. The incident plane is defined by $\mathbf{k}_\alpha$ and the surface normal Oz, the scattering plane by $\mathbf{k}_\alpha$ and $\mathbf{k}_\beta$.

compared to solid surfaces the range of correlations of smectic membranes is much larger: the layer-displacement correlation function $C_{mn}(r_\perp)$, which is analogous to $H(r_\perp)$, diverges logarithmically with $r_\perp$ (see Sec. IV.B).

3. Types of scans and their resolution

The scattering geometry for surfaces and films is depicted in Fig. 14. Various types of scans allow mapping of the scattered intensity in different cuts through reciprocal space. In a specular reflectivity scan α and β are kept equal and varied together in the plane defined by $\psi=\delta=0$. *Specular scans* probe the scattered intensity along q_z with $q_y=q_x=0$. In *rocking scans* $\omega=\alpha-\beta$ is varied keeping the total scattering angle $2\theta=\alpha+\beta$ fixed. In such a scan mainly q_x is probed while in addition a small variation of q_z is introduced. In a rocking scan the in-plane range of q_x is limited by $\omega=\pm\theta$; the accessible range before the sample surface blocks either the incident or the scattered beam. To avoid this restriction one can make a *transverse diffuse scan* out of the scattering plane. In such a scan $\alpha=\beta$ is kept constant with respect to the surface and the detector is moved out of the scattering plane over an angle δ, while rotating the sample over $\psi=\delta/2$. Hence the scattered intensity is measured mainly along q_y at fixed q_z, while a small component q_x is introduced. Finally, in *longitudinal diffuse scans* q_z is varied at constant finite offset q_y while $q_x=0$. In this case α and β are varied together with respect to the surface at a fixed angle $\psi=\delta/2$.

In principle a rocking scan should show so-called Yoneda peaks when either α or β is equal to the critical angle (Yoneda, 1963; Dosch, 1992). In that situation the electric field of the evanescent wave at the surface reaches a maximum of twice the incident field, resulting in a larger diffuse scattering. In smectic membranes Yoneda peaks have not been reported so far. Originating at the surface, they might be hidden in the large kinematic diffuse scattering which stems from all layers. Hence the best chance to observe them would be in thin membranes of just a few layers.

The intensity measured experimentally is always found as a convolution of the structure factor Eq. (18) with the resolution function $R(\mathbf{q}')$:

$$I(\mathbf{q})=\int d^3q'\,S(\mathbf{q}-\mathbf{q}')R(\mathbf{q}'), \tag{41}$$

where S is the scattering intensity in the first Born approximation given by Eq. (18), $\mathbf{q}'$ denotes the stochastic deviation from the ideal wave vector $\mathbf{q}$, and $R(\mathbf{q}')$ describes the distribution of $\mathbf{q}'$. Hence it is essential to calculate the resolution for the various types of scans. The experimental resolution accounts for the divergence and size of the incoming beam, the solid angle defined by the finite aperture of the detector, and the wavelength dispersion. Usually the x-ray beam is highly monochromatic and the wavelength dispersion can be disregarded.

To describe the dispersions relative to $\mathbf{k}_\alpha$ and $\mathbf{k}_\beta$ random deviations α',ψ' and β',δ' are introduced around the angles α, ψ, β, and δ, respectively. Suitable analytical approximations for $R(\mathbf{q}')$ have been derived assuming these deviations to be small, statistically independent and described by Gaussian distributions (Sentenac, Fera, *et al.*, 2000; Sentenac, Shalaginov, *et al.*, 2000). In that situation linear relations can be given between the mean-square deviations of $\mathbf{q}$ and of the angles: $\Delta\alpha^2=\langle(\alpha')^2\rangle$ and similarly for $\Delta\beta^2$, $\Delta\psi^2$, and $\Delta\delta^2$. The resulting equations define the elements of the matrix $\hat{A}=A_{ij}=\langle q_i' q_j'\rangle$ where $i,j=x,y,z$. To calculate $R(\mathbf{q}')$ in Eq. (41) we can resort to a simplified form using the eigenvalues of $\hat{A}$, denoted as Δq_x^2, Δq_y^2, and Δq_z^2. Referring now (O,x,y,z) to the corresponding eigenvector coordinate system, $R(\mathbf{q}')$ reduces to (Sentenac, Shalaginov, *et al.*, 2000)

$$R(\mathbf{q}')=\frac{(2\pi)^{-2/3}}{\Delta q_x\Delta q_y\Delta q_z}\exp\left(-\frac{1}{2}\frac{q_x^2}{\Delta q_x^2}\right)\times\exp\left(-\frac{1}{2}\frac{q_y^2}{\Delta q_y^2}\right)\exp\left(-\frac{1}{2}\frac{q_z^2}{\Delta q_z^2}\right). \tag{42}$$

For the small angles involved in reflectivity experiments the eigenvector coordinate system does not differ much from the original system. For that situation first-order approximations of the resolution parameters for both the rocking geometry and diffuse scans out of the plane of incidence were given by Sentenac, Shalaginov, *et al.* (2000). The final step consists of calculating the scattered intensity by carrying out the integration in Eq. (41) using the relevant approximation for the resolution function of Eq. (42). This will be done for diffuse scattering from smectic membranes in Sec. IV.C.1.

B. Theory of the static structure factor

In this section we shall summarize the theory of the static structure factor of smectic membranes in which the layer displacement-displacement fluctuations play an essential role. According to the kinematic approximation, the scattering intensity $S(\mathbf{q})$ is given by Eq. (18). For the present purpose this can be generalized to

$$S(\mathbf{q})=\int d^3r_1 d^3r_2\langle\rho(\mathbf{r}_1)\rho(\mathbf{r}_2)\rangle\exp[\imath\mathbf{q}\cdot(\mathbf{r}_1-\mathbf{r}_2)]. \tag{43}$$

Using $\mathbf{r}=(\mathbf{r}_\perp,z)$ the electron density can be expressed in terms of the layer displacements as

$$\rho(\mathbf{r},t)=\sum_n \rho_s[z-nd-u_n(\mathbf{r}_\perp,t)]$$
$$=\int dz'\sum_n \rho_s(z')\delta[z-z'-nd-u_n(\mathbf{r}_\perp,t)]. \tag{44}$$

The summation is carried over the layers indexed by n, while ρ_s is the electron density of a single layer. We assume ρ_s to be independent of n; in other words, we neglect any possible profile. This assumption may break down close to a phase transition. If the random displacements u_n of the layers are Gaussian, the structure factor is given by

$$S=|\rho_s(q_z)|^2\int d^2r_\perp \times\sum_{m,n}\exp\left(\imath q_z(m-n)d+\imath\mathbf{r}_\perp\cdot\mathbf{q}_\perp-\frac{1}{2}q_z^2 g_{mn}(\mathbf{r}_\perp)\right), \tag{45}$$

where $\rho_s(q_z)$ is the molecular form factor, the Fourier transform of the density $\rho_s(z)$. Furthermore, in agreement with Eq. (11), the correlation function is given by

$$g_{mn}(\mathbf{r}_\perp)=\langle[u_m(0)-u_n(\mathbf{r}_\perp)]^2\rangle$$
$$=\langle u_m^2(0)\rangle+\langle u_n^2(\mathbf{r}_\perp)\rangle-2\langle u_m(0)u_n(\mathbf{r}_\perp)\rangle$$
$$=2\sigma_m^2(0)-2C_{mn}(\mathbf{r}_\perp). \tag{46}$$

A central consideration is the displacement-displacement correlation function $g_{mn}(\mathbf{r}_\perp)$, or in a continuous representation, $g(r_\perp,z,z')$. Theoretical models of thin smectic membranes have been developed that include the effect of surface tension at the interfaces (Hołyst *et al.*, 1990; Hołyst, 1991; Romanov and Shaliginov, 1992). The original formulation by Hołyst (1991) uses discretized fluctuations as a function of z. Later continuous versions (Poniewierski and Hołyst, 1993; Shaliginov and Romanov, 1993) have been shown to be equivalent.

1. The displacement-displacement correlation function

In order to calculate the displacement-displacement correlation function for smectic membranes we have to include the effect of the outer surfaces. The free energy for a smectic membrane can be written as the sum of the bulk and a surface contribution:

$$F=F_B+F_S. \tag{47}$$

F_B has been given in Eq. (5), F_S can be written as (Hołyst, 1991)

$$F_S=\frac{1}{2}\gamma\int d^2r\{[\nabla_\perp u(\mathbf{r}_\perp,z=L/2)]^2 +[\nabla_\perp u(\mathbf{r}_\perp,z=-L/2)]^2\}. \tag{48}$$

The surface terms, which are proportional to the surface tension γ, describe the energy cost associated with an increase in the surface area of the two free surfaces located at $z=L/2$ and $z=-L/2$. Within the framework of the present theory bulk elastic constants are used; the values of B and K are independent of layer number and film thickness. Hence the possibility of an increased smectic order parameter and thus a larger value of B at the surfaces will be disregarded. Furthermore, we shall not take the surface elastic constant for bending K_s (Shalaginov and Romanov, 1993) into account. The introduction of K_s, which does not have to be related to K (Poniewierski and Hołyst, 1993), would lead to a rescaling of the surface tension to $\gamma_{\text{eff}}=\gamma+q_\perp^2K_s$.

In this section we shall summarize the continuous version of the theory as developed by Shalaginov and Romanov (1993). The most convenient approach is to calculate $C(\mathbf{r}_\perp,z,z')$ in the $(\mathbf{q}_\perp,z,z')$ representation and subsequently take the inverse Fourier transform with respect to $\mathbf{q}_\perp$. Using

$$u(\mathbf{q}_\perp,z)=\int d\mathbf{r}_\perp\exp(-\imath\mathbf{q}_\perp\cdot\mathbf{r}_\perp)u(\mathbf{r}_\perp,z) \tag{49}$$

we arrive at

$$F=\frac{1}{(2\pi)^2}\int d^2q_\perp F(\mathbf{q}_\perp), \tag{50}$$

where $F(\mathbf{q}_\perp)$ is the contribution from fluctuations with wave vector $\mathbf{q}_\perp$:

$$F(\mathbf{q}_\perp)=\frac{1}{2}\int_{-L/2}^{L/2}dz[B|\partial_z u(\mathbf{q}_\perp,z)|^2 +Kq_\perp^4|u(\mathbf{q}_\perp,z)|^2]+\frac{1}{2}q_\perp^2\gamma[|u(\mathbf{q}_\perp,z=L/2)|^2 +|u(\mathbf{q}_\perp,z=-L/2)|^2]. \tag{51}$$

The surface term vanishes if the fluctuations $u(\mathbf{q}_\perp,z)$ satisfy the following boundary conditions:

$$\gamma q_\perp^2 u(\mathbf{q}_\perp,\pm L/2)\pm B\partial_z u(\mathbf{q}_\perp,\pm L/2)=0. \tag{52}$$

Using partial integration Eq. (51) can be transformed into a quadratic form,

$$F(\mathbf{q}_\perp)=\frac{1}{2}\int_{-L/2}^{L/2}dz\,u^*(\mathbf{q}_\perp,z)\hat{A}u(\mathbf{q}_\perp,z), \tag{53}$$

where the operator $\hat{A}$ is defined as

$$\hat{A}=B(-\nabla_z^2+\lambda^2q_\perp^4) \tag{54}$$

and $\lambda=\sqrt{K/B}$ has been introduced. $\hat{A}$ is self-adjoint so that an arbitrary function can be expanded into its complete series of eigenfunctions $f_n(\mathbf{q}_\perp)$ (fluctuation modes). The use of the boundary conditions does not impose restrictions, because any given fluctuation can be approximated by a linear combination of eigenfunctions $f_n(\mathbf{q}_\perp,z)$ [see also Valkov *et al.* (2001)]. Using the equipartition theorem we can now write

$$\langle u(\mathbf{q}_\perp,z)u^*(\mathbf{q}_\perp,z')\rangle=k_BT\sum_n\frac{1}{\Gamma_n}f_n(\mathbf{q}_\perp,z)f_n^*(\mathbf{q}_\perp,z'), \tag{55}$$

where the $\Gamma_n(\mathbf{q}_\perp)$ are the corresponding eigenvalues. This is the conventional approach to calculating the correlation function. However, the analysis is not straightforward because the eigenfunctions remain unknown. The sum in Eq. (55) is equal to the inverse operator $\hat{A}^{-1}$, which in turn is the resolvent of the operator $-\nabla_z^2$ defined as

$$\mathcal{R}_\Gamma(z,z')=B[-\nabla_z^2-\Gamma]^{-1}(z,z'), \tag{56}$$

calculated at $\Gamma=-\lambda^2 q_\perp^4$. Therefore we find

$$\langle u(\mathbf{q}_\perp,z)u^*(\mathbf{q}_\perp,z')\rangle=k_B T\,\mathcal{R}_{-\lambda^2 q_\perp^4}(\mathbf{q}_\perp)(z,z'). \tag{57}$$

Here we shall just present the expression for the resolvent $\mathcal{R}$ and refer the reader for analytical details of the derivation to Shalaginov and Romanov (1993):

$$\begin{aligned}\mathcal{R}_{-\lambda^2 q_\perp^4}(z,z')=&\frac{L}{2v[(v+w)^2+(v-w)^2e^{-2v}]}\\&\times\{(v+w)^2\exp(-v|z-z'|/L)\\&+2(v^2-w^2)\exp(-v)\cosh(v|z+z'|/L)\\&+(v-w)^2\exp(-2v+v|z-z'|/L)\},\end{aligned} \tag{58}$$

with v and w defined as

$$v=\lambda q_\perp^2 L,\quad w=\gamma q_\perp^2 L/B. \tag{59}$$

Carrying out the Fourier transform and introducing

$$\nu=\gamma/\sqrt{KB},\quad \varrho=r_\perp/\sqrt{\lambda L}, \tag{60}$$

we finally arrive at the correlation function:

$$\begin{aligned}g(r_\perp,z,z')=&\frac{k_B T}{8\pi\sqrt{KB}}\\&\times\int_{\xi_1}^{\xi_0}d\xi\,\frac{1}{\xi[(1+\nu)^2+(1-\nu)^2\exp(-2\xi)]}\\&\times[f(\xi,2z,z_0)+f(\xi,2z',z_0)\\&-2J_0(\varrho\sqrt{\xi})f(\xi,z_+,z_-)],\end{aligned} \tag{61}$$

where $\xi=L\lambda q_\perp^2$, $\xi_0=L\lambda(2\pi/a_0)^2$, $\xi_1=L\lambda(2\pi/W)^2$, with a_0 and W defined near Eq. (8), $z_+=z+z'$ and $z_-=|z-z'|$ (with minimal cutoff value z_0). J_0 is the Bessel function of order zero, while the function f is given by

$$\begin{aligned}f(\xi,z_+,z_-)=&2(1-\nu^2)\exp(-\xi)\cosh(\xi z_+/L)\\&+(1+\nu)^2\exp(-\xi z_-/L)\\&+(1-\nu)^2\exp[-\xi(2-z_-/L)].\end{aligned}$$

Equation (61) for the correlation function will be used in the analysis of the experimental results. A cutoff chosen as $z_0\simeq d/4$ reproduces essentially the results from the discrete model of Hołyst (1991). Such a cutoff is reasonable as the layers have a finite thickness and there is smearing of the layers due to the thermal motion of the molecules. For $\mathbf{r}_\perp=0$ the displacement-displacement correlation function $C(0,z,z')$ and the mean-square layer displacements $\langle u^2(0,z)\rangle$ reveal information about the compressional modes that depend on B. By studying $C(r_\perp,z=z')$, one can obtain information about the undulations (and thus K).

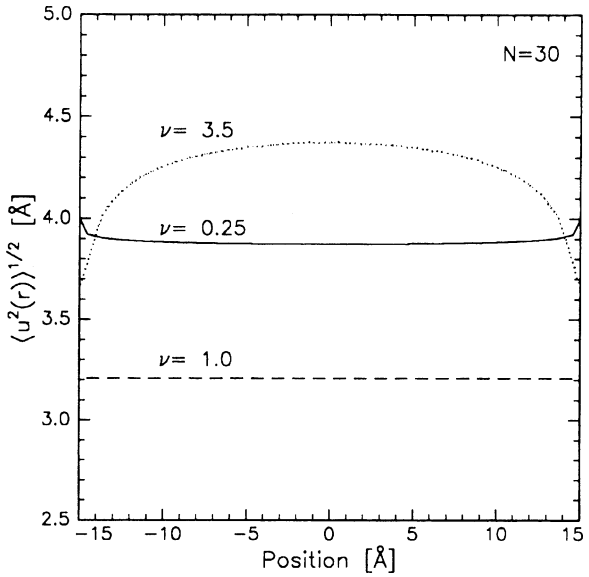

FIG. 15. Layer displacement fluctuation profile for a 30-layer membrane calculated with $\gamma=0.025$ N/m, $K=10^{-11}$ N, and $d=2.94$ nm: solid line, $\nu<1$ ($B=10^9$ N/m^2); dashed line, $\nu=1$ ($B=6.3\times10^7$ N/m^2); dotted line, $\nu>1$ ($B=5\times10^6$ N/m^2).

The fluctuation profile depends upon ν, as defined in Eq. (60). For $\nu>1$ surface damping of the fluctuations is expected, while for $\nu<1$ the fluctuation amplitudes will be enhanced at the surfaces (see Fig. 15). "Cutting" a smectic membrane out of the bulk by introducing two interfaces would increase the fluctuation amplitude at the free surfaces because of the absence of an elastic response from the missing material at the outside. For $\gamma=\sqrt{BK}$ the surface tension exactly compensates for this effect and the hydrodynamic fluctuation profile is flat. Aksenova *et al.* (2001) derived from the present theory an analytical expression for the fluctuations away from the surfaces:

$$\langle u^2(0)\rangle=\frac{k_B T}{8\pi\sqrt{KB}}\left[\frac{\nu-1}{\nu}\ln\left(\frac{L}{d}\right)+\frac{2}{\nu}\ln\left(\frac{W}{a}\right)\right]. \tag{62}$$

This result is valid for $Ld\ll W^2$. In the opposite case the perpendicular dimension takes over and the divergence takes the form $2\ln(W/a)$. An interesting consequence of Eq. (62) is that for $\nu<1$ the fluctuations in the middle of the membrane no longer diverge with L, but continue decreasing. In other words, in this situation the boundary conditions at $z=\pm L/2$ remove the Landau-Peierls instability [cf. Eq. (8)]. This scenario has been observed in thin films of the compound FPP (Mol *et al.*, 1996).

2. Conformal and nonconformal fluctuations

Fluctuations in a smectic membrane are called *conformal* if they are uniform across the film, i.e., all layers fluctuate in unison. For $L\to\infty$ one anticipates the fluctuations at the surfaces to become independent; hence

with increasing thickness conformality is somewhere lost. Before this threshold is reached, at large wavelengths all the layers still fluctuate conformally and $C(r_\perp,z,z')$ decays logarithmically with increasing $r_\perp$. In contrast, at short wavelengths a strong dependence of $C(r_\perp,z,z')$ on the layer position $r_\perp$ will be found. In this section we shall calculate the threshold $r_{\perp c}$ of the wavelength above which a membrane undulates uniformly and that separates the two regimes for the $r_\perp$ dependence of $C(r_\perp,z,z')$. A distortion with in-plane wave number $q_\perp=2\pi/r_\perp$ decays slowly from one layer to the other, due to the small compressibility of the system in the z direction. The characteristic decay length of the distortion is given by $l(q_\perp)=1/(\lambda q_\perp^2)$ (de Gennes and Prost, 1993). Therefore, within this approximation and taking a maximum value $l_{\max}(q_{\perp c})=L$ at a critical wavelength $q_{\perp c}$, a smectic membrane is expected to fluctuate conformally for $r_\perp>r_{\perp c}\simeq 2\pi\sqrt{L\lambda}$. This argument explains in principle the two regimes and gives $r_{\perp c}$ for thick membranes. However, it does not provide the proper value of $r_{\perp c}$ for a thin membrane, in which case the surface tension must be taken into account.

To work out how the surface tension affects $r_{\perp c}$ we consider the first principal mode of the fluctuations, which gives the main contribution to the correlation function [see Eq. (55)]. It corresponds to the smallest eigenvalue of the operator defined by Eq. (54). A general solution to

$$\hat{A}f(z)=\Gamma f(z) \tag{63}$$

reads $f(z)=a\cos(\kappa z)+b\sin(\kappa z)$ where $\kappa^2=(\Gamma-Kq_\perp^4)/B$. The symmetry of the system allows us to treat odd and even eigenfunctions separately, and the mode with the lowest eigenvalue is $\cos(\kappa z)$. Higher modes can be disregarded when the difference between the second and the first eigenvalue is larger than the first eigenvalue itself. As this difference is proportional to L^{-2} (Shalaginov and Romanov, 1993), the present considerations are only valid for thin membranes. The layers can be expected to fluctuate conformally if $\cos(\kappa z)$ does not change considerably across the film, i.e., if $\kappa L\ll 2\pi$. A general solution has been specified above, for which κ has to be found from the boundary conditions, Eq. (52). Taking in this equation $f(z)=a\cos(\kappa z)$ instead of $u(z)$ we arrive at

$$\frac{\gamma q_\perp^2}{B\kappa}=\tan(\kappa L/2)\simeq\kappa L/2\,. \tag{64}$$

Hence in real space the boundary of the region of conformality can be obtained using $r_\perp=2\pi/q_\perp$ as

$$r_\perp\gg r_{\perp c}\simeq\sqrt{2\gamma L/B}\,. \tag{65}$$

If we take $L=200$ nm ($N\simeq 65$), $K=10^{-11}$ N, $B=2.5\times10^6$ N/m^2, and $\gamma=0.03$ N/m, Eq. (65) gives $r_{\perp c}\simeq 70$ nm. In the limiting cases of $B\to\infty$ we find that $r_{\perp c}=0$ as expected. A fully incompressible film fluctuates conformally at all length scales.

In the particular case of $\gamma=\sqrt{KB}$, the integral in Eq. (61) can be evaluated analytically, leading to

$$g(r_\perp,z,z')=\frac{k_BT}{4\pi\gamma}\left[\ln\left(\frac{r_\perp^2}{4\lambda z_0}\right)+E_1\left(\frac{r_\perp^2}{4\lambda z_-}\right)+\gamma_E\right]. \tag{66}$$

The right-hand side does not depend on $z+z'$ and therefore the fluctuation profile over the membrane is completely flat; see also Shalaginov and Romanov (1993). As a consequence information about the film thickness is lost; Eq. (66) does not contain L. This result coincides with Eq. (12) for bulk Sm-A for $z_0=(d^2/\lambda)\exp(\gamma_E)$. It is also similar to an equation derived by Gunther *et al.* (1980) for an infinite sample, with the assumption $z_-\gg d$. A proper choice of z_0 makes them identical. The exponential decay of the exponential integral E_1 makes the second term in Eq. (66) negligible if the argument is larger than 1. For this range of $r_\perp$ we find that $g(r_\perp,z,z')$ depends neither on z nor on z' and varies logarithmically with $r_\perp$. Since $z_-<L$, this range can be estimated as

$$r_\perp\gg r_{\perp l}=2\sqrt{L\lambda}\,, \tag{67}$$

still for $\nu=1$. The length $r_{\perp l}$ is a second characteristic in-plane distance besides $r_{\perp c}$.

A uniformly undulating film can be taken as incompressible. To develop this approximation we take the limit $B\to\infty$ in Eq. (61) and arrive at

$$g(r_\perp,z,z')=g(r_\perp)=\frac{k_BT}{2\pi\gamma}\int_0^{q_{\max}}dq_\perp\ \frac{1-J_0(r_\perp q_\perp)}{q_\perp(1+q_\perp^2r_{\perp0}^2)}, \tag{68}$$

where $q_{\max}=2\pi/a_0$ and $r_{\perp0}=\sqrt{LK/(2\gamma)}$. For a thin film of four layers with $d=3$ nm, $K=10^{-11}$ N, $\gamma=0.03$ N/m, and $a_0=0.4$ nm, we find $r_{\perp0}q_m\simeq 10$. Thus, keeping in mind that the integrand decays as v^{-3}, the upper limit can be replaced by infinity. The integration can be carried out analytically and gives

$$g(\mathbf{r}_\perp)=\frac{k_BT}{2\pi\gamma}[\ln(r_\perp/r_{\perp0})+K_0(r_\perp/r_{\perp0})+\gamma_E-\ln 2]\,. \tag{69}$$

Due to rapid decay of the Bessel function K_0, in this situation of $B\to\infty$ we find $r_{\perp c}=0$. In addition $r_{\perp l}$ now coincides with $r_{\perp0}$, and Eq. (67) can be replaced by

$$r_{\perp l}\simeq\sqrt{\frac{LK}{2\gamma}}\,. \tag{70}$$

In summary we find that in general two characteristic in-plane lengths are needed to describe the fluctuations: $r_{\perp l}$ and $r_{\perp c}$. For $r_\perp>r_{\perp l}$ the correlation function has a logarithmic dependence on $r_\perp$ and for $r_\perp>r_{\perp c}$ the layers undulate conformally throughout the film. In the case of a thin film the surface tension strongly affects the fluctuations, and $r_{\perp c}=\sqrt{2\gamma L/B}$ [Eq. (65)]. If $\gamma\simeq\sqrt{KB}$ we find $r_{\perp l}\simeq r_{\perp c}\simeq 2\sqrt{L\lambda}$. If B tends to infinity, $r_{\perp c}$ tends to zero, but $r_{\perp l}$ remains finite. Equation (70) gives the functional dependence of $r_{\perp l}$ on the physical parameters when $\gamma\ll\sqrt{KB}$. The prefactor $k_BT/(2\pi\gamma)$ in the logarithmic region of the correlation function does not depend on the elastic parameters K and B, but is affected only by the surface tension.

C. Comparison with experiments

1. Interpretation of diffuse reflectivity

The diffusely reflected intensity is given by Eq. (45), which we shall write for the present purpose in the form

$$S(\mathbf{q}) = R_F \int d^2 r_\perp \exp(\imath \mathbf{q}_\perp \cdot \mathbf{r}_\perp) G(q_z, r_\perp), \tag{71}$$

where the correlation function $G(q_z, r_\perp)$ is given by

$$G(q_z, r_\perp) = \sum_{m,n}^{N} \exp\left(\imath q_z (m-n) d - \frac{1}{2} q_z^2 g_{mn}(r_\perp) \right). \tag{72}$$

Convoluting Eq. (71) with the resolution Eq. (42) leads to the final equation

$$I(\mathbf{q}) = R_F \frac{\Delta q_x \Delta q_y}{2\pi} \left[\int dx dy \, G(q_z, r_\perp) \times \exp\left(\imath (q_x x + q_y y) - \frac{1}{2} x^2 \Delta q_x^2 - \frac{1}{2} y^2 \Delta q_y^2 \right) \right] \times \exp\left(-\frac{1}{2} \frac{q_z^2}{\Delta q_z^2} \right). \tag{73}$$

In the reflectivity geometry the convolution in the xy plane ($\perp$ direction) and in the z direction can be carried out separately.

In order to discuss the general behavior of Eq. (73) we assume for the moment that the membranes fluctuate conformally, which means that $g_{mn}(\mathbf{r}_\perp)$ does not depend on n,m and is given by Eq. (69). The usual procedure for discussing x-ray reflectivity is to separate the specular and the diffuse parts. The specular reflectivity is generated at $q_\perp = 0$ and is due to $G(q_z, \infty)$; the diffuse scattering is determined by $[G(q_z, r_\perp) - G(q_z, \infty)]$. This procedure is generally valid for systems with a finite correlation distance, in which $G(q_z, r_\perp)$ decays exponentially to a constant value $G(q_z, \infty) \sim \exp[-q_z^2 \langle u(0)^2 \rangle]$. Integration of this constant with $\exp(\imath \mathbf{r}_\perp \cdot \mathbf{q}_\perp)$ provides a delta function. In the case of smectics, $G(q_z, r_\perp)$ decays algebraically to zero and $\langle u(0)^2 \rangle \to \infty$. However, $r_\perp$ cannot be larger than the sample size and $\langle u(0)^2 \rangle$ cannot reach infinity. The resolution factor forces the integral in Eq. (73) to converge to a finite value and the accessible range of the fluctuation spectrum depends on the parametrization of the resolution function (Sentenac, Shalaginov, *et al.*, 2000).

Rocking scans and diffuse scans out of the plane of incidence are compared for smectic membranes of the compound 4O.8 in Fig. 16. The data at the high-$q_\perp$ range (curve c) relate to the q_y part of a delta scan, those on the left follow a rocking scan, and those at the lowest $q_\perp$ range the q_x part of the same delta scan (cf. Sec. IV.A.3). All curves exhibit a large plateau region at low $q_\perp$, followed by an abrupt falloff at $q_\perp \simeq \Delta q_\perp$ and a smooth negative slope at higher $q_\perp$. The falloff separates specular and off-specular dominated regions. The diffuse region is influenced both by the resolution, which depends on the specific geometry chosen, and by the correlation function. This leads to a further division into two parts. First, there is a region where the logarithmic term in $g(r_\perp)$ is dominant (in between the plateau and high-$q_\perp$ regions). In this range the intensity follows a law close to an algebraic decay of the form

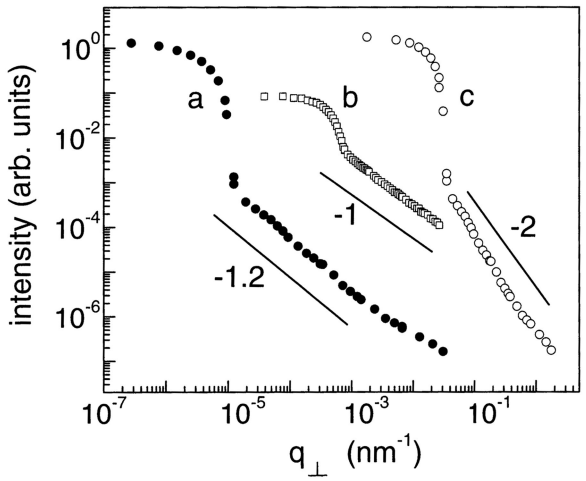

FIG. 16. Diffuse reflectivity scans of an eight-layer membrane of 4O.8. For the rocking scan (curve b) q_x is effectively varied, while for the delta scan both q_y (curve c) and q_x (curve a) are changed. Curve b has been shifted down for clarity.

$$I(q_\perp) \sim \int d\mathbf{r}_\perp \exp(\imath \mathbf{q}_\perp \cdot \mathbf{r}_\perp) r_\perp^{-\eta} \sim q_\perp^{-D+2\eta}. \tag{74}$$

We estimate $\eta \simeq 0.02$ while $D = 1$ or 2 depending on whether the experimental setting requires a one- or a two-dimensional integration. In curve c of Fig. 16 the transverse diffuse q_y scan out of the plane of incidence follows a law according to $q_\perp^{-2+2\eta}$ as a result of the two-dimensional integration needed. For the rocking scan (curve b) the diffuse part shows a slope of -1 corresponding to a one-dimensional integration and thus a behavior as $q_\perp^{-1+2\eta}$. However, to achieve this situation the predetector slit should be wide open in the direction out of the scattering plane. If this is not the case the integration over y can no longer be fully disregarded, and an intermediate slope of -1.25 is found (Sentenac, Shalaginov, *et al.*, 2000). This situation also applies to the q_x part of the delta scan, curve a of Fig. 16. Finally, for values of $q_\perp \gtrsim 0.01$ nm^{-1}, there is a nonlinear deviation from the algebraic decay. This higher-order effect is due to the bending modulus K in the correlation function. It can be understood from the simplified development of $g(q_z, r_\perp)$ in Eq. (69). For the present choice of q_z at the first Bragg position, this deviation can only be seen clearly in diffuse delta scans out of the plane of incidence.

Figure 17 shows transverse diffuse delta scans for 4O.8 membranes of varying thickness, both in the Sm-A and in the Cr-B phase. The results in the Sm-A phase were interpreted using Eq. (73), incorporating the average z component q_z' of the wave-vector transfer inside the membrane, as discussed below Eq. (39). Equation (73) was also smeared with a Gaussian of width σ_{loc} to

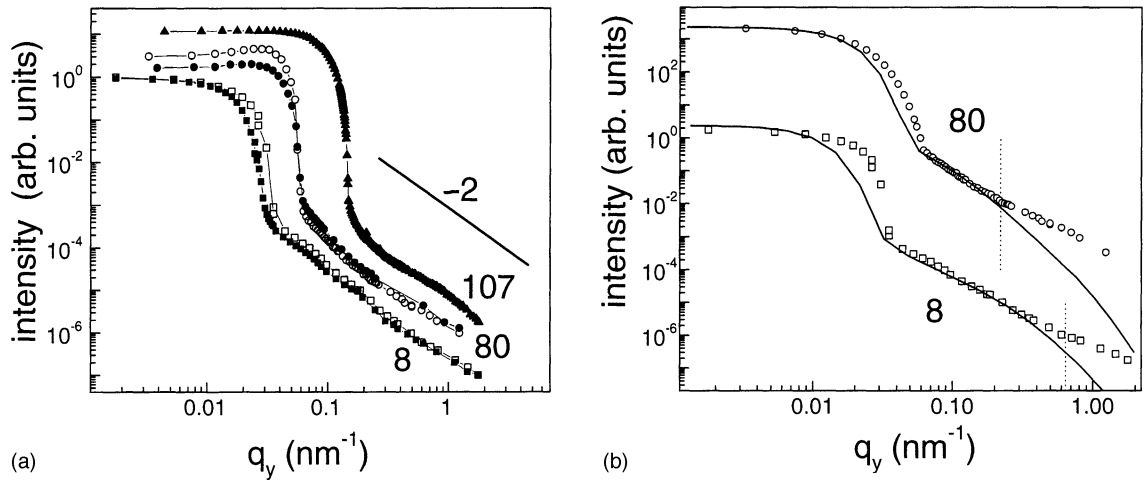

FIG. 17. Diffuse delta scans for N-layer 4O.8 membranes: (a) experimental results in the Sm-A phase (open symbols) and the Cr-B phase (filled symbols); (b) intensity calculation with the 4O.8 parameters from Table III. The vertical dotted lines indicate $2\pi/r_{\perp c}$.

approximate the local (short-wavelength) contribution to the total fluctuations. This allows us in principle to separate $\sigma_{\rm hyd}$ and $\sigma_{\rm loc}$, and to quantify to what extent the full fluctuations can be described by hydrodynamic theory. Assuming Gaussian fluctuations, the total fluctuations are given by

$$\sigma_{\rm tot}^2=\sigma_{\rm hyd}^2+\sigma_{\rm loc}^2. \tag{75}$$

As $\sigma_{\rm tot}$ is measured directly by the specular reflectivity, we shall postpone a further discussion of this relation to Sec. IV.C.3. The final fitting results for the elastic parameters of 4O.8 are given in Table III. They lead to $\nu>1$: the surface tension suppresses the fluctuations (cf. Fig. 15). In fact the values for B, K, and γ are very similar to those of other smectic compounds (Fisch *et al.*, 1984; Vertogen and de Jeu, 1988; Benzekri *et al.*, 1990). Another interesting aspect of Fig. 17 is the similarity of the diffuse reflectivity in the Sm-A and Cr-B phases. In practice, the diffuse intensities could be fitted with the same Sm-A parameters. Only for the thickest film (107 layers) could the effect of the shear constant C_{44} between the crystalline layers be measured. As will be discussed in Sec. V.D this can be understood from the Cr-B Hamiltonian in the so-called "easy-shear" approximation.

The diffuse scattering of the compound FPP has been investigated in some detail (Mol *et al.*, 1996, 1997), using the same methods as discussed above for 4O.8. Figure 18 shows rocking scans of a thin and a thick FPP membrane at various q_z positions. In thin films the line shapes at various q_z are very similar, indicating conformality. For the 150-layer film deviations occur at large q_x values, indicating an approach to loss of conformality at the corresponding in-plane distances. With the values obtained for N and d, the transverse line shapes at fixed q_z were fitted for each film separately, varying only γ, K, and B. For the present rocking curves Eq. (73) can be simplified by restricting the integration to the (x,z) plane. As dif-

TABLE III. Typical parameters for some of the compounds discussed (at temperatures in the middle of the smectic range).

Parameter	FPP	HPP	4O.8	7AB
d/nm	2.94	2.82	2.85	2.88
$d_{\rm core}/d$	0.62	0.50	0.51	0.54
$\delta_{\rm core}/\delta_{\rm tail}$	0.88	1.51	1.57	1.50
$\sigma_{\rm tot}$/nm	0.46	0.30	0.27−0.40[a]	0.35−0.54[a]
$\sigma_{\rm loc}$/nm	0.26	0.08		0.1−0.4[a]
$B/(10^7$ N/m$^2)$	75±25	3.0±1.5	$1.0^{-0.5}_{+10}$	1.0±0.5
$K/(10^{-12}$ N)	10±5	15[b]	25±10	12[c]
$\gamma/(10^{-3}$ N/m)	13.0±0.5	25±1	20±1[d]	25.0±0.5[d]
$\eta_3/[10^3$ N/(m s)]	0.015		0.04[e]	

[a]At surface–at center.
[b]Estimated from related compounds.
[c]de Jeu and Claassen (1977).
[d]Mach, Huang, *et al.* (1998).
[e]Price *et al.* (1999).

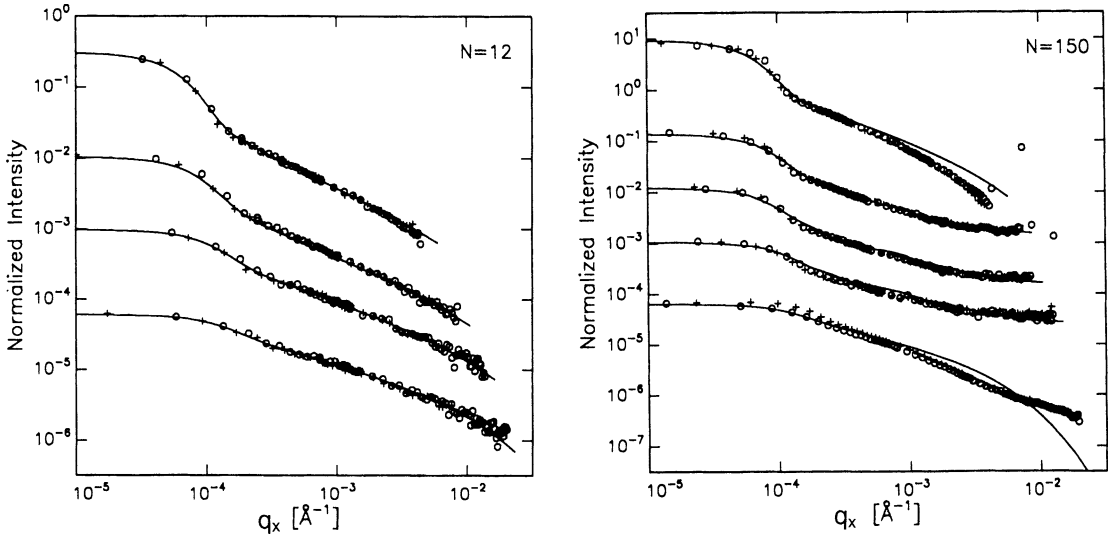

FIG. 18. Rocking scans for FPP membranes of various thicknesses. Top and bottom curves were taken at the first and second Bragg peak, middle curves at extrema of interference fringes in between. Crosses and circles refer to positive and negative q_x, respectively (compare Mol *et al.*, 1996).

fuse scans were made at various values of q_z (in contrast to the situation for 4O.8) for FPP $\sigma_{\rm loc}$ could also be quantified. Best fits to the rocking curves of a whole series of films, shown as solid lines in Fig. 18, occur for the values of γ, B, and K given in Table III.

For FPP the value of $\gamma=13\times10^{-3}$ agrees well with an independent direct measurement (Mach *et al.*, 1995). It is about a factor of 2 smaller than the values reported for nonfluorinated liquid crystals, which is due to a reduction of the surface energy due to fluorination of the alkyl chain (Pang and Clark, 1994). The value obtained for K is quite normal but the value of B is much larger than the others in Table III. This can be attributed to the increased stiffness of a fluorinated chain, which has an average cross section approximately 30% larger than that of a hydrocarbon chain (Rieker and Janulis, 1994). In addition, gauche conformers can practically be excluded, leading to a rigid rodlike structure (Lobko *et al.*, 1993). Clearly our FPP system is nearly incompressible, with layers fluctuating in unison down to the shortest in-plane wavelengths measured. Using Eq. (65) this leads to $r_{\perp c}\simeq2$ nm for a 34-layer film, which is of the order of molecular dimensions. If the 150-layer membrane is approximated as a bulk system, Eq. (66) gives $r_{\perp c}\simeq14$ nm, which is just within experimental reach. In fact, the upward curvature in the intensity at fringe positions between the Bragg peaks can be interpreted as such. The relatively small surface tension in combination with the large value of B leads for FPP to $\nu=0.15<1$, giving a stronger diffuse scattering than expected from the theory for bulk systems (cf. Fig. 15).

2. Loss of conformality

To go beyond the crossover from conformal to independent fluctuations requires specific choices for the scattering geometry as well as for the experimental conditions. According to Eq. (65) the required value of $q_{\perp c}$ can be lowered by choosing thick (large-L), easily compressible films (small B). The compound 7AB that has been investigated shows a second-order Sm-A–N phase transition (Gramsbergen and de Jeu, 1988), at which B is expected to vanish or to reach a small finite value (Nelson and Toner, 1981; Lubensky, 1983; de Gennes and Prost, 1993). Specular and diffuse longitudinal q_z scans for a 24-layer 7AB membrane are presented in Fig. 19(a). At the specular ridge ($q_y=0$) fluctuations at all length scales are probed, while for increasing q_y the long-wavelength side of the fluctuation spectrum is cut off at an increasingly shorter wavelength $2\pi/q_y$. If the fluctuations of the top and bottom interface are correlated, the exponential term with $q_z(m-n)d$ in Eq. (72) gives interference between the diffusely scattered amplitudes. Now the diffuse scattering is the coherent superposition of scattering from each layer, showing maxima and minima, e.g., Bragg peaks and Kiessig fringes, at the same positions in q_z as the specular reflectivity (Sinha, 1991). For independent fluctuations the correlation function vanishes for $m\neq n$ and the diffuse scattering is an incoherent superposition of the fluctuations of each interface. From Fig. 19(a) we note that at small offset q_y the film is conformal. The disappearance of the interference fringes at $q_y=0.191$ nm^{-1} ($r_\perp\simeq33$ nm) indicates that the top and bottom of the film no longer fluctuate in unison. The persistence of the Bragg peak up to the largest q_y value measured, however, shows that lateral correlation between adjacent layers still exists. The broadening and weakening of the Bragg peak reveals that the correlation length $\xi_\parallel$ becomes smaller than the total film thickness. With increasing $q_\perp$ more layers fluctuate independently and thus fewer layers are contributing coherently to the diffuse signal.

More direct information about the displacement-displacement correlation function can be obtained from the delta scans shown in Fig. 19(b). At small q_y the

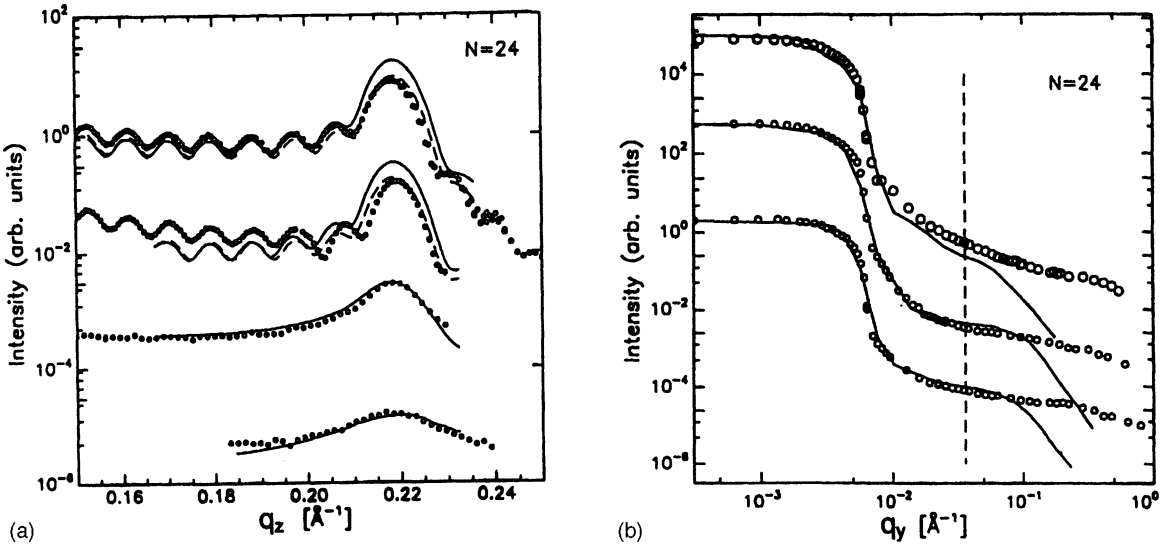

FIG. 19. Loss of conformality in a 24-layer 7AB membrane: (a) q_z scans with offsets from top to bottom, $q_y=0$, $q_y=0.064$, $q_y=0.191$, and $q_y=0.414$ nm^{-1}. Fits are described in the text; curves have been shifted for clarity; (b) delta scans at from top to bottom: $q_z=q_0$, $q_z=0.5q_0$, and $q_z=0.7q_0$. Fits are described in the text, the vertical dashed line indicates $2\pi/r_{\perp c}$. Curves have been shifted for clarity (Mol *et al.*, 1997).

slopes of the transverse scans at different q_z values are approximately parallel. Therefore all the layers are fluctuating in unison. The development of different slopes in the various scans is the signature of loss of conformality for fluctuations with increasing $q_\perp$. For further details of the quantitative analysis of the data using Eq. (73) we refer the reader to Mol *et al.* (1996). The resulting values for B, K, and γ are given in Table III. Using these values and d, $d_{\rm core}$, and $\delta_{\rm core}/\delta_{\rm tail}$ from Sec. IV.C.3 (see again Table III), the longitudinal diffuse scans were fitted as the solid line in Fig. 19(a). As no new parameters were introduced, the agreement is satisfactory. The vertical dashed line in Fig. 19(b) indicates the in-plane wave-vector transfer where loss of conformality is expected according to Eq. (65), which agrees reasonably well with the experimental observations. Nevertheless the fitting at large $q_\perp$ values still presents a serious problem to the interpretation. With increasing $q_\perp$ the fluctuations approach the bulk behavior described by Eq. (19) and the intensity should vary as $q_\perp^{-4}$. This transition is clearly visible in the theoretical curves as a steep falloff around $q_\perp \simeq 1$ nm^{-1} ($r_\perp \simeq 6$ nm). Though one would expect the hydrodynamic theory still to be valid in this region, the experimental data show no inclination to follow this behavior!

3. Interpretation of specular reflectivity

Early work on the interpretation of specular reflectivity curves began with Eq. (39) and was augmented with Eq. (40) in order to take a Gaussian roughness of the interfaces into account. Nowadays Parrat's recursive matrix formalism (see Sec. IV.A.1) is usually incorporated directly. In any case, a model is needed of the smectic membrane in terms of an electron-density profile along the normal. This profile is matched via an inverse Fourier transformation (after convolution with the experimental resolution) to the reflected intensity curve. In principle two approaches can be used to construct the electron-density profile. Phenomenologically it can be expressed as a Fourier series, retaining as many terms as needed to fit the data (Gierlotka *et al.*, 1990; Lambooy *et al.*, 1992). Here we shall take as a starting point the form factor of a smectic layer, which for orthogonal smectic phases is equal to the up-down averaged molecular form factor. The latter can be calculated by Fourier transformation of the electron density obtained from molecular modeling (Gramsbergen *et al.*, 1986). The results are in reasonable agreement with the simplified box model of Fig. 20 (Lobko *et al.*, 1993). Usually the central aromatic core has a larger electron density than the aliphatic tails.

Using the box model without fluctuations, the electron-density profile would be as shown in Fig. 21 for a two-layer smectic membrane. At any finite temperature fluctuations occur, due both to hydrodynamic modes of the layers ($\sigma_{\rm hyd}$) and to local movements of the centers of mass of the molecules around their equilibrium positions in the layers ($\sigma_{\rm loc}$). In a Gaussian approximation the total fluctuations are determined by $\sigma_{\rm tot}$ as given by Eq. (75). Hence the resulting density modulation is obtained by convolution of the box function with a Gaussian of width $\sigma_{\rm tot}$. While $\sigma_{\rm loc}$ is obtained from the diffuse scattering together with $G(r_\perp,z,z')$, the total fluctuations can be derived from the specular x-ray reflectivity (see Fig. 20). The value of $\sigma_{\rm tot}$ can in principle differ for each interface, leading to a fluctuation profile across the membrane. The combination of specular and diffuse reflectivity measurements allows us to separate the extent of local smectic disorder and the magnitude of the long-length-scale thermal fluctuations and to test Eq. (75). Note that the Gaussian approximation fixes the distribution function of the centers of mass

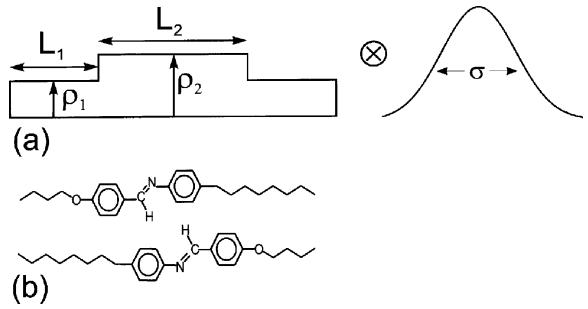

FIG. 20. Model for the smectic layer form factor: (a) box model used to represent the electron density smeared with a Gaussian function to take fluctuations into account; (b) two 4O.8 molecules with opposite up-down orientations.

$f(z)$ as defined in Sec. II.A and thus also the smectic order parameters τ_n. This is not in agreement with experiments and shows the limitations of this approach. Software packages have been developed to calculate the reflected intensity using the box model in combination with the recursive matrix formalism, for example, REFLAN (Samoilenko *et al.*, 1996, 1999).

We shall now turn to some applications. Figure 22 shows reflectivities for the compounds HPP and FPP at various thicknesses. We note a relatively strong second-order Bragg peak for FPP. This is well known for fluorinated molecules and can be attributed to the relatively high electron-density contrast due to the fluorinated tails (Lobko *et al.*, 1993; Rieker and Janulis, 1995; Takanishi *et al.*, 1995). The final fitting parameters using the box model are given in Table III. In the block model obviously $d=d_{\rm core}+2d_{\rm tail}$, while the critical angle is determined by the average density $\delta_0=(\delta_{\rm core}d_{\rm core}+2\delta_{\rm tail}d_{\rm tail})/d$. Two parameters strongly influence the fitting: $\delta_{\rm tail}/\delta_{\rm core}$, which determines the strength of the Bragg peaks, and $\delta_{\rm tail}/d$, which affects the relative strength of the second to the first Bragg peak. These parameters show very little interdependence. For $N=20$ the results for the two compounds can be directly compared. Note the important difference between HPP and FPP in the region around the first Bragg peak. For HPP we have a low-density termination at the interfaces ($\delta_{\rm core}/\delta_{\rm tail}>1$) leading to a minimum in the intensity for q_z values just above the Bragg position. FPP has fluorinated tails leading to the reverse situation. Now $\delta_{\rm core}/\delta_{\rm tail}<1$ and the minimum in q_z is shifted to the opposite side of the first Bragg peak. For $d_{\rm core}=0.5d$ the form factor has a minimum at the second Bragg peak, which will then be absent. This situation obviously applies to HPP. In the case of FPP the minimum is positioned at the low-q side of the second Bragg peak, indicating a box model with $d_{\rm core}>0.5d$.

FPP has been studied in depth by Mol *et al.* (1996), who give details of the fitting. In short there is a remarkable agreement with both the specular and diffuse experiments for a single set of stable parameters (see Table III), which are essentially independent of both film thickness and layer position. From the specular reflectivity the total fluctuation amplitude varies from $\sigma_{\rm tot}=0.48$ nm for a four-layer membrane and $\sigma_{\rm tot}=0.45$ nm for a 34-layer film. The parameters from the diffuse reflectivity include a value $\sigma_{\rm loc}=0.26$ nm for the local fluctuations, independent of the film thickness. Using Eq. (75) we can now calculate $\sigma_{\rm hyd}=0.37$ nm for the hydrodynamic part of the fluctuations. Even though the quantitative aspects of this calculation may be questioned, it is evident that for FPP both the hydrodynamic and the local fluctuations give a non-negligible contribution. The result for $\sigma_{\rm hyd}$ can be compared with a direct calculation of the hydrodynamic fluctuations from the correlation function. The value of $\sqrt{\langle u^2(0)\rangle}=\sigma_{\rm hyd}$ in the center of the thicker films is of the order of 0.36 nm. The excellent agreement with the value calculated using Eq. (75) gives some confidence in the reliability of the procedure used.

Specular reflectivities for membranes of various thickness of the compound 4O.8 have been given by Fera, Dolbnya, *et al.* (2001). The results of the final fitting are summarized in Table III. In contrast to the rather flat profiles of FPP, for 4O.8 a strong dependence on layer position is observed [Fig. 23(a)]. The flat top in the Sm-A profiles of the 38- and 80-layer membranes is an artifact: the value of σ_i of the central layers was constrained to be constant in order to reduce the number of parameters. For 7AB specular data are also available at various temperatures (Mol *et al.*, 1998); see Fig. 24 for a 24-layer membrane. They can again be fitted with stable parameters (see Table III). For 7AB the σ_i values also indicate a fluctuation profile over the membranes that becomes more pronounced with increasing temperature. The data for the highest temperature (56.2 °C) are well above the bulk Sm-A–N transition temperature of 52.9 °C. It is evident that thin membranes can be stable under these circumstances of increased smectic ordering at the surfaces. This leads to the phenomenon of thinning transitions (see Sec. VI.A).

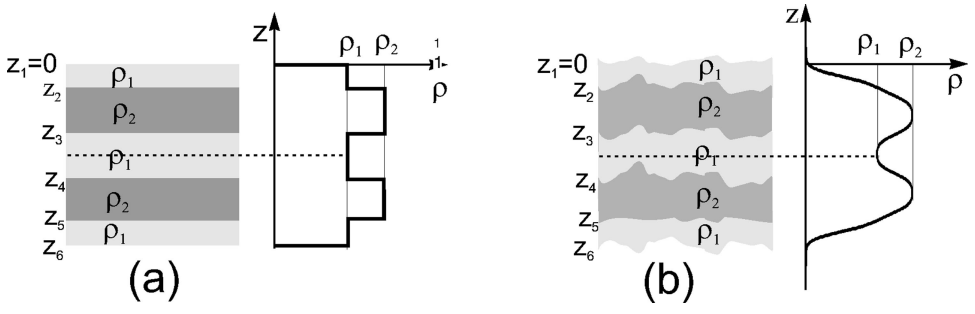

FIG. 21. Electron-density modulation in a two-layer membrane: (a) without thermal fluctuations; (b) including smearing by fluctuations.

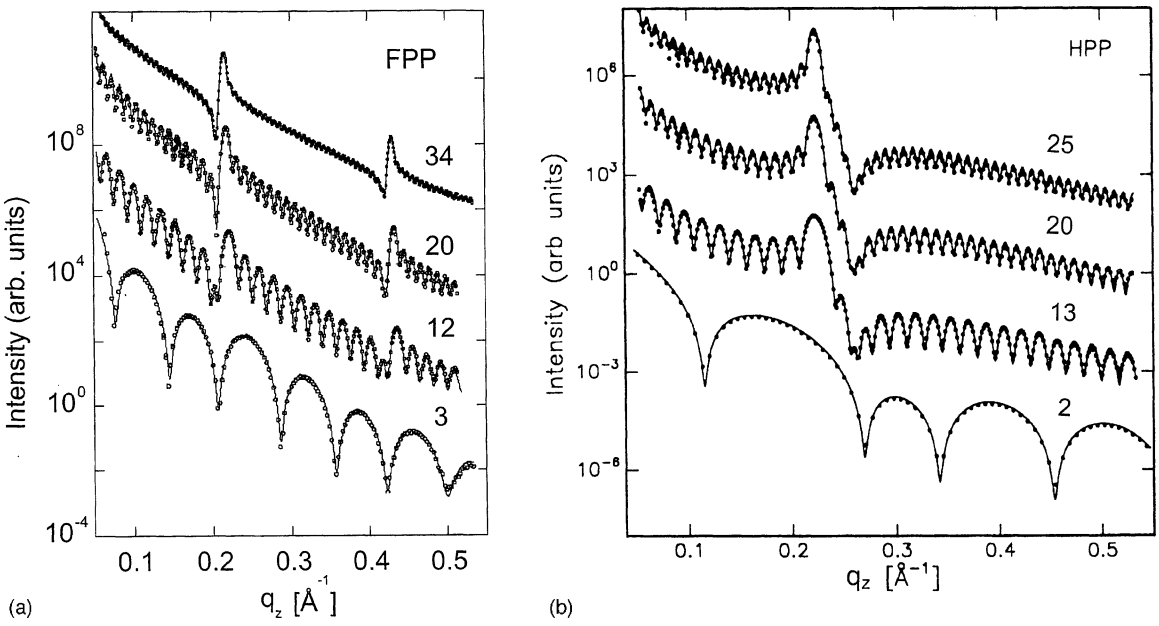

FIG. 22. Specular x-ray reflectivity of membranes with a different number of layers N for two related compounds: (a) FPP; (b) its hydrogenated analog HPP.

For both 4O.8 and 7AB the hydrodynamic profiles as discussed so far do not suffice to explain the experimental profiles. This is demonstrated for a 15-layer 4O.8 membrane in Fig. 23(b). The curve that fits the data ($\nu=6.5$) is far outside the experimental range of $\sqrt{BK}$ as determined by the diffuse reflectivity: the hydrodynamic profile is much weaker than the total one. Clearly a local fluctuation profile with an appreciable curvature is required to complete the picture. The same applies to 7AB for which we calculate $\nu=2.2$ from Table III. The associated hydrodynamic fluctuation amplitudes of the 24-layer membrane are $\sigma_{\mathrm{hyd}}=0.34$ nm and $\sigma_{\mathrm{hyd}}=0.37$ nm at the surface and center, respectively: again the profile of the hydrodynamic fluctuations is weak. Using σ_{tot} from Fig. 24 we can use Eq. (75) to calculate a profile for the local disorder with amplitudes $\sigma_{\mathrm{loc}}=0.1$ nm and $\sigma_{\mathrm{loc}}=0.5$ nm at the surface and the interior of the membrane, respectively. This is supported by the fitting of the results in Fig. 19(b). The original fit to the data (solid line) was performed using $\sigma_{\mathrm{loc}}=0.1$ nm. In fact the specular scan and the longitudinal diffuse scan at $q_y=0.64\times10^{-3}$ nm^{-1} can be better modeled when σ_{loc} is varied from 0.1 to 0.4 nm from the surface to the interior of the film (dashed line). For both 4O.8 and 7AB local fluctuations with a clear curvature have to be introduced to explain the experiments.

D. Conclusions and outlook

The major results and problems from this central section can be summarized as follows.

- The resolution problem that has hampered the interpretation of the specular and diffuse reflectivity of

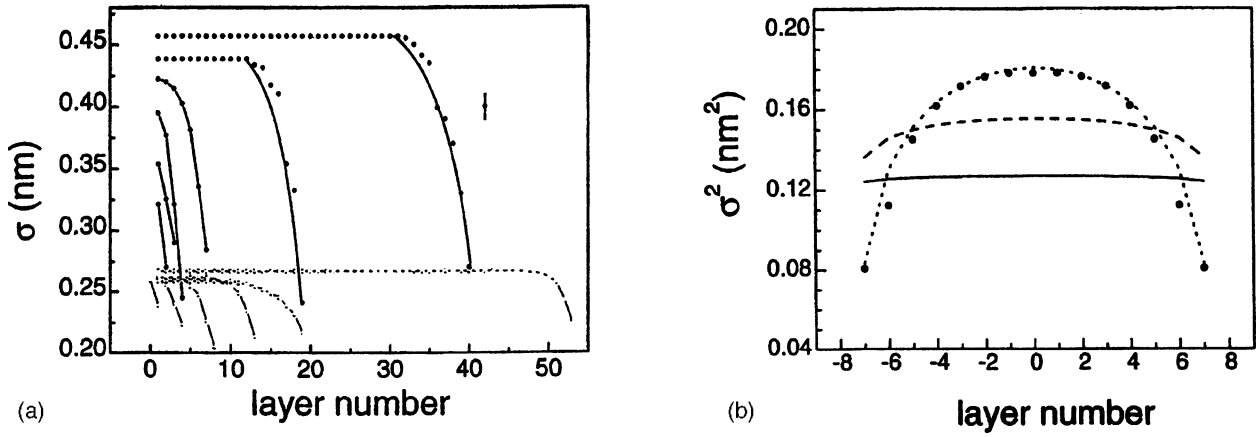

FIG. 23. Fluctuation profiles of 4O.8 membranes: (a) specular reflectivity at various thicknesses: solid line, Sm-A phase; dashed line, Cr-B phase; (b) experimental profile of the 15-layer membrane compared with hydrodynamic profiles. Solid line, parameters from Table III giving $\nu=1.3$; dashed line, $\nu=2.1$; and dotted line, $\nu=6.5$.

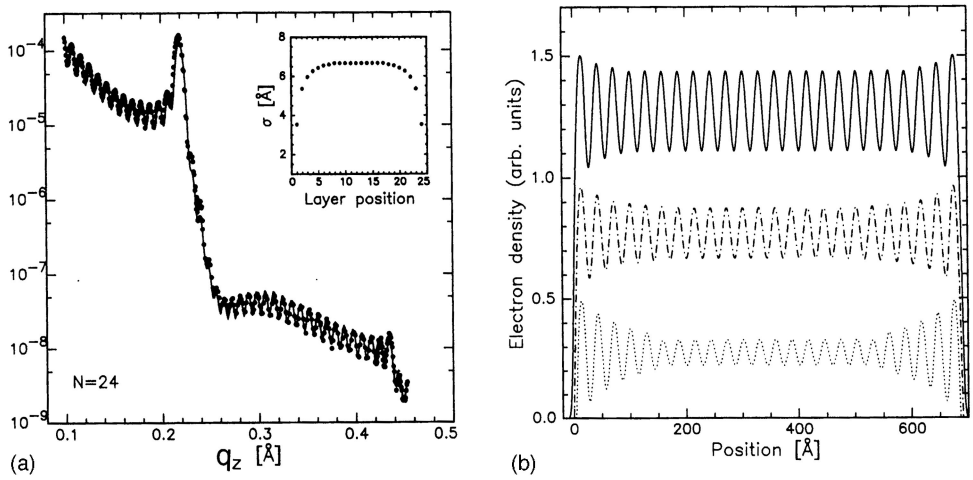

FIG. 24. Specular reflectivities of a 24-layer 7AB membrane with $T_c(24) = 56.3\,^\circ$C: (a) at 52.2 °C with the fluctuation profile as inset; (b) density profiles at 45.0, 52.2, and 56.2 °C, top to bottom (Mol *et al.*, 1998).

smectic membranes for some time has, in principle, been solved. This allows us to arrive at a quantitative interpretation of the fluctuation behavior. However, the possible effects of (partial) coherence of the x-ray beam still have to be further implemented.

- The occurrence of dynamic effects like Yoneda peaks in smectic membranes still remains to be proven experimentally.
- The diffuse reflectivity can be used to establish nicely the crossover from conformal to independent fluctuations. However, the intensity at moderately large values of $q_\perp$ does not approach the theoretically predicted $q_\perp^{-4}$ bulk behavior.
- For several systems fluctuation profiles have been observed in smectic membranes, which involve either quenched or enhanced fluctuations at the surfaces. In the latter case the fluctuations in the middle should continue to decrease with increasing membrane thickness and no Landau-Peierls divergence should occur. It would be worthwhile to investigate this behavior for a wide range of thicknesses.
- Theoretically the relative role of the hydrodynamic and the local fluctuations is not clear. It is evident that at values of $q_\perp$ approaching inverse molecular dimensions hydrodynamic theory no longer applies. Independent local fluctuations have been added in an approximate way using Gaussians to explain the experimental fluctuation profiles. In other words, a microscopic model that would correlate the positions of the molecules along the director is missing.
- A fluctuation profile over a smectic membrane implies in principle a profile of the smectic order parameter, and thus of the layer compressibility B. The possible effects of a nonconstant B on fluctuation behavior have not yet been incorporated theoretically.

V. DYNAMICS OF SMECTIC FLUCTUATIONS

A. Introduction

If coherent radiation is incident on a material, the scattered intensity shows a so-called speckle pattern that reflects the instantaneous configuration of the scatterers. Movement of the scatterers causes a corresponding change in this pattern and thus contains information on the dynamics of the system. Photon correlation spectroscopy or dynamic light scattering measures the time-dependent intensity autocorrelation function of the speckle pattern. Using visible light, it has developed into a well-established technique since lasers became available (Chu, 1991). In contrast, correlation spectroscopy with coherent x rays has been developed only recently at third-generation high-brilliance synchrotron sources (Dierker, 1995; Grübel and Abernathy, 1997; Abernathy *et al.*, 1998). Dynamic light-scattering studies of smectic membranes were carried out by Böttger and Joosten (1987) and Nallet *et al.* (1989). So far, the feasibility of x-ray photon correlation spectroscopy has been demonstrated for various hard (Brauer *et al.*, 1995; Dierker *et al.*, 1995; Tsui and Mochrie, 1998) and soft (Mochrie *et al.*, 1997; Thurn-Albrecht *et al.*, 1999; Grübel *et al.*, 2000; Lumma *et al.*, 2000; Lurio *et al.*, 2000; Riese *et al.*, 2000; Lal *et al.*, 2001) condensed systems, including capillary waves on liquid surfaces (Seydel *et al.*, 2001). Emphasis has been on relatively slow dynamics (ms range) like those of colloidal particles suspended in various liquids. More recently applications to smectic membranes have been made (Poniewierski *et al.*, 1998; Price *et al.*, 1999; Fera *et al.*, 2000; Sikharulidze *et al.*, 2002) as well as to liquid-crystalline surfaces (Madsen *et al.*, 2003). A considerable advantage of x rays is that they do not suffer from multiple scattering problems, so that opaque systems can also be studied. In the context of smectic membranes other differences between the two methods are important. Light-scattering experiments are sensitive to either orientational fluctuations of the director associated with layer undulations (Sprunt *et al.*, 1992; Shalaginov and Romanov, 1993) or to long-wavelength fluctuations of the air-liquid interface (as in the case of Böttger and Joosten, 1987). In contrast, x-ray photon correlation spectroscopy is sensitive to the layer fluctuations and gives a much better spatial resolution. In Fig.

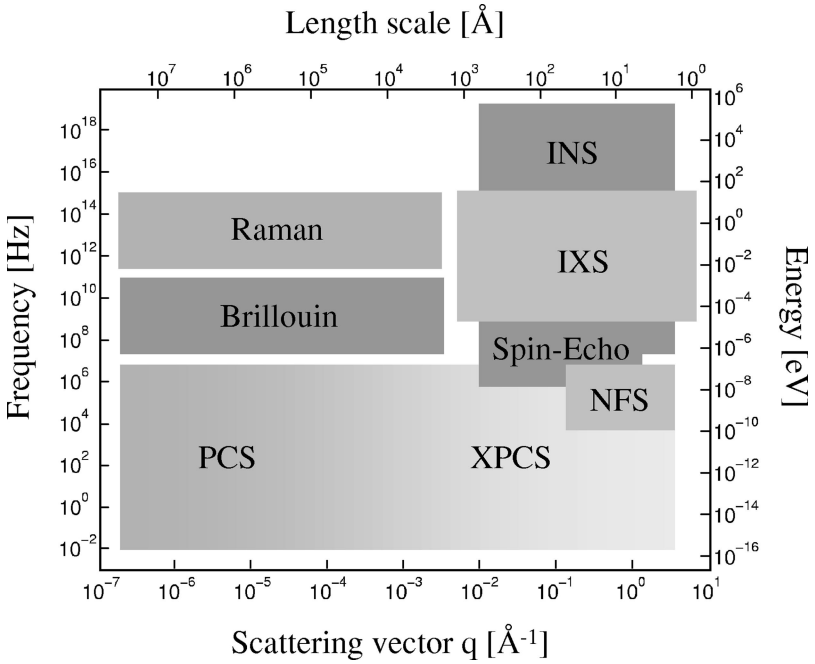

FIG. 25. Diagram of frequency vs wave vector comparing various dynamic techniques.

25 various dynamic scattering techniques are compared in terms of the energy and wavelength scales involved.

The analysis of x-ray photon correlation spectroscopy is more complicated than that of light-scattering studies. In the latter case, it is often sufficient to calculate the two-time displacement-displacement correlation function in the wave vector, frequency $(\mathbf{q},\omega)$ representation. X-ray photon correlation spectroscopy needs the position, time $(\mathbf{r},t)$ representation, which requires taking inverse Fourier transformations. For both light scattering and x-ray scattering of smectic membranes, finite-size and surface effects, depending on the surface tension and perhaps other surface parameters, should be taken into account. Most importantly, the finite thickness of a smectic membrane leads to quantization, producing a set of modes dependent on surface parameters, instead of a continuous spectrum as in bulk systems.

B. Theory of the dynamic structure factor

To analyze x-ray photon correlation spectroscopy, the two-time correlation function of the thermal displacements of the layers is required. Recently, this has been examined by a discrete model (Poniewierski *et al.*, 1998, 1999; Romanov and Ulyanov, 2001) as well as by a continuous one (Chen and Jasnow, 2000; Shalaginov and Sullivan, 2000). Both types of model are based on the hydrodynamic equations for bulk systems, supplemented by boundary conditions, and give essentially the same characteristic times. Here we concentrate on a continuous model that directly yields a closed-form expression for the correlation function in the $(\mathbf{q},\omega)$ representation (Shalaginov and Sullivan, 2000) The relaxation times of the modes correspond to the poles of this function.

A coherent x-ray beam enables one to measure $\langle I(t)I(0)\rangle$ and to obtain information about dynamic processes in the system under consideration. Let us consider in more detail the correlation between the intensities $I(t)$ at different times. We recall that the intensity at time t is proportional to $E(t)E^*(t)$, where E is the scattered field. The measured correlation function is therefore proportional to $\langle E(0)E^*(0)E(t)E^*(t)\rangle$. The fluctuations of the scattered field contain two contributions that can be considered separately. The first one is due to variations in the incoming field and thus comprises the bunch structure of the storage ring. The second one stems from the scattering amplitude of the sample (density fluctuations) and is our direct concern. If the fluctuations of the field are Gaussian, then the intensity-intensity correlation factorizes as

$$\begin{aligned}\langle E(0)E^*(0)E(t)E^*(t)\rangle &= \langle E(0)E(t)\rangle\langle E(0)^*E^*(t)\rangle \\ &+ \langle E(0)E^*(0)\rangle\langle E(t)E^*(t)\rangle \\ &+ \langle E(0)E^*(t)\rangle\langle E^*(0)E(t)\rangle.\end{aligned} \tag{76}$$

As the field changes with time as $\exp(\iota\omega t)$, the first term becomes zero after averaging over the period $2\pi/\omega$. The second term does not depend on time, because the system is stationary (i.e., the single-time correlation function does not depend on time). The third term contains all the information about the dynamics of the sample and is proportional to $|S|^2$, where in the first Born approximation S is given by Eq. (45), with

$$g_{mn}(\mathbf{r}_\perp,t) = \langle [u_m(0,0) - u_n(\mathbf{r}_\perp,t)]^2\rangle. \tag{77}$$

Hence the time dependence in the displacements $u_n(\mathbf{r}_\perp,t)$ is retained and incorporated in the displacement-displacement correlation function $g_{mn}(\mathbf{r}_\perp,t)$, which is central to the following considerations. The analysis of $g_{mn}(\mathbf{r}_\perp,t)$ carried out by Poniewierski *et al.* (1998, 1999) is based on the following

approach. First, they apply hydrodynamic equations for bulk Sm-A liquid crystals written in terms of a continuous displacement $u(\mathbf{r}_\perp,z,t)$. Second, they replace the derivative $\nabla_z u$ by $(u_n-u_{n-1})/d$, taking into account additional terms for interfacial effects (surface tension), and obtain a set of coupled equations for the displacements $u_n(\mathbf{r}_\perp,t)$. Here we use the same hydrodynamic equations to calculate

$$g(\mathbf{r}_\perp,z,z',t)=\langle[u(0,z',0)-u(\mathbf{r}_\perp,z,t)]^2\rangle, \tag{78}$$

where z remains a continuous variable. To calculate the scattering we set

$$g_{mn}(\mathbf{r}_\perp,t)=g(\mathbf{r}_\perp,z_n,z_m,t), \tag{79}$$

where z_m and z_n are the z coordinates of smectic layers m and n, respectively.

1. Hydrodynamic equations

Full sets of hydrodynamic equations for a Sm-A liquid crystal can be found, for instance, in the work of Martin *et al.* (1972), Landau and Lifshitz (1986), de Gennes and Prost (1993), and Kats and Lebedev (1993). Here we use a simplified version. We note that three characteristic time scales occur in the hydrodynamics of Sm-A (de Gennes and Prost, 1993; Chaikin and Lubensky, 1995). The first one is related to the permeation process, which can be viewed as the penetration of flux through the smectic layer structure. This process is very weak and its characteristic time scale is very large. It will not be further considered here. The second time is associated with the viscous forces responding to inertia. This motion is sometimes denoted in the literature as the *fast mode* and its time scale is the shortest of the three. The final time scale stems from the balance between viscous and elastic forces. This is often referred to as the *slow mode*, although its time scale is in fact intermediate between the other two. The characteristic time scales of the slow and the fast modes are related via the parameter $\rho_0 K/\eta_3^2$ (de Gennes and Prost, 1993), in which η_3 is the sliding viscosity of the smectic layers. This parameter, which can be considered as the ratio of inertia to elastic forces, is small in bulk smectics (of the order of 10^{-6},) and one can consider the slow and fast modes separately. This is due to the absence of a term proportional to $q_\perp^2$ in the bulk elastic energy. In this situation, equations for the slow mode can be obtained from the general hydrodynamic equations neglecting inertial terms. However, one should be cautious in the case of smectic membranes because they involve a surface contribution proportional to $q_\perp^2$ due to the surface tension. If the layers undulate conformally, then this contribution effectively acts like a bulk one. For small $q_\perp$ this term may prevail over the layer-bending term $Kq_\perp^4$ and inertia can no longer be disregarded.

In the following we neglect thermodiffusion as being a slow process. Compressibility is disregarded because B is much smaller than the compressibility coefficient. Furthermore, we take $\nabla\cdot\mathbf{v}=0$ in the calculation of viscous forces; $\mathbf{v}$ is the velocity, which only has a z component with $v_z=\partial u/\partial t$. We also neglect rolls, and finally assume that the temperature is constant ($\nabla T=0$). The dynamic equation then reads

$$\rho_0\frac{\partial v_z}{\partial t}=-\frac{\delta F}{\delta u}-\frac{\delta R_{\rm dis}}{\delta v_z}, \tag{80}$$

in which $R_{\rm dis}$ is a dissipation function and F the free energy. The first term on the right-hand side of Eq. (80) is the elastic force and the second term the viscous force. The dissipation function is given by

$$R_{\rm dis}=\frac{1}{2}\int d^3r\,\eta_3(\nabla_\perp v_z)^2. \tag{81}$$

The elastic and viscous forces acting in the z direction can be expressed as the derivatives of F and $R_{\rm dis}$ with respect to u and v_z, respectively. The free energy of a Sm-A membrane has been given in Eq. (47), and the elastic force is equal to the variational derivative

$$\frac{\delta F}{\delta u}=(-B\nabla_z^2+K\Delta_\perp^2)u. \tag{82}$$

Using these results in Eq. (80) and taking the Fourier transform over $\mathbf{r}_\perp$, we get

$$\rho_0\frac{\partial^2 u(\mathbf{q}_\perp,z,t)}{\partial t^2}=\left[-\eta_3 q_\perp^2\frac{\partial}{\partial t}+B\nabla_z^2-Kq_\perp^4\right]u(\mathbf{q}_\perp,z,t). \tag{83}$$

We shall apply the same boundary conditions as in the static case, Eq. (52), which can be obtained by minimizing F with respect to the surface displacements $u(\mathbf{r}_\perp,z=\pm L/2,t)$. These conditions represent the balance of elastic forces at the interfaces and implicitly assume that relaxation at the interfaces is much faster than in the bulk (i.e., the viscosity at $z=\pm L/2$ is negligible). The same boundary conditions were employed by Chen and Jasnow (2002). Although they appear different from those used in the discrete dynamic model, the same characteristic times of the relaxation modes are obtained.

2. Two-time correlation function

The correlation function $g_{mn}(\mathbf{r}_\perp,t)$ can be expressed as

$$\begin{aligned}g_{mn}(\mathbf{r}_\perp,t)=\frac{1}{(2\pi)^2}\int d^2q_\perp[&C(\mathbf{q}_\perp,z_m,z_m,0)\\&+C(\mathbf{q}_\perp,z_n,z_n,0)-C(\mathbf{q}_\perp,z_m,z_n,t)\\&\times\exp(\imath\mathbf{r}_\perp\cdot\mathbf{q}_\perp)-C(\mathbf{q}_\perp,z_n,z_m,-t)\\&\times\exp(-\imath\mathbf{r}_\perp\cdot\mathbf{q}_\perp)],\end{aligned} \tag{84}$$

where

$$C(\mathbf{q}_\perp,z,z',t)\equiv\langle u^*(\mathbf{q}_\perp,z',0)u(\mathbf{q}_\perp,z,t)\rangle. \tag{85}$$

To calculate C we use the method developed by Shalaginov and Romanov (1993), which is based on the resolvent of the operator $-\nabla_z^2$. Mathematically this method is formulated as follows. Multiplying Eq. (83) by $u^*(\mathbf{q}_\perp,z',0)$ and averaging, we get the equation

$$\rho_0 \frac{\partial^2 C(\mathbf{q}_\perp,z,z',t)}{\partial t^2} = -\eta_3 q_\perp^2 \frac{\partial C(\mathbf{q}_\perp,z,z',t)}{\partial t} - [-B\nabla_z^2 + Kq_\perp^4] C(\mathbf{q}_\perp,z,z',t), \tag{86}$$

with boundary conditions equivalent to Eq. (52):

$$\gamma q_\perp^2 C(\mathbf{q}_\perp,z=\pm L/2,z',t) \pm B\nabla_z C(\mathbf{q}_\perp,z=\pm L/2,z',t) = 0, \tag{87}$$

and the initial conditions

$$C(\mathbf{q}_\perp,z,z',0) = C(\mathbf{q}_\perp,z,z'), \tag{88a}$$

$$\frac{\partial}{\partial t} C(\mathbf{q}_\perp,z,z',t=0) = 0. \tag{88b}$$

The last condition assumes that u and v_z are statistically independent (see also Poniewierski *et al.*, 1999). $C(\mathbf{q}_\perp,z,z')$ is the single-time correlation function that coincides with Eq. (57).

To solve the dynamic equations we make the following transformation:

$$C^+(\mathbf{q}_\perp,z,z',\omega) = \int_0^\infty dt \exp(\iota\omega t) C(\mathbf{q}_\perp,z,z',t). \tag{89}$$

Applying this to Eq. (86), integrating by parts, and taking into account that the correlation function vanishes for $t\to\infty$, we obtain

$$B[-\nabla_z^2 - \Gamma] C^+(\mathbf{q}_\perp,z,\omega) = (\eta_3 q_\perp^2 - \iota\rho_0\omega) C(\mathbf{q}_\perp,z,z'), \tag{90}$$

in which Γ is now given by

$$B\Gamma(\mathbf{q}_\perp,\omega) = \iota\omega\eta_3 q_\perp^2 + \rho_0\omega^2 - Kq_\perp^4. \tag{91}$$

The solution to this equation can be expressed in terms of the resolvent $\mathcal{R}_\Gamma(z,z')$ defined by Eq. (56). We recall that the single-time correlation function can also be expressed in terms of the resolvent as in Eq. (57). Then C^+ can be expressed as

$$C^+(\mathbf{q}_\perp,z,z',\omega) = \frac{(\eta_3 q_\perp^2 - \iota\rho_0\omega) k_B T}{B^2} \times (\mathcal{R}_{\Gamma(\mathbf{q}_\perp,\omega)} \cdot \mathcal{R}_{\Gamma(\mathbf{q}_\perp,0)})(z,z'), \tag{92}$$

and the full correlation function is

$$C(\mathbf{q}_\perp,z,z',\omega) = C^+(\mathbf{q}_\perp,z,z',\omega) + C^+(\mathbf{q}_\perp,z,z',-\omega), \tag{93}$$

where we have used time-reversal symmetry. The product on the right-hand side of Eq. (92) can be calculated using the first formula for resolvents of self-adjoint operators (Reed and Simon, 1972):

$$(\mathcal{R}_\mu \cdot \mathcal{R}_\nu)(z,z') = \frac{1}{\mu-\nu}[\mathcal{R}_\mu(z,z') - \mathcal{R}_\nu(z,z')]. \tag{94}$$

Then one obtains

$$C(\mathbf{q}_\perp,z,z',\omega) = \frac{2k_B T}{\omega B} \operatorname{Im} \mathcal{R}_{\Gamma(\mathbf{q}_\perp,\omega)}(z,z'). \tag{95}$$

The displacement-displacement correlation function in the real-space and real-time representation is obtained from the Fourier transform

$$C(\mathbf{q}_\perp,z,z',t) = \langle u(0,z',0) u(\mathbf{r}_\perp,z,t)\rangle = \frac{1}{(2\pi)^3} \int_{2\pi/\Lambda}^{2\pi/a} d\omega d^2 q_\perp \times \exp(-\iota\omega t + \iota\mathbf{q}_\perp\cdot\mathbf{r}_\perp) C(\mathbf{q}_\perp,z,z',\omega). \tag{96}$$

The integration over $q_\perp$ is cut off in the short- and long-wavelength limits by the intermolecular distance a and an in-plane dimension of the system Λ, respectively. However, for coherent x-ray experiments the cutoff Λ is usually taken equal to the in-plane footprint, which is in practice much smaller than the system size (Hołyst, 1991; Mol *et al.*, 1996).

3. Eigenmodes and their characteristic times

The singularities of the resolvent $\mathcal{R}$ as a complex function of ω have a crucial physical significance. According to Eq. (56), the singularities of $\mathcal{R}$ correspond to values of $\Gamma(\mathbf{q}_\perp,\omega)$ which are eigenvalues of the operator $-\nabla_z^2$. Since this operator is self-adjoint for the given boundary conditions, its eigenvalues must be real. Hence, according to Eq. (91), the frequencies ω corresponding to these singularities of $\mathcal{R}$ must be complex. From its definition, Eq. (89), the function C^+ is regular in the region $\operatorname{Im}\omega > 0$, and therefore each singular value of ω can be written as $-\iota/\tau$. Evaluating the Fourier transform over ω in Eq. (96), these singularities yield contributions with a time dependence $\exp(-|t|/\tau)$, indicating that the set of τ's are the relaxation times of the various modes. In the case of an infinite system one would obtain a continuous spectrum, with the relaxation times $\tau(q_z)$ being continuous functions of q_z. The finiteness of the smectic membrane in the z direction leads to quantization and as a result produces a discrete spectrum.

To calculate the characteristic times, one needs to find the roots of the denominator in Eq. (58). The denominator is zero if

$$\tan(wZ) = \frac{2Z}{Z^2-1}, \tag{97}$$

where $v = \lambda q_\perp^2 L$ and $w = \gamma q_\perp^2 L/B$ were defined in Eq. (59) and $Z = -\iota v/w$. The singular values of v define the singular values of Γ, which in turn determine via Eq. (91) the corresponding singular values of ω. The relaxation times are now the roots of the equation

$$\rho_0 \frac{1}{\tau^2} - \eta_3 q_\perp^2 \frac{1}{\tau} + Kq_\perp^4 + \frac{\gamma^2 q_\perp^4}{B} Z_m^2 = 0, \tag{98}$$

where the Z_m are the roots of Eq. (97) and will be ordered as $Z_1 < Z_2 < Z_3 < \cdots$. Hence, for any Z_m, we find two characteristic times. The larger one corresponds to the slow mode, the other to the fast mode. Expanding Eq. (97) in powers of w leads to

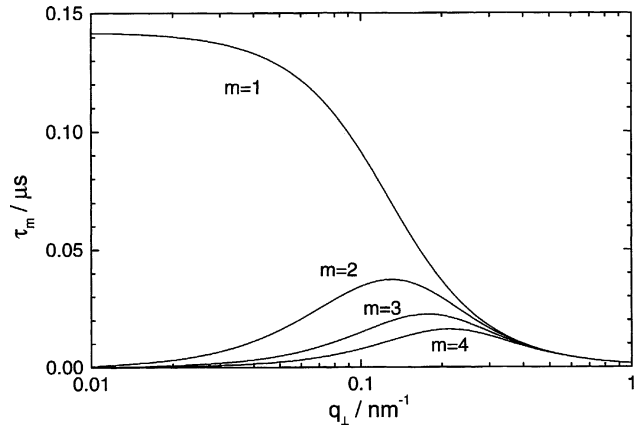

FIG. 26. Relaxation times τ_m, $m=1,2,3,4$ vs in-plane wave-vector transfer for a 50-layer membrane in the noninertial approximation (calculated for 4O.8 parameters from Table III).

$$Z_1^2 \simeq \frac{2}{w} - \frac{1}{3} = \frac{2B}{\gamma L q_\perp^2} - \frac{1}{3}. \tag{99}$$

Inserting this result in Eq. (98) gives

$$\rho_0 \frac{1}{\tau_1^2} - \eta_3 q_\perp^2 \frac{1}{\tau_1} + K\left(1 - \frac{\gamma^2}{3KB}\right) q_\perp^4 + \left(\frac{2\gamma}{L}\right) q_\perp^2 = 0. \tag{100}$$

As a starting point we shall neglect inertia, which means disregarding the first quadratic term in τ. In this *no-inertia approximation* the lowest-order solution is

$$\tau_1 \simeq \eta_3 \left[\frac{2\gamma}{L} + \left(1 - \frac{\gamma^2}{3KB}\right) K q_\perp^2\right]^{-1}. \tag{101}$$

This expression is valid only for $q_\perp^2 \ll B/\gamma L$. For $q_\perp = 0$ it agrees with the result of Poniewierski *et al.* (1998):

$$\tau_1 = \frac{\eta_3 L}{2\gamma}. \tag{102}$$

Note that, in this range of $q_\perp$, τ_1 decreases with $q_\perp$ if $\gamma^2 < 3KB$ and increases if $\gamma^2 > 3KB$. The first situation always applies in the limit $B \to \infty$. A more detailed consideration shows that for $q_\perp = 0$ only the first relaxation time is nonzero, while all the others vanish in the no-inertia approximation. Figure 26 shows the first few characteristic times versus $q_\perp$.

As stressed above, in the long-wavelength limit the inertia term has to be taken into account. Expanding the roots of Eq. (100) in powers of $q_\perp$, we obtain

$$\frac{1}{\tau_1} \simeq \mp \iota \frac{1}{2} \sqrt{\frac{8\gamma}{\rho_0 L}} q_\perp + \frac{\eta_3}{2\rho_0} q_\perp^2. \tag{103}$$

As we can see, the relaxation time becomes complex. Moreover, in this approximation τ is no longer finite for $q_\perp \to 0$. The relaxation times depend on the wave number $q_\perp$, and are real only for sufficiently large $q_\perp$. For

$$q_\perp^2 < q_{\perp fs}^2 = \frac{8\rho_0\gamma}{L(\eta_3^2 - 4\rho_0 K)} \simeq \frac{8\rho_0\gamma}{L\eta_3^2}, \tag{104}$$

the roots of Eq. (103) are complex. Again using the 4O.8 parameters from Table III, this criterion yields $q_{\perp fs} < 1.3 \times 10^{-3}$ nm^{-1}. For $q_\perp < q_{\perp fs}$ we can write $\tau = \tau' \pm \iota\tau''$ with real and positive values of τ' and τ''. The value $(\tau'^2 + \tau''^2)/\tau'$ is the characteristic time for exponential decay, while $\tau''/(\tau'^2 + \tau''^2)$ determines the frequency of the oscillations.

4. High-compressibility approximation

In the case of thin films that undulate conformally we can neglect the layer compressibility and assume B to be infinitely large. In this limit the correlation function does not depend on z and z', and the film can be considered as a two-dimensional system. Taking the limit $B \to \infty$ in Eq. (95), which requires some cumbersome calulations, we arrive at

$$C(\mathbf{q}_\perp, \omega) = \frac{2k_B T}{L\omega} \mathrm{Im}\left[\frac{2\gamma}{L} q_\perp^2 + K q_\perp^4 - \rho_0 \omega^2 - \iota\omega\eta_3 q_\perp^2\right]^{-1}. \tag{105}$$

As before the singular points of this function define the characteristic times. Using $\omega = -\iota/\tau$ we obtain Eq. (100) with $B \to \infty$. For small $q_\perp$ this yields the same relaxation times as Eq. (103): the real parts of the roots are positive, while their imaginary parts are equal but of opposite sign. Let us denote the roots as τ_s and τ_f, in which the indices stand for slow and fast, respectively. Fourier transformation of Eq. (105) yields

$$\begin{aligned} C(\mathbf{q}_\perp, t) &= \frac{1}{2\pi} \int_{-\infty}^{\infty} d\omega e^{-\iota\omega t} C(\mathbf{q}_\perp, \omega) \\ &= \frac{2k_B T \tau_s \tau_f}{L\rho_0(\tau_s - \tau_f)} [\tau_s \exp(-|t|/\tau_s) \\ &\quad - \tau_f \exp(-|t|/\tau_f)]. \end{aligned} \tag{106}$$

The relaxation times τ_s and τ_f depend on the wave number $q_\perp$ and, for sufficiently large $q_\perp$, both relaxation times are real. In the range of large $q_\perp$ values Eq. (106) describes relaxation with a single characteristic time τ_s.

To find out how the result affects the x-ray scattering, we calculate the time-dependent part of the intensity. We recall that for a thin conformally undulating film the displacement-displacement correlation function is independent of the layer numbers m and n. Therefore Eq. (73) becomes

$$\begin{aligned} S(\mathbf{q}, t) \propto \int\int dx dy \exp\Big(&-\iota(q_x x + q_y y) - \frac{1}{2}(\Delta q_x x)^2 \\ &- \frac{1}{2}(\Delta q_y y)^2\Big) \exp\Big(-\frac{1}{2} q_z^2 g(r_\perp, t)\Big). \end{aligned} \tag{107}$$

As the resolution Δq_y is usually an order of magnitude larger than Δq_x, the corresponding exponential can be approximated by a delta function, which reduces the integration in Eq. (107) to the x direction only. Finally the correlation function is calculated from

$$g(r_\perp,t)=\frac{1}{\pi}\int_{2\pi/\Lambda}^{2\pi/a} dq_\perp q_\perp [C(q_\perp,0) - J_0(r_\perp q_\perp)C(q_\perp,t)], \tag{108}$$

in which $C(q_\perp,t)$ is given by Eq. (96). Equations (106), (107), and (108) allow us to calculate the intensity-intensity correlation function measured in coherent x-ray experiments.

C. Dynamic x-ray experiments

1. X-ray photon correlation spectroscopy

Let us start with a discussion of the coherent properties of synchrotron radiation. The longitudinal coherence length ξ_l associated with electromagnetic radiation is the distance along the direction of propagation at which two plane waves with wavelength λ and $\lambda-\Delta\lambda$ are in phase (Als-Nielsen and McMorrow, 2000; Lengeler, 2001). Expressed in wavelength units, this length is inversely proportional to the degree of monochromaticity $\Delta\lambda/\lambda=\Delta E/E$ of the beam. Hence we find

$$\xi_l \simeq \frac{\lambda}{2(\Delta E/E)}. \tag{109}$$

The transverse coherence length ξ_t is defined in the plane perpendicular to the direction of propagation. It is related to the deviations from a perfectly planar wave front and is thus inversely proportional to the source size s scaled to the distance R. Hence we find

$$\xi_t \simeq \frac{\lambda R}{2s}. \tag{110}$$

Clearly the sample to be studied should be effectively positioned inside the coherence volume thus defined. The coherent intensity is proportional to the second power of the wavelength (Attwood *et al.*, 1985):

$$I_{\mathrm{coh}} \propto \lambda^2 \mathcal{B}(\Delta E/E), \tag{111}$$

where $\mathcal{B}$ is the brilliance of the source. The equations for the coherence volume and intensity are quite general. The "problem" of applying these results to x rays lies in the resulting numbers for the small wavelengths involved. At the Troika undulator beamline at the ESRF (Grenoble, France), typically the following values for the coherence of the beam can be reached for $\lambda \simeq 0.1$ nm (Grübel and Abernathy, 1997). The longitudinal coherence length is $\xi_l \simeq 1.7$ μm for a relative bandwidth $\Delta E/E \simeq 6\times10^{-5}$ set by a Si(220) monochromator. At a distance $R=46$ m from the anisotropic effective source, the transverse coherence lengths are about 4 and 150 μm in the horizontal and the vertical directions, respectively. From Eq. (111) it will be clear that soft x rays (say $\lambda>1$ nm) can be used advantageously, but their application is limited by the attendant increased absorption.

An x-ray beam impinging on a smectic membrane defines an illuminated volume and a coherence volume (Lengeler, 2001), which in general will be anisotropic. A transverse coherence area is defined by the product of the two transverse coherence lengths projected on the sample surface. Along the beam, coherent illumination means that the maximum path-length difference Δ has to be smaller than ξ_l. The ratio between the dimensions of the coherence volume and those of the illuminated volume of the sample determines what is measured. When in a particular situation the coherence volume is smaller than the illuminated one, the total scattered intensity is the sum of the intensities scattered from each "coherence domain" (cf. Sec. IV.A.2). In the reverse case, the signal results from the sum of the amplitudes of the scattered photons. In the z direction perpendicular to a smectic membrane, the maximum path-length difference Δ is reached for reflections from the top and bottom interfaces. This difference depends on the thickness of the membrane and on the incoming angle via $\Delta = 2L\sin\alpha$. For the value $\xi_l \simeq 1.7$ μm given above and $\alpha \simeq 1.5°$, a typical Bragg position, this gives a maximum thickness $L_{\max} \simeq 30$ μm. Up to a thickness of this order of magnitude, Kiessig fringes due to the interference of x rays from the top and bottom of a film can be observed (compare Sec. IV.A.1). Real experiments will also depend on the detector resolution, which has here been assumed to be sufficient.

Along the surface of a smectic membrane the illuminated area is in general much larger than the coherence area. To observe interference effects in this direction, it is necessary to reduce the dimensions of the beam to a size comparable to ξ_t. The coherently reflected waves then interfere, creating a speckle pattern. Motion of the scatterers is observed by analyzing the intensity variation of a single speckle in time. At delay times τ short compared to a typical time scale τ_0 of the membrane, the intensity is correlated with the initial intensity. Conversely, for large delay times the position of the scatterers will be independent of the initial one. At intermediate time scales a transition is observed corresponding to τ_0. More formally the intensity-intensity autocorrelation function is measured, which is defined as $\langle I(\mathbf{q},t)I(\mathbf{q},t+\tau)\rangle$. Normalizing this function and setting the time axis such that the origin coincides with the beginning of the experiment, we can write

$$g_2(\mathbf{q},\tau)=\frac{\langle I(\mathbf{q},0)I(\mathbf{q},\tau)\rangle}{\langle I(\mathbf{q},0)\rangle^2}. \tag{112}$$

In practice the required reduction of the illuminated area is realized by positioning a pinhole of dimensions comparable to ξ_t in the beam before the sample. The situation can be compared with a single-slit experiment in visible optics. The pinhole acts as a secondary coherent source, creating the well-known Fraunhofer pattern on a far-field screen, but now on the scale of x-ray wavelengths (Robinson *et al.*, 1995; Vlieg *et al.*, 1997). Clearly this procedure cuts down the emitted intensity considerably, while the small size of the pinhole creates at the same time a very high resolution. One of the virtues of smectic membranes as model systems for x-ray photon correlation spectroscopy is that they combine an appro-

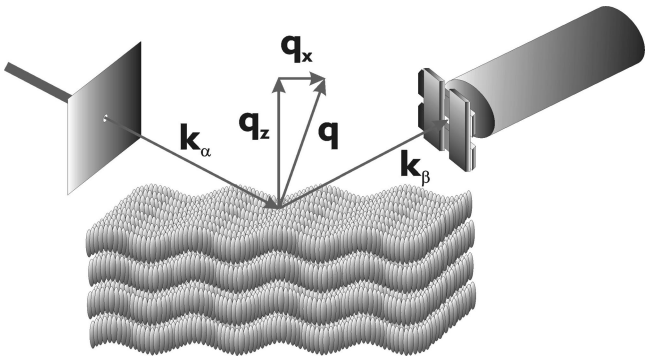

FIG. 27. Scheme of the experimental setup for x-ray photon correlation spectroscopy.

priate thickness $L \lesssim \Delta$ with a small mosaic comparable to the experimental resolution.

In the experiments to be discussed (Fera *et al.*, 2000; Sikharulidze *et al.*, 2002) at beamline ID10A (Troika I, ESRF), at about 46 m from the storage ring a pinhole of approximately 10 μm diameter was placed 0.25 m upstream of the sample to provide a collimated and partially coherent beam (see Fig. 27). Typically this reduced the intensity from about 10^{14} cts/s to about 10^8 cts/s. Smectic membranes were mounted vertically in a reflection geometry and illuminated with 8-keV radiation. Most experiments so far have been done at the Bragg position on the specular ridge, but some measurements have also been made at off-specular positions ($q_x \neq 0$) by rocking the sample.

Fundamentally the time scales that can be reached by x-ray photon correlation spectroscopy are limited by the pulsed structure of the synchrotron source, in which the electrons or positrons go around in very narrow bunches. At the ESRF the revolution time is 2.8 μs, and the minimum time that can be correlated depends on the bunch structure of the ring, in particular the bunch-to-bunch interval. Constant spacings are required to avoid spurious signals generated by the revolution time and its higher harmonics. In the so-called uniform-filling mode 992 bunches are equally spaced in the storage ring at 2.8-ns intervals, which sets the fundamental lower limit. Using avalanche photodiodes as detectors, which can have an intrinsic time response down to a few ns (Baron, 2000), this limit can be reached. In practical experiments a final limit is determined by the availability of fast correlators. Standard commercial correlators nowadays allow a minimum lag time of about 10 ns, but certainly this can be improved. An alternative way to determine the auto-correlation function is to store the arrival times of all individual pulses from the detector in a buffer memory (Fera *et al.*, 2000). Subsequently the stored data can be used to construct the autocorrelation function using appropriate software.

2. Results for smectic-A membranes

Sorensen and co-workers (Price *et al.*, 1999) performed the first measurements of smectic membranes by x-ray photon correlation spectroscopy employing soft x

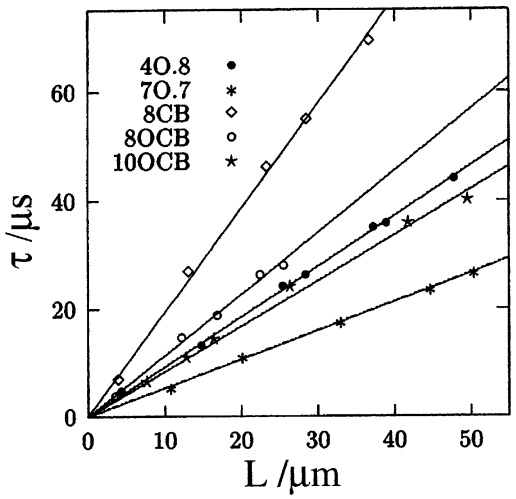

FIG. 28. Fundamental relaxation time as a function of film thickness for various compounds (Price *et al.*, 1999). The straight lines are fits to Eq. (102).

rays at a wavelength of 4.4 nm. The measurements were centered on the specular ridge at the Bragg position. For several compounds a single exponential decay was observed in the range of tens of μs, which depends linearly on the membrane thickness (see Fig. 28). The fluctuations can be expected to be dominated by the lowest-order surface mode, in which case the decay time is given by Eq. (102). The results are consistent with the theoretically expected linear dependence of the decay time on the thickness. The slope η_3/γ for each of the linear relations in Fig. 28 can be compared with independent measurements of η_3 and γ. As far as these values are available, the results are in good agreement. The largest wavelength in a finite-size membrane is determined by the size of the frame. In coherent x-ray experiments the largest wavelength detected would be determined instead by the footprint, or projected coherence length, at the given q_z position (Hołyst, 1991; Shalaginov and Sullivan, 2000). For the soft x rays used, $\xi_t \simeq 35$ μm. At the Bragg angle this gives a coherent footprint along the beam of about 50 μm, and the dominating wavelengths in the fluctuation spectrum can be expected around this value.

de Jeu and co-workers have shown the feasibility of performing x-ray photon correlation spectroscopy using standard x rays with a wavelength around 0.1 nm (Fera *et al.*, 2000; Sikharulidze *et al.*, 2002). They could realize film mosaics as low as 2 mdeg, which matches the high resolution in the experiments that results from the small pinhole. As a consequence at the Bragg position count rates as high as 100 MHz were obtained, allowing a considerable increase in the quality of the measurement. The results for a few moderately thick films are in agreement with those of Fig. 28. More interestingly a rather different behavior was found in thin films. Figure 29 shows experimental data for 4O.8 membranes of various thicknesses. For the thinnest membranes the correlation function shows a decay of the layer fluctuations in the time scale of μs and oscillatory behavior in the range of

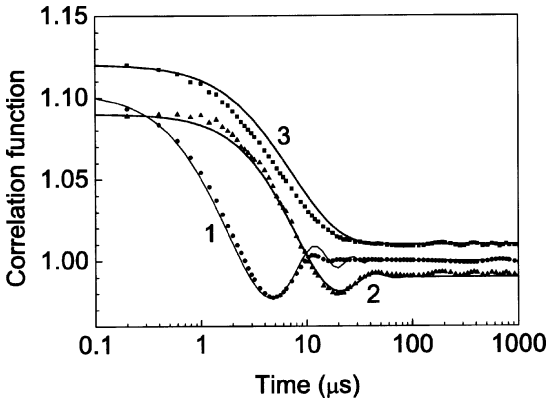

FIG. 29. Autocorrelation function at q_0 for 4O.8 membranes of various thicknesses; ●, $L=0.3$ μm; ▲, $L=4.0$ μm; ■, $L=7.0$ μm. Solid lines are fits with the parameters $\gamma=0.021$ N/m, $K=5\times10^{-12}$ N, $\eta_3=0.05$ kg/(m s), $\rho_0=103$ kg/m^3, $\Delta q_x=5\times10^{-5}$ nm^{-1}. Λ values are 180, 160, and 50 μm, for the curves 1, 2, and 3, respectively. Curves 2 and 3 have been shifted for clarity. From Sikharulidze *et al.*, 2002.

tens of μs. The oscillations become less pronounced and finally disappear with increasing membrane thickness. This can be contrasted with membranes of the compound FPP, which show oscillations up to the largest thickness (15 μm) reached experimentally. Figure 30 shows a series of off-specular measurements of this compound. At the specular ridge (curve 1) the data show oscillatory behavior, but even for a small offset in q_x corresponding to 25 mdeg the oscillations disappear. The relaxation times have also moved to values well below 1 μs.

The normalized experimental intensity-intensity correlation functions were fitted for both 4O.8 and FPP to the expression $aS^2(t)+b$, where a and b are constants indicating contrast and offset, and $S(t)$ is the dynamic structure factor. For a thin uniformly undulating film the

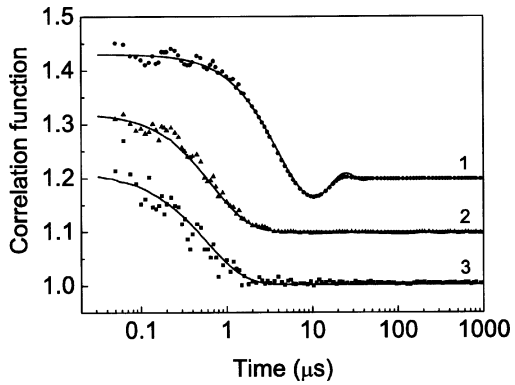

FIG. 30. Autocorrelation functions of a 2.83-μm-thick FPP membrane at q_0; ●, specular Bragg position at $q_x=0$; ▲, at an offset $q_x=0.95\times10^{-3}$ nm^{-1}; ■, at $q_x=3.8\times10^{-3}$ nm^{-1}. Solid lines are fits with the parameters $\gamma=0.013$ N/m, $K=10^{-11}$ N, $\eta_3=0.015$ kg/(m s), $\rho_0=103$ kg/m^3, $\Delta q_x=9\times10^{-5}$ nm^{-1}. Λ has been fitted to 90 μm. Curves 2 and 3 have been shifted by 0.25 and 0.50, respectively (Sikharulidze *et al.*, 2002).

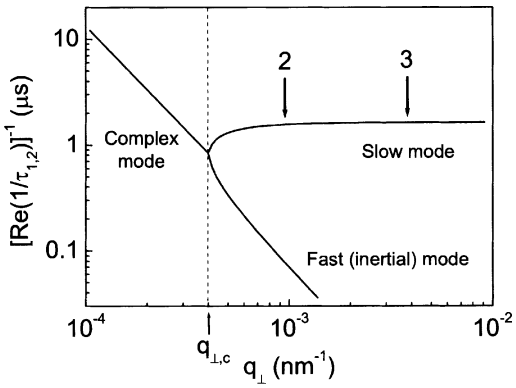

FIG. 31. Calculation of the lowest-order relaxation times of the FPP membrane of Fig. 30; $B=7.5\times10^8$ N/m^2. The arrows correspond to the off-specular positions of curves 2 and 3.

displacement-displacement correlation function is independent of layer numbers m and n and for $S(t)$ Eq. (107) can be used. In Eq. (108) for $g(r_\perp,t)$ the short-wavelength cutoff is defined by the intermolecular distance a, taken as 0.4 nm. The long-wavelength cutoff Λ influences the damping time and the form of the correlation function. In fitting the experimental curves Λ varies around 100 μm, which is compatible with the interpretation as a projected coherence length given above. Fluctuations with larger wavelengths could nevertheless still be important, as they also disturb the position of the scatterers. A proper implementation of the coherence and the resolution in the theory would probably introduce some weight function in Eq. (108), which would suppress the contribution of the longer wavelengths more smoothly. The fitting parameters for FPP agree very well with those in Table III from static measurements, those for 4O.8 less so. This reflects the large value of B for FPP, which makes the high-compressibility approximation used more appropriate than in the case of 4O.8.

The relaxation times can be found from Eq. (100) for $B\to\infty$; the relevant solutions are displayed in Fig. 31 using FPP parameters. Two roots, τ_{1s} and τ_{1f}, are found and the relaxation times are given by $[\mathrm{Re}(1/\tau_{1s})]^{-1}$ and $[\mathrm{Re}(1/\tau_{1f})]^{-1}$, respectively. For small values of $q_\perp$ the roots are complex-conjugate numbers, and both relaxation times coincide. This implies oscillatory damping of the fluctuations (complex mode). If $q_\perp$ exceeds a crossover value $q_{\perp fs}$, τ_{1s} and τ_{1f} are different real numbers corresponding to a slow and a fast relaxation. In this regime the correlation function shows simple exponential decay. The fast relaxation is related to the presence of the inertia term in Eq. (83). From Fig. 31 one notes that this relaxation time decreases rapidly with increasing $q_\perp$ and will not be accessible experimentally. The crossover wave number $q_{\perp fs}$ is determined by Eq. (104). The total signal measured at a specular position corresponds to the superposition of fluctuations with different wave vectors. The observed relaxation behavior depends strongly on the fluctuations with the longest wavelength detectable. If the crossover wave vector $q_{\perp fs}$ is within the integration interval of Eq. (108), the correlation function exhibits oscillatory damping. This situation cor-

responds to curve 1 of Fig. 30. As soon as $q_{\perp fs}$ is outside this integration interval, an exponential decay is observed. This region corresponds to curves 2 and 3 of Fig. 30. The slow relaxation branch in Fig. 31 exhibits a plateau for $q_\perp > q_{\perp fs}$ between 10^{-3} and 10^{-2} nm^{-1}. Indeed, in Fig. 30 no change in the experimental relaxation time is observed for the different off-specular positions in q_x. Larger offset positions could not be measured because of the rapidly decreasing count rate.

As $q_{\perp fs}$ scales with the membrane thickness as $1/\sqrt{L}$ we can use the parameter Λ to determine a cutoff thickness:

$$L_c = \frac{2\rho_0 \gamma}{\pi^2 \eta_3^2} \Lambda^2. \tag{113}$$

For membranes with $L < L_c$ oscillatory behavior will be pronounced. As the membrane thickness approaches L_c the oscillatory behavior starts to vanish and for $L > L_c$ only an exponential decay is observed. This is in agreement with the results for the 4O.8 membranes presented in Fig. 29. For FPP the viscosity η_3, as determined from the fits, is several times smaller than for 4O.8. According to Eq. (113) then L_c is an order of magnitude larger for FPP than for 4O.8. This is outside the experimental range of thicknesses studied and explains why the crossover was not observed.

In conclusion, the complex behavior predicted theoretically for the dynamics of smectic fluctuations has been observed for membranes of different types of liquid-crystalline molecules. A crossover is found between an oscillatory and an exponential regime of fluctuation damping, as a function both of membrane thickness and of the off-specular wave-vector transfer.

D. Crystalline-B membranes as fluctuating systems

Crucial for our present understanding of the Cr-B phase is the existence of a (small) coupling between the crystalline layers leading to three-dimensional positional order (see Sec. II.A). According to the elastic theory for solid plates (Landau and Lifshitz, 1986), undulation of a thin plate gives rise to extension of one side (top or bottom) and compression of the other side. The bending rigidity in this case is on the order of L^2E, where L is the film thickness and E is Young's modulus. Estimating the order of magnitude of the bending rigidity using the value of E expected for a hexagonal two-dimensional crystal (Zakri *et al.*, 1997), one finds that the crystalline rigidity should drastically affect the diffuse x-ray scattering. However, in transverse diffuse scans, only small changes are seen between the results for Sm-A and Cr-B membranes [see Fig. 17(a)], which indicates that the rigidity remains nearly the same. The observed small bending rigidity is due to well-developed shear deformations in a Cr-B plate (Fera, Dolbnya, *et al.*, 2001).

Although the Cr-B phase has a finite shear modulus C_{44}, mechanical (Cagnon and Durand, 1980; Dubois-Violette *et al.*, 1993) and ultrasonic (Thiriet and Martinoty, 1982) studies indicate that its value is very small. Hence the conventional analysis of bending ignoring shear is not valid. Instead the *easy-shear approximation* can be used in which all in-plane deformations are neglected while shear deformations are large. The corresponding elastic energy can be written as (Shalaginov and Sullivan, 2000)

$$F = \frac{1}{2} \int d^3r \left[C_{33} (\nabla_z u)^2 + K (\Delta_\perp u)^2 + \frac{1}{4} C_{44} (\nabla_\perp u)^2 \right], \tag{114}$$

where the elastic modulus C_{33} is equivalent to the smectic compressibility B. However, the value of C_{33} may differ from that of B in the Sm-A phase. As the shear elastic coefficient C_{44} is finite but small, it is justified to keep the next-order term with respect to in-plane derivatives (the bending term), which is dominant in the smectic phase. A crucial consequence of shear elastic deformations is that they produce a bulk term proportional to $(\nabla_\perp u)^2$, which is forbidden for smectic phases in which the layers slide freely. The absence of such a term leads to the Landau-Peierls instability of bulk smectics. Any finite value of C_{44} makes the mean-square fluctuations converge independently of the size of the system. This point has been demonstrated in Fig. 23(a), Sec. IV.C.3, for Sm-A and Cr-B membranes of different thickness. Specular reflectivity scans show that in the Cr-B phase the amplitude of the fluctuations in the interior of the film does not depend on the thickness.

Shalaginov and Sullivan (2000) have extended the continuous dynamic model of Sm-A to make predictions for the dynamic behavior of Cr-B membranes. Introducing boundary conditions to Eq. (114), one can still write the resulting fundamental relaxation time as Eq. (103), but with γ replaced by

$$\gamma_{\text{eff}} = \gamma + L C_{44}/8. \tag{115}$$

As far as the fundamental relaxation is concerned, a thin Cr-B film is in the easy-shear approximation equivalent to a Sm-A membrane, the effect of C_{44} being essentially a renormalization of γ. Using $\gamma = 0.02$ N/m (Mach, Huang, *et al.*, 1998) and $C_{44} = 0.12 \times 10^6$ N/m^2 (Cagnon and Durand, 1980; Pindak *et al.*, 1980), we calculate that according to Eq. (115) the correction to γ becomes appreciable only for rather thick films and is equal to γ for about 450 layers. This explains the equivalence between specular and diffuse reflectivity results on Sm-A and Cr-B membranes in Fig. 17. The remaining difference between the results can be accounted for by an increase of the effective surface tension γ_{eff} from 0.02 N/m to about 0.03 N/m.

The dynamic nature of the fluctuations in Cr-B membranes has been explicitly demonstrated by a measurement of the intensity-intensity autocorrelation function $g_{(2)}(\mathbf{q},t)$; see Fig. 32. The behavior of the correlation function is very similar to that in Fig. 29 for Sm-A films. In fact, the associated times hardly change upon heating from the Cr-B into the Sm-A phase. As the thickness of the investigated membrane ($L = 0.27$ μm, $N = 95$) is well below the value of 450 layers calculated above, this is indeed as expected. Like for Sm-A films (Sec. V.B.3) in

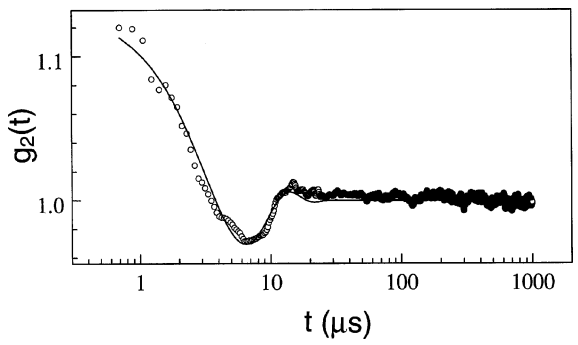

FIG. 32. Normalized autocorrelation function at q_0 of a 0.27-μm-thick 4O.8 membrane in the Cr-B phase (Fera, Dolbnya, *et al.*, 2001).

the thin-film regime, inertia cannot be neglected and the autocorrelation function of a Cr-B film also shows oscillatory behavior. Because the C_{44} term in γ_{eff} is still small, these oscillations result from inertial effects due to surface tension rather than shear effects.

In conclusion, the main effect of the crystallinity of Cr-B membranes can be incorporated for thin films by a renormalization of the surface tension [see Eq. (115)]. This explains why Cr-B membranes, like Sm-A membranes, can only exist when spanned on a frame. It also allows the material to flow (slowly) under the influence of external forces, so that the surface area can be changed.

E. Conclusions and outlook

The study of the dynamics of smectic fluctuations is still in its early stages. In Sm-A membranes only the first fundamental surface mode has been observed, which depends on the surface tension γ. In addition the effects of inertia, leading to complex behavior, have been seen in thin films and at off-specular positions. Several problems still remain to be investigated:

- Can the higher-order (elastic) modes, which also depend on K and B, be observed? This requires further measurements at off-specular positions, in which situation the intensity decreases steeply.
- Can the fast (inertial) mode be measured? This might be possible by extending the time scale of x-ray photon correlation spectroscopy to a few ns, and then continuing to faster times with neutron spin echo techniques.
- What is the role of the long-wavelength cutoff Λ? Further investigations are needed regarding its possible relation to the projected coherence length. A proper implementation of coherence and resolution in the theory would probably introduce some weight function instead of a simple cutoff, which would suppress the contribution of the longer wavelengths more smoothly.
- How do thick membranes fit into the picture? The theoretical model has so far been restricted to thin membranes. No expression is available for the limit $L\to\infty$, for which the relaxation spectrum is continuous rather than discrete.

Thermally driven fluctuations in thin Cr-B films are remarkably similar to those in Sm-A membranes. The limits of this behavior for thicker films, for which the shear elastic constant C_{44} becomes dominant, still have to be investigated.

VI. MISCELLANEOUS TOPICS

A. Thinning transitions

Smectic membranes can in many cases be heated above the bulk smectic disordering temperature without immediately rupturing, and instead undergo successive layer-by-layer thinning transitions as the temperature is increased. Though the effect was observed relatively early (Böttger *et al.*, 1988), the field really started to develop with the work of Huang and co-workers (Stoebe *et al.*, 1994; Johnson *et al.*, 1997; Pankratz *et al.*, 1998). An example is shown in Fig. 33. Thinning transitions have been found rather systematically at the Sm-A–isotropic transition of fluorinated liquid-crystalline compounds, and less so in their nonfluorinated counterparts. However, the thinning phenomenon observed in 54COOBC (Jin *et al.*, 1996) indicates that the nature of this process must be more universal. Moreover, thinning transitions have also been found at the Sm-A–nematic phase transition (Demikhov *et al.*, 1995; Mol *et al.*, 1998). A key experimental observable is the variation of the layer-thinning transition temperature $T_c(N)$ with the number of film layers N, which is found to be well fit by the power-law relation $N\propto t^{-\nu}$, where $t=[T_c(N)-T_0]/T_0$, $\nu\simeq 0.70\pm 0.10$, and T_0 is close to the bulk transition temperature (see Fig. 33).

The persistence of smectic layering in an overheated membrane can be attributed to enhanced ordering associated with the free surfaces of the film, as is known to occur in other contexts. As discussed at the end of Sec. IV.B.1, in that situation one expects $\gamma/\sqrt{BK}>1$. Such fluctuation profiles have been given in Fig. 24 for the compound 7AB near the Sm-A–nematic phase transition, where thinning occurs. This situation provides direct evidence that melting during the thinning process occurs at the innermost layers. Unfortunately the surface damping behavior of the fluctuation profile has not been investigated near the smectic-isotropic transition temperature. In fact, FPP, the only fluorinated compound for which the fluctuation profile has been measured, gives at lower temperatures $\gamma/\sqrt{BK}<1$. Preliminary experiments indicate that this ratio might increase to values larger than one upon approaching the isotropic phase. Another observation is that layer thinning is not a homogeneous process in the smectic plane, but involves nucleation and development of dislocation loops (Pankratz *et al.*, 1999, 2000).

Theoretically there is no clear consensus about the mechanism by which layer thinning occurs. According to

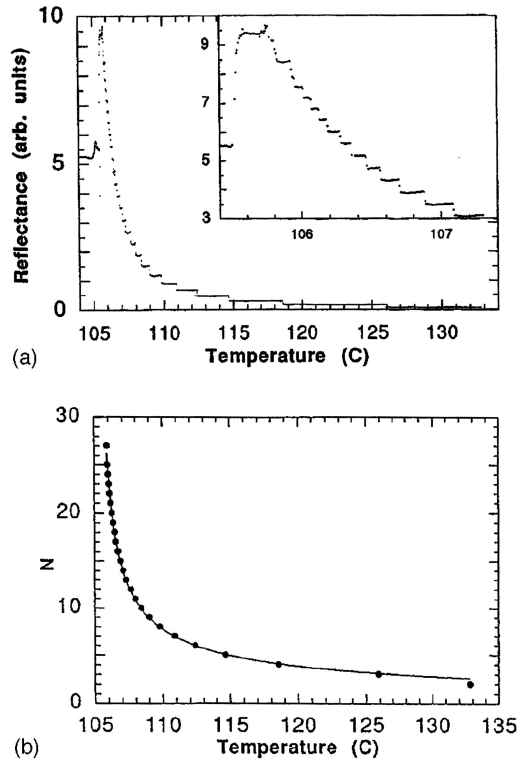

FIG. 33. Thinning transitions of the compound F3MOCPF6H5OB (Pankratz *et al.*, 1998): (a) thinning sequence as obtained from the reflectance in the bulk isotropic temperature range; (b) plot of N vs $T_c(N)$ giving an exponent $\zeta=0.61$.

one set of theories (Mirantsev, 1996; Martínez-Ratón *et al.*, 1997; Gorodetskii *et al.*, 1999; Shalaginov and Sullivan, 2001), thinning takes place when the smectic layer structure in the middle of a film vanishes. In an alternative theory (Pankratz *et al.*, 1999), supported by experimental studies (Pankratz *et al.*, 2000), layer thinning occurs by spontaneous nucleation of dislocation loops prior to the melting of the layer structure in the film interior. This inhomogeneous mechanism is not necessarily unrelated to the former, since a sufficient reduction in the degree of interior smectic ordering is required for it to proceed. Various mathematical relations (Gorodetskii *et al.*, 1999; Pankratz *et al.*, 1999; Picano *et al.*, 2001) and upper bounds (Shalaginov and Sullivan, 2001) for $T_c(N)$ have been derived theoretically. With appropriate fitting parameters, these alternative relations all agree well with the power-law expression and thus are not able to distinguish between the various mechanisms.

At present it is not clear whether the experimental results on thinning at (first-order) smectic-isotropic transitions and (second- and first-order) smectic-nematic transitions all can be treated within the same framework. Another question is the special role of fluorinated compounds. Although there is some progress in the understanding of static inhomogeneities (Picano *et al.*, 2001), a theoretical model that describes dynamic processes in inhomogeneously thinning films has yet to be developed. In practice, dislocation-mediated thinning of an overheated smectic membrane may preempt a uniform thinning mechanism. In this way for a given N thinning occurs at a lower temperature than that predicted by considering a purely uniform film (Shalaginov and Sullivan, 2001).

We conclude that, in spite of considerable theoretical effort, no full understanding of the layer-thinning phenomenon has been reached to date. Experimental data on fluctuation profiles over smectic membranes at the thinning transitions are very much needed.

B. Smectic membranes of chiral molecules

The structure and origin of the polar behavior of tilted smectic liquid crystals formed by chiral molecules have been intensely debated over the last decade; reviews have been given by Goodby *et al.* (1991), Fukuda *et al.* (1994), and Lagerwall (1999). These phases are of technological importance due to their potential as fast and low-voltage electro-optical switches. In addition to Sm-A a variety of tilted smectic phases exist in which the average orientation of the long molecular axis with respect to the layer normal $\mathbf{z}$ is described by a tilt angle $\theta(z)$ and an azimuthal angle $\varphi(z)$. In the case of the classical Sm-C phase the azimuthal orientations in adjacent layers are in the same direction: $\varphi(z)$ is constant. Such a synclinic ordering leads to ferroelectricity in a Sm-C phase of chiral molecules (Sm-C*). The symmetry allows in each layer for a spontaneous electric polarization P along $\mathbf{n}\times\mathbf{z}$ (perpendicular to the tilt plane; Meyer *et al.*, 1975). In addition, the molecular chirality generates a helical twist with a pitch of the order of microns due to the azimuthal angle's varying slowly from one layer to another. For opposite tilt directions of adjacent layers, the resulting anticlinic ordering corresponds to an antiferroelectric Sm-C_A^* phase in which the polarization direction alternates from layer to layer. Tilted phases with ferrielectric (Sm-C_γ^*) and mixed antiferroelectric–ferrielectric (Sm-C_α^*) properties have also been identified (Fukuda *et al.*, 1994). On the temperature scale the order is usually

$$\text{Sm-C}_\text{A}^*\leftrightarrow\text{Sm-C}_\gamma^*\leftrightarrow\text{Sm-C}^*\leftrightarrow\text{Sm-C}_\alpha^*\leftrightarrow\text{Sm-A}.$$

An alternative route to polar order has been discovered in fluid smectic phases of achiral molecules with a bent core (Niori *et al.*, 1996) and in polymer-monomer mixtures (Soto Bustamante *et al.*, 1996). In these phases the macroscopic ordering of molecular subunits results in polar smectic layers, which can be arranged in tilted synclinic or anticlinic assemblies (Brand *et al.*, 1998; Diele *et al.*, 1998; Link *et al.*, 1999; Link *et al.*, 2000).

Smectic membranes have been extensively used to obtain structural information from well-ordered samples. The director field in the Sm-C_γ^* and the Sm-C_α^* phase is characterized by a complex distribution of the molecular tilt, and the exact interlayer structure of these phases is still subject to debate. A first structural model was based on the one-dimensional Ising model (Isozaki *et al.*, 1993;

Fukuda *et al.*, 1994). It predicted an infinitely large number of structural states ("devil's staircase") characterized by various sequences of synclinic/anticlinic interfaces. Alternative "clock models" assume a discrete variation of the azimuthal angle $\Delta\varphi = 2\pi/k$ across the layers, where k is an integer (Čepič and Žekš, 1995; Lorman, 1995). The integer value of k is 3 or 4 in the various ferrielectric phases and varies continuously from 5 to larger values in the Sm-C^*_α phase.

Resonant x-ray scattering has proved to be a powerful tool for discriminating between the various modulated structures (Mach, Pinďak, *et al.*, 1998; Levelut and Pansu, 1999; Mach *et al.*, 1999). In such an experiment the x-ray energy is selected at the absorption edge of one of the atoms of the molecule. Due to the anisotropic environment of this resonant atom, both the polarization and the phase of the scattered radiation depend on the orientation of the molecule with respect to the polarization of the incident beam. This leads to additional satellite peaks not observed in conventional x-ray diffraction. The results obtained so far with sulfur, bromine, and selenium as resonant atoms, provide direct evidence of three-layer and four-layer superlattices in the ferrielectric phases, which is consistent with the clock model. Figure 34 shows an example of resonant scattering from a thick smectic membrane of the compound 10OTBBB1M7 at the sulfur K-edge. Note the peaks at 1/4, 1/3, and 1/2 integral values, characteristic of a four-layer, three-layer, and two-layer (antiferroelectric) superlattice periodicity, respectively. Because the pitch of the induced helix is in the optical range, the proposed structures are intrinsically uniaxial. In contrast, optical measurements (optical rotatory power, ellipsometry) indicate that the Sm-C* subphases are highly biaxial (Akizuki *et al.*, 1999; Johnson *et al.*, 2000). The latter observations rule out a simple uniaxial clock model and favor a biaxial structure with out-of-plane distortions. These different structural models for ferrielectric phases can be reconciled by assuming three- and four-layer superstructures with a nearly planar configuration and azimuthal deviations of about twenty degrees.

The picture sketched so far is in practice more complicated because the ordering is strongly influenced by finite-size and surface effects. For example, as mentioned in Sec. III.A.5 for a Sm-A–Sm-C transition, a free surface often induces a tilt, causing the Sm-C phase to grow continuously from the surface into the Sm-A interior of the film as T_{CA} is approached from above. As a consequence a tilt-magnitude profile $\theta(z)$ appears across the film. For Sm-C films this will be accompanied by a tilt-direction profile $\varphi(z)$. The combination of x-ray reflectivity and optical ellipsometry allows us to determine both profiles (Fera, Opitz, *et al.*, 2001).

The physics and chemistry of the different ferroelectric phases, due either to intrinsic chirality or to the banana shape of the molecules, is at the time of this writing still under development. Though important structural conclusions have been reached regarding the different types of Sm-C* phases, one should not be surprised at the observation of new variations.

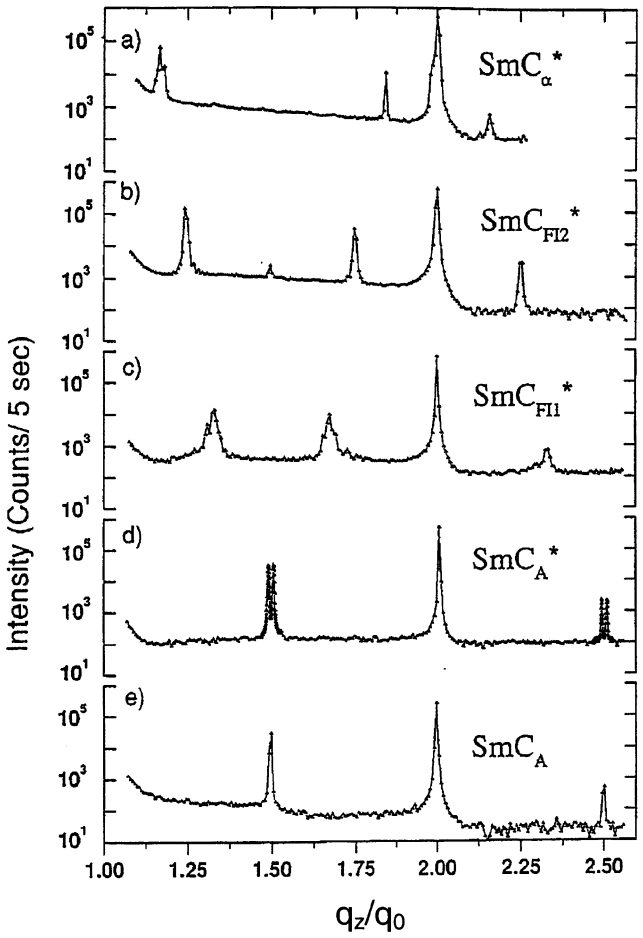

FIG. 34. Anomalous x-ray scattering in the various types of chiral C* phase (Mach, Pindak, *et al.*, 1998).

C. Smectic films on a substrate

Ordered smectic films on a substrate can be obtained by conventional techniques like spin coating (Olbrich *et al.*, 1993; Shi *et al.*, 1993) or the Langmuir-Blodgett method (Geer *et al.*, 1995). In both cases the resulting film will be aligned due to anchoring forces at the film-air and film-substrate interfaces. Homeotropic anchoring of the molecules at the air-film surface leads to smectic layering parallel to that interface, which is quite common for many classes of liquid crystals. The anchoring at the film-substrate interface might be either homeotropic or planar, or with an intermediate tilt of the director (Blinov and Chigrinov, 1994). It can be modified and controlled by mechanical and/or chemical treatment of the substrate. In the case of conflicting anchoring at the two interfaces, a complex director distribution is found across the film.

Thin liquid-crystalline films on a solid substrate are often unstable with respect to dewetting, like isotropic liquid films. The dewetting proceeds via an increase of the average roughness at the free surface. At a certain

stage large-size holes can be formed, which may reach the initial film thickness after prolonged annealing. Dewetting of thin liquid and polymer films on solid substrates has been attributed to two different mechanisms (Herminghaus *et al.*, 1998; Reiter *et al.*, 1999). The first is nucleation at defects and subsequent growth of the dewetted area. The second possibility is amplification of the thermal fluctuations at the free surface, leading to so-called spinodal dewetting. However, examples also exist in which a restructuring of the molecules at the substrate destabilizes the free surface (Demirel and Jérôme, 1999; Ostrovskii *et al.*, 2001). With regard to these points, liquid-crystal films do not behave very differently from organic films in general.

An alternative way to create smectic films on a substrate is to transfer freely suspended smectic membranes. In this way ultrathin and highly ordered supported molecular films can be produced on solid substrates like glass, mica, or silicon (Decher *et al.*, 1991; Maclennan *et al.*, 1991). This method is based on the possibility of inflating smectic membranes by external pressure to form bubbles similar to soap bubbles (Oswald, 1987; Stannarius and Cremer, 1998). The substrate is then moved towards the top of the smectic bubble until it touches and the film adheres. The preservation of uniform smectic layering after transfer has been confirmed by x-ray reflectivity. A comparison of transferred membranes and Langmuir-Blodgett films of the same material, found the ordering in the former films to be much more perfect than in the latter (Overney *et al.*, 1993). Nevertheless, for tilted Sm-C films characteristic features of the **c**-director field are lost during the transfer process. Examination of transferred films with an atomic force microscope indicates many small holes with a depth close to the total thickness of the film and a lateral size of tenths of microns (Chikina *et al.*, 1998). In this context one should realize that after transfer the meniscus is gone: the smectic "membrane" has changed into a smectic "film" and the tension is reduced to $\Gamma = \gamma_{\text{sm-air}} + \gamma_{\text{sm-solid}}$ [compare Eq. (28)]. In addition the curved shape of a membrane that does not perfectly match a flat substrate may play a role during the transfer. Transfer of a smectic membrane onto another membrane in a different phase has also been accomplished (Lucht and Bahr, 1997a).

In smectic membranes the lateral inhomogeneities are due to thermally induced layer fluctuations. In smectic films on a substrate another source of layer distortions is the propagation of static substrate roughness into the film. In this case the amplitude of the layer distortions decays exponentially with distance from the substrate (de Gennes and Prost, 1993). The characteristic decay length of a distortion with lateral wave number $q_\perp = 2\pi/r_\perp$ is given by $l(q_\perp) = 1/(\lambda q_\perp^2)$, where $\lambda = \sqrt{K/B}$. Because of the small compressibility of the system and the remarkable $q_\perp^{-2}$ dependence of the decay length, static layer undulations of long wavelengths penetrate deeply into the film. For typical values $\lambda \simeq 0.1$ nm and $q_\perp \simeq 0.01$, the decay length can be as large as tens of μm. At wavelengths for which the film thickness is smaller than the decay length, the film-air interface will reproduce conformally the static roughness of the substrate, and thermal fluctuations will be suppressed. In thicker films thermal fluctuations gradually take over, starting at short wavelength. The transition has been studied theoretically by de Boer (1999). The results account nicely for the experimental behavior observed for multilayers of smectic monomer-polymer mixtures by diffuse x-ray scattering (Geer and Shashidar 1995; Geer *et al.*, 1995). A similar crossover from conformal substrate roughness to capillary waves has been observed in thin liquid films (Tidswell *et al.*, 1991).

A vast literature exists on liquid and polymeric films, which has only been touched upon here. Though smectic films (monomeric and polymeric) have so far received limited attention in this context, they seem to fit rather well in the general pattern.

D. Surfactant and lipid membranes

Much of the discussion of the structure and fluctuations of smectic membranes so far can be applied to surfactant systems (lyotropic liquid crystals) and to membranes of biologically relevant materials. Stacks of surfactant membranes in solution can lead to a highly swollen phase. Examples are hydrated phospholipids, in which lipid bilayers alternate with water layers, and ternary systems of surfactants, water and oil, in which surfactant monolayers separate layers of water and oil. A wide range of periodicity can be found (1–100 nm), which can be tuned by a proper adjustment of the dilution. The total interactions are usually understood as involving several contributions. At small interlayer distances an exponentially decaying repulsive force (the *hydration force*) occurs, which is related to the osmotic pressure. In that situation it balances the attractive van der Waals interactions (Rand and Parsegian, 1989; Petrache *et al.*, 1998). In addition neighbors limit the space available for fluctuations, causing an entropic membrane repulsion (*undulation forces* or *Helfrich effect*). This effect depends strongly on the intermembrane distance (Safinya *et al.*, 1989). At small dilution the membranes may be rigid and flat, in which case thermal fluctuations are not important. In contrast, for diluted systems the undulation forces overwhelm the van der Waals interactions and stabilize the membranes at large separations. From x-ray measurements on uniformly aligned stacked membranes both the bending constant and the multilayer compressibility have been determined (Lei *et al.*, 1995).

Regarding the role of thermal fluctuations in membrane systems, a large body of theoretical work exists (Lipowsky, 1991; Ben-Shaul *et al.*, 1994; Safran, 1994). This work shows the importance of the dynamics to the insertion of proteins as well as to the direct transport of small molecules. The bending dynamics may extend down to the millisecond range. Between this region and the much smaller time scale of molecular movements, collective mesoscopic motions emerge, which are to some extent similar to those in smectic liquid crystals. In

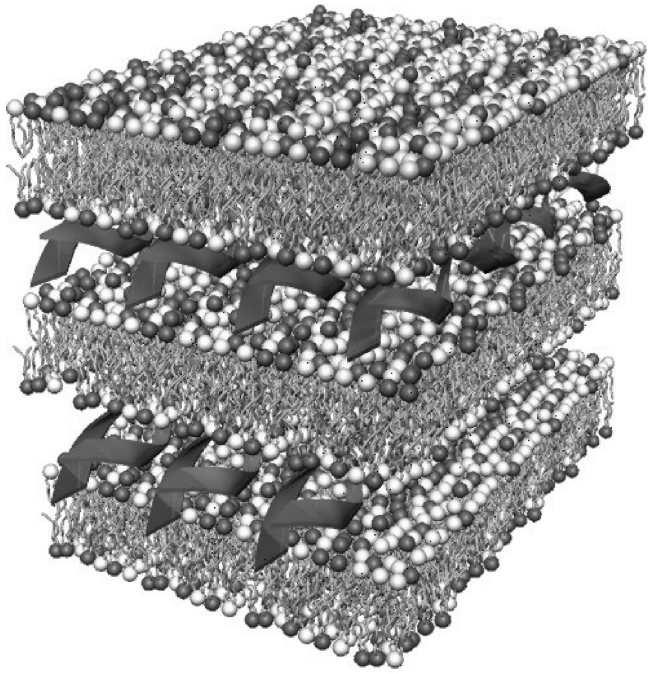

FIG. 35. Schematic model of DNA ordering in a lipid membrane. After Rädler *et al.*, 1997.

this intermediate regime the physical basis for important biological properties may be found. Recently freely suspended black lipid membranes have been investigated by dynamic light scattering over time scales from nanoseconds to over milliseconds (Hirn *et al.*, 1999). These first experiments indicate that significant changes occur in the dynamic response upon tight binding of a protein to the surface of the membrane. The mesoscopic undulations and thickness fluctuations have also been studied by Monte Carlo (Goetz *et al.*, 1999) as well as by molecular-dynamics simulations (Lindahl and Edholm, 2000). The results indicate that bending undulations are already present as soon as the wavelength is slightly larger than the membrane thickness.

Smectic ordering also plays a role in the organization of DNA chains in lipid membranes. Linear DNA chains and cationic liposomic mixtures can self-assemble into a quasi-two-dimensional smectic phase of DNA embedded between a three-dimensional smectic phase of lipid layers (Rädler *et al.*, 1997; Salditt *et al.*, 1997; Wong *et al.*, 1998; see Fig. 35). These complexes are able to carry (transfect) DNA across cell membranes for gene therapy applications. In that sense they mimic certain characteristics of natural viruses. Moreover, if the membranes' bending rigidity is lowered, an inverted hexagonal (columnar) phase can be found with a strong tendency for membrane fusion (Koltover *et al.*, 1998). New theoretical models for the ordering in these DNA-cationic complexes have been developed (Golubović and Golubović, 1998; O'Hern and Lubensky, 1998) that combine strong long-length-scale undulations of DNA (two-dimensional smectic) with the conventional three-dimensional undulations of the lipid bilayers. The predicted phase behavior depends on the transmembrane lattice interactions. It includes a new "sliding columnar" phase with quasi-long-range in-plane order and short-range out-of-plane order. Some preliminary x-ray results (Artzner *et al.*, 1998) are consistent with this model.

In the above examples membranes were investigated in thermodynamic equilibrium, i.e., the shape fluctuations have a thermal origin. In contrast, biological membranes of living cells are in a nonequilibrium steady state with shape fluctuations governed by the activity of incorporated proteins. The embedded proteins serve as ion pumps, translocating ions from one side of the membrane to another. The activity of ion pumps creates subtle undulations of the membranes, which have a nonthermal origin. Nonequilibrium shape fluctuations in active membranes have been studied both experimentally (Manneville *et al.*, 1999) and theoretically (Ramaswamy *et al.*, 2000). Coherent x rays could be used to investigate the dynamics of these low-energy undulation modes.

Clearly a full discussion of the field of biomembranes is outside the scope of this review. Nevertheless it seems that much of the physics of smectic membranes is highly relevant in describing the fluctuation behavior and associated properties of biological systems.

VII. CONCLUDING REMARKS

This review has examined experimental studies (mainly by x rays) and theoretical calculations of phase transitions and fluctuations in smectic membranes, accounting for the effects of film interfaces and reduced dimensionality. In this context a crucial property of smectic membranes is their thickness variation, from the limit where the molecular interactions are three dimensional to the thin-film limit where the interactions are constrained to two dimensions. The central point with respect to the in-plane structure is the nature of the liquid-hexatic-crystalline phase transitions, or the development of bond-orientational and positional correlations. In spite of extensive experimental and theoretical work, there is no definite conclusion yet regarding the mechanism of these transitions.

Our present knowledge of the low-dimensional ordering and phase transitions in smectic membranes is primarily based on x-ray and electron-diffraction studies. The main features of the phases are fairly well understood. Thanks to x-ray reflectivity techniques, much progress has been made regarding the structure and dynamics of the layer fluctuations in smectic membranes. However, a microscopic model that connects hydrodynamic theory with the smectic distribution of the molecular centers of mass is still lacking. This is needed in order to understand the behavior at large in-plane wave-vector transfer. It would also allow a quantitative assessment of the fluctuation profiles associated with quenched or enhanced fluctuations at the surfaces of smectic membranes.

X-ray photon correlation spectroscopy shows great promise for increasing our knowledge of the dynamics of smectic fluctuations. This method offers unique possibilities for studying fairly rapid dynamic processes in

films and membranes of various types down to molecular length scales. Rapid processes at these length scales in condensed media (10^7–10^{12} Hz) are traditionally studied by inelastic neutron scattering. X-ray photon correlation spectroscopy allows us now to measure routinely rather slow processes (10^{-2}–10^6 Hz) at length scales of typically 10^{-1}–10^3 nm. Recently the time scales accessible by x-ray photon correlation spectroscopes have been brought down by two orders of magnitude, creating overlap with neutron spin-echo methods. X-ray free-electron lasers, which are expected to be operational within a decade, will significantly expand upon these possibilities. Information on some of these projects can be found on the websites http://tesla.desy.de and http://www-ssrl.slac.stanford.edu/lcls/

The most interesting open question is probably the applicability of the various methods (experimental and theoretical) to membranes of biological materials. X-ray photon correlation spectroscopy spans the time and wave-vector range of collective mesoscopic motions that provide a physical basis for several important biological properties. Now that the statics and dynamics of simple smectic systems are to some extent understood, the fluctuations of related biologically relevant membrane systems provide a fascinating and still open field to be explored.

ACKNOWLEDGMENTS

Working on smectic membranes at the FOM-Institute AMOLF in Amsterdam, we benefited from the cooperation of several Ph.D. students and postdocs: Andrea Fera, Stan Gierlotka, Peter Lambooy, Liesbeth Mol, Ricarda Opitz, Daniel Sentenac, Joe Shindler, Irakli Sikharulidze, and Gerard Wong, whom we thank for their scientific contributions and also for much fun during those years. We would not have survived extensive synchrotron runs without the local support. We thank at ESRF (Grenoble, France) Gerhard Grübel, Dough Abernathy and Anders Madsen at beamline ID10A, Oleg Konovalov at ID10B, François Rieutord and Jean-Marc Petit at BM32, and Igor Dolbnya at BM26 for valuable discussions and participation in experiments. The same applies to Robert Feidenhans'l, Maurits Nielsen, and Oliver Bunk at beamline BW2 at HASYLAB (Desy, Hamburg, Germany). We are grateful to Vladimir Kaganer and Efim Kats for sharing their theoretical insights. This work is part of the research program of the Stichting voor Fundamenteel Onderzoek der Materie (FOM), which is financially supported by the Nederlandse Organisatie voor Wetenschappelijk Onderzoek (NWO). B.I.O. and A.N.S. acknowledge support from the NWO in the framework of the cooperation program of the NWO with the Russian Federation.

APPENDIX: LIST OF SMECTIC COMPOUNDS

In the following we list the smectic liquid-crystalline compounds mentioned most frequently in this review, together with the acronym used for indentification, the structural formula, and the phase sequence with transition temperatures in °C. A full compilation of liquid-crystalline compounds and their phase behavior can be found in various databases, for example, LiqCryst4.2, http://www.lci-publisher.com/liqcryst.html

1. nO.m

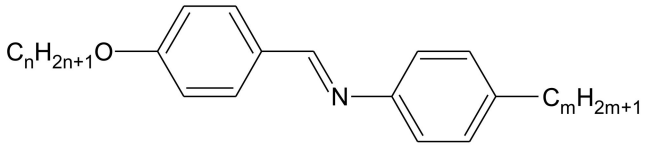

4O.8: Cr 33 Cr-B 48.5 Sm-A 63.5 N 78 I
5O.6: Cr 36 Cr-G 38 Sm-F 42 Cr-B 50 Sm-C 52 Sm-A 60 N 73 I
7O.7: Cr 33 Cr-G 55 Cr-B 69 Sm-C 72 Sm-A 83.7 N 84 I
9O.4: Cr 48 Cr-G 67 Sm-F 70 Sm-A 82 I

2. 7AB

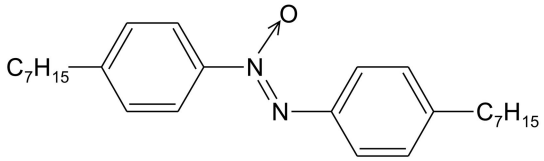

Cr 32 Sm-A 53 N 70 I

3. 8CB

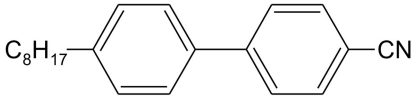

Cr 21.5 Sm-A 33.5 N 40.5 I

4. nOCB

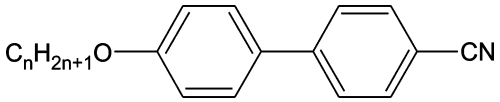

8OCB: Cr 55 Sm-A 67 N 80 I
10OCB: Cr 59 Sm-A 84 I

5. nmOBC

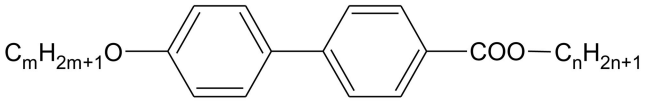

3(10)OBC: Cr 40 Sm-B 68 Sm-A 100 I
46OBC: Sm-B 67 Sm-A 92 I
65OBC: Cr-E 61 Sm-B 67 Sm-A 85 I
75OBC: Cr-E 59 Sm-B 67 Sm-A 81 I

6. 54COOBC

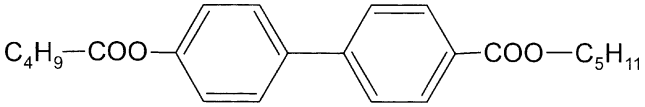

Cr-B 53 Sm-B 55 Sm-A 70 I

7. FPP

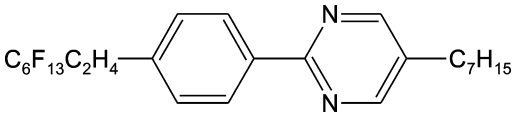

Cr 72 Sm-C 79 Sm-A 123 I

8. HPP

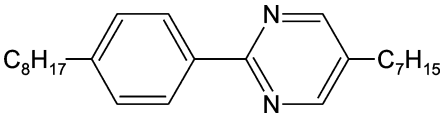

Cr 18 Sm-A 48 I

REFERENCES

Abernathy, D. L., G. Grübel, S. Brauer, I. McNulty, G. B. Stephenson, S. G. J. Mochrie, A. R. Sandy, N. Mulders, and N. Sutton, 1998, J. Synchrotron Radiat. **5**, 37.

Aeppli, G., and R. Bruinsma, 1984, Phys. Rev. Lett. **53**, 2133.

Aharony, A., R. J. Birgeneau, J. D. Brock, and J. D. Litster, 1986, Phys. Rev. Lett. **57**, 1012.

Aharony, A., and M. Kardar, 1988, Phys. Rev. Lett. **61**, 2855.

Ajdari, A., L. Peliti, and J. Prost, 1991, Phys. Rev. Lett. **66**, 1481.

Akizuki, T., K. Miyashi, Y. Takanishi, K. Ishikawa, H. Takezoe, and A. Fukuda, 1999, Jpn. J. Appl. Phys., Part 1 **38**, 4832.

Aksenova, E. V., A. Y. Val'kov, W. H. de Jeu, and I. Sikharulidze, 2002, *19th International Liquid Crystal Conference*, Edinburgh, UK.

Alexander, S., and J. McTague, 1978, Phys. Rev. Lett. **41**, 702.

Als-Nielsen, J., 1980, in *Ordering in Strongly Fluctuating Condensed Systems*, edited by T. Riste (Plenum, New York), p. 57.

Als-Nielsen, J., 1986, in *Structure and Dynamics of Surfaces II*, edited by W. Schommers and P. von Blanckenhagen, Topics in Current Physics No. 43 (Springer, Berlin), Chap. 5, p. 181.

Als-Nielsen, J., F. Christensen, and P. S. Pershan, 1982, Phys. Rev. Lett. **48**, 1107.

Als-Nielsen, J., D. Jacquemain, K. Kjaer, F. Leveiller, M. Lahav, and L. Leiserowitz, 1994, Phys. Rep. **246**, 251.

Als-Nielsen, J., J. D. Litster, R. J. Birgeneau, M. Kaplan, C. R. Safinya, A. Lindegaard-Andersen, and S. Mathiesen, 1980, Phys. Rev. B **22**, 312.

Als-Nielsen, J., and D. McMorrow, 2000, *Elements of Modern X-ray Physics* (Wiley, Chichester).

Amador, S. M., and P. S. Pershan, 1990, Phys. Rev. A **41**, 4326.

Amador, S., P. S. Pershan, H. Stragier, B. D. Swanson, D. Tweet, L. B. Sorensen, E. B. Sirota, G. E. Ice, and A. Habenschuss, 1989, Phys. Rev. A **39**, 2703.

Andreeva, P. O., V. K. Dolganov, C. Gors, R. Fouret, and E. I. Kats, 1999, Phys. Rev. E **59**, 4143.

Artzner, F., R. Zantl, G. Rapp, and J. O. Rädler, 1998, Phys. Rev. Lett. **81**, 5015.

Attwood, D., K. Halbach, and K.-J. Kim, 1985, Science **228**, 1265.

Bagchi, K., H. C. Andersen, and W. Swope, 1996, Phys. Rev. E **53**, 3794.

Bahr, C., 1994, Int. J. Mod. Phys. B **8**, 3051.

Bahr, C., C. J. Booth, D. Fliegner, and J. W. Goodby, 1996, Phys. Rev. Lett. **77**, 1083.

Bahr, C., and D. Fliegner, 1993, Phys. Rev. Lett. **70**, 1842.

Baron, A. Q. R., 2000, Hyperfine Interact. **125**, 29.

Bates, M. A., and D. Frenkel, 2000, Phys. Rev. E **61**, 5223.
Benattar, J. J., J. Doucet, M. Lambert, and A. M. Levelut, 1979, Phys. Rev. A **20**, 2505.
Ben-Shaul, A., W. Gelbart, and D. Roux, 1994, Eds., *Membranes, Microemulsions and Monolayers* (Springer, New York).
Benzekri, M., J. P. Marcerou, H. T. Nguyen, and J. C. Rouillon, 1990, Phys. Rev. B **41**, 9032.
Berezinskii, V. L., 1972, Sov. Phys. JETP **34**, 610.
Binder, K., 1986, in *Phase Transitions and Critical Phenomena*, edited by C. Domb and J. L. Lebowitz (Academic, London), Vol. 8, p. 1.
Birgeneau, R. J., and J. D. Litster, 1978, J. Phys. (Paris) Lett. **39**, L399.
Bishop, D. J., W. O. Sprenger, R. Pindak, and M. E. Neubert, 1982, Phys. Rev. Lett. **49**, 1861.
Bladon, P., and D. Frenkel, 1995, Phys. Rev. Lett. **74**, 2519.
Blinov, L. M., and V. G. Chigrinov, 1994, *Electrooptic Effects in Liquid Crystalline Materials* (Springer, New York).
Born, M., and E. Wolf, 1959, *Principles of Optics* (Pergamon, Oxford).
Böttger, A., D. Frenkel, J. G. H. Joosten, and G. Krooshof, 1988, Phys. Rev. A **38**, 6316.
Böttger, A., and J. G. H. Joosten, 1987, Europhys. Lett. **4**, 1297.
Brand, H. R., P. E. Cladis, and H. Pleiner, 1998, Eur. Phys. J. B **6**, 347.
Brauer, S., G. B. Stephenson, M. Sutton, R. Bruning, E. Dufresne, S. G. J. Mochrie, G. Grübel, J. Als-Nielsen, and D. L. Abernathy, 1995, Phys. Rev. Lett. **74**, 2010.
Brazovskii, S. A., 1975, Sov. Phys. JETP **41**, 85.
Brock, J. D., A. Aharony, R. J. Birgeneau, K. W. Evans-Lutterode, J. D. Litster, P. M. Horn, G. B. Stephenson, and A. R. Tajbakhsh, 1986, Phys. Rev. Lett. **57**, 98.
Brock, J. D., D. Y. Noh, B. R. McClain, J. D. Litster, R. J. Birgeneau, A. Aharony, P. M. Horn, and J. C. Liang, 1989, Z. Phys. B: Condens. Matter **74**, 197.
Bruinsma, R., and D. R. Nelson, 1981, Phys. Rev. B **23**, 402.
Cagnon, M., and G. Durand, 1980, Phys. Rev. Lett. **45**, 1418.
Caillé, A., 1972, C. R. Seances Acad. Sci., Ser. B **247**, 891.
Čepič, M., and B. Žekš, 1995, Mol. Cryst. Liq. Cryst. Sci. Technol., Sect. A **263**, 61.
Chaikin, P. M., and T. C. Lubensky, 1995, *Principles of Condensed Matter Physics* (Cambridge University, Cambridge, UK).
Chao, C. Y., C. F. Chou, J. T. Ho, S. W. Hui, A. Jin, and C. C. Huang, 1996, Phys. Rev. Lett. **77**, 2750.
Chao, C. Y., S. W. Hui, J. E. Maclennan, C. F. Chou, and J. T. Ho, 1997, Phys. Rev. Lett. **78**, 2581.
Chao, C. Y., Y. H. Liu, T. C. Pan, B. N. Chang, and J. T. Ho, 2001, Phys. Rev. E **64**, 050703.
Chao, C. Y., T. C. Pan, C. F. Chou, and J. T. Ho, 2000, Phys. Rev. E **62**, R1485.
Chen, H. Y., and D. Jasnow, 2000, Phys. Rev. E **61**, 493.
Cheng, M., J. T. Ho, S. W. Hui, J. W. Goodby, R. Pindak, R. Geer, and C. C. Huang, 1991, Phys. Rev. A **44**, R7891.
Cheng, M., J. T. Ho, S. W. Hui, and R. Pindak, 1987, Phys. Rev. Lett. **59**, 1112.
Cheng, M., J. T. Ho, S. W. Hui, and R. Pindak, 1988, Phys. Rev. Lett. **61**, 550.
Chikina, I. V., N. Limodin, A. Langlois, M. Brazovskaia, C. Even, and P. Pieranski, 1998, Eur. Phys. J. B **3**, 189.
Chou, C. F., J. T. Ho, and S. W. Hui, 1997, Phys. Rev. E **56**, 592.
Chou, C. F., J. T. Ho, S. W. Hui, and V. Surendrath, 1996, Phys. Rev. Lett. **76**, 4556.
Chou, C. F., A. J. Jin, C. Y. Chao, S. W. Hui, C. C. Huang, and J. T. Ho, 1997, Phys. Rev. E **55**, R6337.
Chou, T., and D. R. Nelson, 1996, Phys. Rev. E **53**, 2560.
Chu, B., 1991, *Laser Light Scattering: Basic Principles and Practice* (Academic, San Diego).
Collett, J., P. S. Pershan, E. B. Sirota, and L. B. Sorensen, 1984, Phys. Rev. Lett. **52**, 356.
Collett, J., L. B. Sorensen, P. S. Pershan, and J. Als-Nielsen, 1985, Phys. Rev. A **32**, 1036.
Daillant, J., and O. Bélorgey, 1992, J. Chem. Phys. **97**, 5824.
Daillant, J., and A. Gibaud, 1999, Eds., *X-Ray and Neutron Reflectivity: Principles and Applications* (Springer, Berlin).
Davey, S. C., J. Budai, J. W. Goodby, R. Pindak, and D. E. Moncton, 1984, Phys. Rev. Lett. **53**, 2129.
Davidson, P., and A. M. Levelut, 1992, Liq. Cryst. **11**, 469.
de Boer, D. K. G., 1999, Phys. Rev. E **59**, 1880.
de Gennes, P. G., 1966, *Superconductivity of Metals and Alloys* (Benjamin, New York).
de Gennes, P. G., 1990, Langmuir **6**, 1448.
de Gennes, P. G., and J. Prost, 1993, *The Physics of Liquid Crystals* (Clarendon, Oxford).
de Jeu, W. H., and W. A. P. Claassen, 1977, J. Chem. Phys. **67**, 3704.
de Jeu, W. H., A. Fera, B. I. Ostrovskii, and O. Konovalov, 2003, Phys. Rev. E (to be published).
Decher, G., J. Maclennan, J. Reiber, and U. Sohling, 1991, Adv. Mater. **3**, 617.
Decher, G., J. Reibel, M. Honig, I. G. Voigt-Martin, A. Dittrich, H. Ringsdorf, H. Poths, and R. Zentel, 1993, Ber. Bunsenges. Phys. Chem. **97**, 1386.
Demikhov, E. I., 1995, Mol. Cryst. Liq. Cryst. Sci. Technol., Sect. A **265**, 403.
Demikhov, E. I., V. K. Delganov, and K. P. Meletov, 1995, Phys. Rev. E **52**, R1285.
Demirel, A. M., and B. Jérôme, 1999, Europhys. Lett. **45**, 58.
Diele, S., D. Demus, and H. Sackmann, 1980, Mol. Cryst. Liq. Cryst. **56**, 217.
Diele, S., S. Grande, H. Kruth, C. Lischka, G. Pelzl, and I. Wirth, 1998, Ferroelectrics **212**, 169.
Dierker, S. B., 1995, NSLS Newslett. July, p. 1.
Dierker, S. B., R. Pindak, R. M. Fleming, I. K. Robinson, and L. Berman, 1995, Phys. Rev. Lett. **75**, 449.
Dietrich, S., 1988, in *Phase Transitions and Critical Phenomena*, edited by C. Domb and J. L. Lebowitz, (Academic, London), Vol. 12, p. 1.
Doerr, A. K., M. Tolan, W. Prange, J.-P. Schlomka, T. Seydel, and W. Press, 1999, Phys. Rev. Lett. **83**, 3470.
Dosch, H., 1992, *Critical Phenomena at Surfaces and Interfaces* (Springer, Berlin).
Dubois-Violette, E., B. Pansu, P. Davidson, and A. M. Levelut, 1993, J. Phys. II **3**, 395.
Fera, A., I. P. Dolbnya, G. Grübel, H. G. Muller, B. I. Ostrovskii, A. N. Shalagionv, and W. H. de Jeu, 2000, Phys. Rev. Lett. **85**, 2316.
Fera, A., I. P. Dolbnya, Ṙ. Opitz, B. I. Ostrovskii, and W. H. de Jeu, 2001, Phys. Rev. E **63**, 020601.
Fera, A., R. Opitz, W. H. de Jeu, B. I. Ostrovskii, D. Schlauf, and C. Bahr, 2001, Phys. Rev. E **64**, 021702.
Fera, A., B. I. Ostrovskii, D. Sentenac, I. Samoilenko, and W. H. de Jeu, 1999, Phys. Rev. E **60**, R5033.

Fisch, M. R., P. S. Pershan, and L. B. Sorensen, 1984, Phys. Rev. A **29**, 2741.
Fradin, C., A. Braslau, D. Luzet, D. Smilgies, M. Alba, M. Boudet, K. Mecke, and J. Daillant, 2000, Nature (London) **4032**, 871.
Friedel, G., 1922, Ann. Phys. (Paris) **18**, 273.
Fukuda, A., Y. Takanishi, T. Isozaki, K. Ishikawa, and H. Takezoe, 1994, J. Mater. Chem. **4**, 997.
Gane, P. A. C., A. J. Leadbetter, J. J. Benattar, F. Moussa, and M. Lambert, 1981, Phys. Rev. A **24**, 2694.
Gang, O., B. M. Ocko, X. Z. Wu, E. B. Sirota, and M. Deutsch, 1998, Phys. Rev. Lett. **80**, 1264.
Geer, R. E., S. B. Qadri, R. Shashidar, A. F. Thibodeaux, and R. S. Duran, 1995, Phys. Rev. E **52**, 671.
Geer, R. E., and R. Shashidar, 1995, Phys. Rev. E **51**, R8.
Geer, R., T. Stoebe, and C. C. Huang, 1992, Phys. Rev. B **45**, 13055.
Geer, R., T. Stoebe, and C. C. Huang, 1993, Phys. Rev. E **48**, 408.
Geminard, J. C., R. Holyst, and P. Oswald, 1997, Phys. Rev. Lett. **78**, 1924.
Gierlotka, S., P. Lambooy, and W. H. de Jeu, 1990, Europhys. Lett. **12**, 341.
Glaser, M. A., and N. A. Clark, 1990, Phys. Rev. A **41**, 4585.
Glaser, M. A., and N. A. Clark, 1993, *Advances in Chemical Physics* (Wiley, London), Vol. 83, p. 543.
Glattli, D. C., E. Y. Andrei, and F. I. B. Williams, 1988, Phys. Rev. Lett. **60**, 420.
Goetz, R., G. Gomper, and R. Lipowsky, 1999, Phys. Rev. Lett. **82**, 221.
Golubović, L., and M. Golubović, 1998, Phys. Rev. Lett. **80**, 4341.
Goodby, J. W., R. Blinc, N. A. Clark, S. T. Lagerwall, M. A. Osipov, S. A. Pikin, T. Sakurai, K. Yoshino, and B. Žekš, 1991, *Ferroelectric Liquid Crystals. Principles, Properties and Applications* (Gordon and Breach, Philadelphia).
Górecka, E., L. Chen, W. Pyzuk, A. Krówczynski, and S. Kumar, 1994, Phys. Rev. E **50**, 2863.
Gorodetskii, E. E., E. S. Pikina, and V. E. Podnek, 1999, Sov. Phys. JETP **88**, 35.
Gramsbergen, E. F., and W. H. de Jeu, 1988, J. Chem. Soc., Faraday Trans. 2 **84**, 1015.
Gramsbergen, E. F., W. H. de Jeu, and J. Als-Nielsen, 1986, J. Phys. (Paris) **47**, 711.
Gray, G. W., and J. W. Goodby, 1984, *Smectic Liquid Crystals; Textures and Structures* (Leonard Hill, Glasgow).
Grübel, G., and D. L. Abernathy, 1997, Proc. SPIE **3154**, 103.
Grübel, G., D. L. Abernathy, D. O. Riese, W. L. Vos, and G. H. Wegdam, 2000, J. Appl. Crystallogr. **33**, 424.
Gunther, L., Y. Imry, and J. Lajzerowicz, 1980, Phys. Rev. A **22**, 1733.
Halperin, B. I., T. C. Lubensky, and S. Ma, 1974, Phys. Rev. Lett. **32**, 292.
Halperin, B. I., and D. R. Nelson, 1978, Phys. Rev. Lett. **41**, 121.
Heinekamp, S., R. A. Pelcovits, E. Fontes, E. Y. Chen, R. Pindak, and R. B. Meyer, 1984, Phys. Rev. Lett. **52**, 1017.
Heiney, P. A., P. W. Stephens, R. J. Birgeneau, P. M. Horn, and D. E. Moncton, 1983, Phys. Rev. B **28**, 6416.
Herminghaus, S., K. Jacobs, K. Mecke, J. Bishof, A. Fery, M. Ibn-Elhaj, and S. Schlagowski, 1998, Science **282**, 916.
Hirn, R., R. Benz, and T. M. Bayerl, 1999, Phys. Rev. E **59**, 5987.
Holý, V., U. Pietsch, and T. Baumbach, 1999, *High-Resolution X-ray Scattering from Thin Films and Multilayers* (Springer, Berlin).
Hołyst, R., 1991, Phys. Rev. A **44**, 3692.
Hołyst, R., 1992, Phys. Rev. B **46**, 15 542.
Hołyst, R., D. J. Tweet, and L. B. Sorensen, 1990, Phys. Rev. Lett. **65**, 2153.
Huang, C. C., J. M. Viner, R. Pindak, and J. W. Goodby, 1981, Phys. Rev. Lett. **46**, 1289.
Imry, Y., and L. Gunther, 1971, Phys. Rev. B **3**, 3939.
Isozaki, T., T. Fujikawa, H. Takezoe, A. Fukuda, Y. Suzuki, and I. Kawamura, 1993, Phys. Rev. B **48**, 13 439.
Jaster, A., 1999, Phys. Rev. E **59**, 2594.
Jin, A. J., M. R. Bjurstrom, and M. H. W. Chan, 1989, Phys. Rev. Lett. **62**, 1372.
Jin, A. J., T. Stoebe, and C. C. Huang, 1994, Phys. Rev. E **49**, R4791.
Jin, A. J., M. Veum, T. Stoebe, C. F. Chou, J. T. Ho, S. W. Hui, V. Surendranath, and C. C. Huang, 1996, Phys. Rev. E **53**, 3639.
Johnson, P. M., P. Mach, E. D. Wedell, F. Lintgen, M. Neubert, and C. C. Huang, 1997, Phys. Rev. E **55**, 4386.
Johnson, P. M., D. A. Olson, S. Pankratz, T. Nguyen, J. W. Goodby, M. Hird, and C. C. Huang, 2000, Phys. Rev. Lett. **84**, 4870.
Kaganer, V. M., G. Brezesinski, H. Möhwald, P. B. Howes, and K. Kjaer, 1999, Phys. Rev. E **59**, 2141.
Kaganer, V. M., and E. B. Loginov, 1995, Phys. Rev. E **51**, 2237.
Kaganer, V. M., H. Möhwald, and P. Dutta, 1999, Rev. Mod. Phys. **71**, 779.
Kaganer, V. M., B. I. Ostrovskii, and W. H. de Jeu, 1991, Phys. Rev. A **44**, 8158.
Kaganer, V. M., I. R. Peterson, R. M. Kenn, M. C. Shih, M. Durbin, and P. Dutta, 1995, J. Chem. Phys. **102**, 9412.
Kats, E. I., and J. Lajzerowicz, 1996, Sov. Phys. JETP **83**, 495.
Kats, E. I., and V. V. Lebedev, 1993, *Dynamics of Liquid Crystals* (Springer, Berlin).
Kats, E. I., V. V. Lebedev, and A. R. Muratov, 1993a, Phys. Rep. **228**, 1.
Kats, E. I., V. V. Lebedev, and A. R. Muratov, 1993b, JETP Lett. **58**, 653.
Kellogg, G. J., P. S. Pershan, E. H. Kawamoto, and W. Foster, 1995, Phys. Rev. E **51**, 4709.
Koltover, I., J. O. Rädler, T. Salditt, K. J. Rothschild, and C. R. Safinya, 1999, Phys. Rev. Lett. **82**, 3184.
Koltover, I., T. Salditt, J. O. Rädler, and C. R. Safinya, 1998, Science **281**, 78.
Kosterlitz, J. M., and D. J. Thouless, 1973, J. Phys. C **6**, 1181.
Kusner, R. E., J. A. Mann, J. Kerins, and A. J. Dahm, 1994, Phys. Rev. Lett. **73**, 3113.
Lagerwall, L. T., 1999, *Ferroelectric and Antiferroelectric Liquid Crystals* (Wiley-VCH, Weinheim).
Lal, J., D. Abernathy, L. Auvray, O. Diat, and G. Grübel, 2001, Eur. Phys. J. E **4**, 263.
Lambooy, P., S. Gierlotka, and W. H. de Jeu, 1992, in *Phase Transitions in Liquid Crystals*, edited by S. Martellucci and A. N. Chester (Plenum, New York), Chap. 17, p. 239.
Landau, L. D., 1937, Phys. Z. Sowjetunion **11**, 545.
Landau, L. D., and E. M. Lifshitz, 1986, *Theory of Elasticity* (Pergamon, Oxford).
Landau, L. D., E. M. Lifschitz, and L. P. Pitaevskii, 1980, *Statistical Physics* (Pergamon, New York).

Leadbetter, A. J., J. C. Frost, and M. A. Mazid, 1979, J. Phys. (Paris) Lett. **40**, L325.
Lei, N., C. Safinya, and R. F. Bruinsma, 1995, J. Phys. II **5**, 1155.
Lengeler, B., 2001, Naturwissenschaften **88**, 249.
Levelut, A.-M., and B. Pansu, 1999, Phys. Rev. E **60**, 6803.
Lindahl, E., and O. Edholm, 2000, Biophys. J. **79**, 426.
Link, D. R., N. A. Clark, B. I. Ostrovskii, and E. A. Soto Bustamante, 2000, Phys. Rev. E **61**, R37.
Link, D. R., G. Natale, N. A. Clark, J. E. MacLennan, M. Walsh, S. S. Keast, and M. E. Neubert, 1999, Phys. Rev. Lett. **82**, 2508.
Lipowsky, R., 1991, Nature (London) **349**, 475.
Lobko, T. A., B. I. Ostrovskii, A. I. Pavluchenko, and S. N. Sulianov, 1993, Liq. Cryst. **15**, 361.
Lorman, V. L., 1995, Mol. Cryst. Liq. Cryst. Sci. Technol., Sect. A **262**, 437.
Lubensky, T. C., 1983, J. Chim. Phys.-Chim. Biol. **80**, 31.
Lucht, R., and C. Bahr, 1997a, Ber. Bunsenges. Phys. Chem. **101**, 968.
Lucht, R., and C. Bahr, 1997b, Phys. Rev. Lett. **78**, 3487.
Lucht, R., P. Marczuk, C. Bahr, and G. H. Findenegg, 2001, Phys. Rev. E **63**, 041704.
Lumma, D., L. B. Lurio, M. A. Borthwick, P. Falus, and S. G. J. Mochrie, 2000, Phys. Rev. E **62**, 8258.
Lurio, L. B., D. Lumma, A. R. Sandy, M. A. Borthwick, P. Falus, S. G. J. Mochrie, J. P. Pelletier, M. Sutton, L. Regan, A. Malik, and G. B. Stephenson, 2000, Phys. Rev. Lett. **84**, 785.
Mach, P., S. Grantz, D. A. Debe, T. Stoebe, and C. C. Huang, 1995, J. Phys. II **5**, 217.
Mach, P., C. C. Huang, T. Stoebe, E. D. Wedell, T. Nguyen, W. H. de Jeu, F. Guittard, J. Nacri, R. Shashidar, N. Clark, I. M. Jiang, F. J. Kao, H. Lui, and H. Nohira, 1998, Langmuir **14**, 4330.
Mach, P., R. Pindak, A.-M. Levelut, P. Barois, H. T. Nguyen, H. Baltes, M. Hird, K. Toyne, A. Seed, J. W. Goodby, C. C. Huang, and L. Furenlid, 1999, Phys. Rev. E **60**, 6793.
Mach, P., R. Pindak, A.-M. Levelut, P. Barois, H. T. Nguyen, C. C. Huang, and L. Furenlid, 1998, Phys. Rev. Lett. **81**, 1015.
Maclennan, J. E., G. Decher, and U. Sohling, 1991, Appl. Phys. Lett. **59**, 917.
Madsen, A., J. Als-Nielsen, and G. Grübel, 2003, Phys. Rev. Lett., in press.
Manneville, J.-B., P. Bassereau, D. Levy, and J. Prost, 1999, Phys. Rev. Lett. **82**, 4356.
Marcus, A. H., and S. A. Rice, 1996, Phys. Rev. Lett. **77**, 2577.
Martin, P. C., O. Parodi, and P. S. Pershan, 1972, Phys. Rev. B **6**, 2401.
Martínez-Ratón, Y., A. M. Somoza, L. Mederos, and D. E. Sullivan, 1997, Phys. Rev. E **55**, 2030.
Meyer, R. B., L. Liebert, L. Strelecki, and P. Keller, 1975, J. Phys. (Paris) Lett. **36**, L69.
Millet, F., J. J. Benatter, and P. Perrin, 1999, Phys. Rev. E **60**, 2045.
Mirantsev, L. V., 1996, Liq. Cryst. **20**, 417.
Mochrie, S. G. J., A. M. Mayes, A. R. S. and M. Sutton, S. Brauer, G. B. Stephenson, D. L. Abernathy, and G. Grübel, 1997, Phys. Rev. Lett. **78**, 1275.
Mol, E. A. L., J. D. Shindler, A. N. Shalaginov, and W. H. de Jeu, 1996, Phys. Rev. E **54**, 536.
Mol, E. A. L., G. C. L. Wong, J.-M. Petit, F. Rieutord, and W. H. de Jeu, 1997, Phys. Rev. Lett. **79**, 3439.
Mol, E. A. L., G. C. L. Wong, J.-M. Petit, F. Rieutord, and W. H. de Jeu, 1998, Physica B **248**, 191.
Moncton, D. E., and R. Pindak, 1979, Phys. Rev. Lett. **43**, 701.
Moncton, D. E., R. Pindak, S. C. Davey, and G. S. Brown, 1982, Phys. Rev. Lett. **49**, 1865.
Murray, C. A., and D. H. van Winkle, 1987, Phys. Rev. Lett. **58**, 1200.
Nachaliel, E., E. N. Keller, D. Davidov, and C. Boeffel, 1991, Phys. Rev. A **43**, 2897.
Nallet, F., D. Roux, and J. Prost, 1989, J. Phys. (Paris) **50**, 3147.
Nelson, D. R., 1983, in *Phase Transitions and Critical Phenomena*, edited by C. Domb and J. L. Lebowitz (Academic, London), Vol. 7, p. 1.
Nelson, D. R., and B. I. Halperin, 1979, Phys. Rev. B **19**, 2457.
Nelson, D. R., and B. I. Halperin, 1980, Phys. Rev. B **21**, 5312.
Nelson, D. R., and L. Peliti, 1987, J. Phys. (Paris) **48**, 1085.
Nelson, D. R., and J. Toner, 1981, Phys. Rev. B **24**, 363.
Nielsen, M., J. Als-Nielsen, J. Bohr, J. P. McTague, D. E. Moncton, and P. W. Stephens, 1987, Phys. Rev. B **35**, 1419.
Niori, T., T. Sekine, J. Wanatabe, and H. Takezoe, 1996, J. Mater. Chem. **6**, 1231.
Noh, D. Y., J. D. Brock, J. O. Fossum, J. P. Hill, W. J. Nuttal, J. D. Lister, and R. J. Birgeneau, 1991, Phys. Rev. B **43**, 842.
Ocko, B. M., 1990, Phys. Rev. Lett. **64**, 2160.
Ocko, B. M., A. Braslau, P. S. Pershan, J. Als-Nielsen, and M. Deutsch, 1986, Phys. Rev. Lett. **57**, 94.
Ocko, B. M., P. S. Pershan, C. R. Safinya, and L. Y. Chiang, 1987, Phys. Rev. A **35**, 1868.
Ocko, B. M., X. Z. Wu, E. B. Sirota, S. K. Sinha, and M. Deutsch, 1994, Phys. Rev. Lett. **72**, 242.
Ocko, B. M., X. Z. Wu, E. B. Sirota, S. K. Sinha, O. Gang, and M. Deutsch, 1997, Phys. Rev. E **55**, 3164.
O'Hern, C. S., and T. C. Lubensky, 1998, Phys. Rev. Lett. **80**, 4345.
Olbrich, E., O. Marinov, and D. Davidov, 1993, Phys. Rev. E **48**, 2713.
Ostrovskii, B. I., 1999, in *Structure and Bonding, Liquid Crystals I*, edited by D. M. P. Mingos (Springer, New York/Heidelberg), p. 199.
Ostrovskii, B. I., D. Sentenac, I. I. Samoilenko, and W. H. de Jeu, 2001, Eur. Phys. J. E **6**, 287.
Oswald, P., 1987, J. Phys. (Paris) **48**, 897.
Oswald, P., and P. Pieranski, 2002, *Les Cristeaux Liquides* (Gordon and Breach), Vol. 2, Chap. C.VIII.
Oswald, P., P. Pieranski, F. Picano, and R. Hołyst, 2002, Phys. Rev. Lett. **88**, 015503.
Overney, R., E. Meyer, J. Frommer, H.-J. Guntherodt, G. Decher, J. Reibel, and U. Sohling, 1993, Langmuir **9**, 341.
Paczuski, M., and M. Kardar, 1988, Phys. Rev. Lett. **60**, 861.
Pang, J., and N. A. Clark, 1994, Phys. Rev. Lett. **73**, 2332.
Pankratz, S., P. M. Johnson, R. Hołyst, and C. C. Huang, 1999, Phys. Rev. E **60**, R2456.
Pankratz, S., P. M. Johnson, H. T. Nguyen, and C. C. Huang, 1998, Phys. Rev. E **58**, R2721.
Pankratz, S., P. M. Johnson, A. Paulson, and C. C. Huang, 2000, Phys. Rev. E **61**, 6689.
Parrat, L. G., 1954, Phys. Rev. **95**, 359.
Peierls, R. E., 1934, Helv. Phys. Acta **7**, supplement II, 81.
Pershan, P. S., 1988, *Structures of Liquid Crystals* (World Scientific, Singapore).
Pershan, P. S., G. Aeppli, J. D. Litster, and R. J. Birgeneau, 1981, Mol. Cryst. Liq. Cryst. **67**, 205.

Pershan, P. S., and J. Als-Nielsen, 1984, Phys. Rev. Lett. **52**, 759.
Pershan, P. S., A. Braslau, A. H. Weiss, and J. Als-Nielsen, 1987, Phys. Rev. A **35**, 4800.
Petrache, H. I., N. Gouliaev, S. Tristram-Nagle, R. Zhang, R. M. Suter, and J. F. Nagle, 1998, Phys. Rev. E **57**, 7014.
Picano, F., R. Holyst, and P. Oswald, 2000, Phys. Rev. E **62**, 3747.
Picano, F., P. Oswald, and E. I. Kats, 2001, Phys. Rev. E **63**, 021705.
Pieranski, P., L. Beliard, J.-Ph. Tournellec, X. Leoncini, C. Furtlehner, H. Dumoulin, E. Riou, B. Jouvin, J.-P. Fenerol, Ph. Palaric, J. Heuving, B. Cartier, and I. Kraus, 1993, Physica A **194**, 364.
Pindak, R., 1992, in *Solitons in Liquid Crystals*, edited by L. Lam and J. Prost (Springer, New York/Berlin), Chap. 7.
Pindak, R., D. J. Bishop, and W. O. Sprenger, 1980, Phys. Rev. Lett. **44**, 1461.
Pindak, R., and D. E. Moncton, 1982, Phys. Today **35** (5), 57.
Pindak, R., D. E. Moncton, S. C. Davey, and J. W. Goodby, 1981, Phys. Rev. Lett. **46**, 1135.
Pitchford, T., G. Nounesis, S. Dumrongrattana, J. M. Viner, C. C. Huang, and J. W. Goodby, 1985, Phys. Rev. A **32**, 1938.
Poniewierski, A., and R. Hołyst, 1993, Phys. Rev. B **47**, 9840.
Poniewierski, A., R. Hołyst, A. C. Price, and L. B. Sorensen, 1999, Phys. Rev. E **59**, 3048.
Poniewierski, A., R. Hołyst, A. C. Price, L. B. Sorenson, S. D. Kelvan, and J. Toner, 1998, Phys. Rev. E **58**, 2027.
Price, A. C., L. B. Sorensen, S. D. Kevar, J. Toner, A. Ponierewski, and R. Hołyst, 1999, Phys. Rev. Lett. **82**, 755.
Prost, J., 1984, Adv. Phys. **33**, 1.
Rädler, J. O., I. Koltover, T. Salditt, and C. Safinya, 1997, Science **275**, 810.
Ramaswamy, S., J. Toner, and J. Prost, 2000, Phys. Rev. Lett. **84**, 3494.
Rand, R. P., and V. A. Parsegian, 1989, Biochim. Biophys. Acta **988**, 351.
Reed, M., and B. Simon, 1972, *Methods of Mathematical Physics* (Academic, Cambridge), Vol. 2.
Reibel, J., M. Brehmer, R. Zentel, and G. Decher, 1995, Adv. Mater. **7**, 849.
Reiter, G., A. Sharmna, R. Khanna, A. Casoli, and M.-O. David, 1999, J. Colloid Interface Sci. **214**, 126.
Rieker, T. P., and E. J. Janulis, 1994, Liq. Cryst. **17**, 681.
Rieker, T. P., and E. J. Janulis, 1995, Phys. Rev. E **52**, 2688.
Riese, D. O., W. L. Vos, G. H. Wegdam, F. J. Poelwijk, D. L. Abernathy, and G. Grübel, 2000, Phys. Rev. E **61**, 1676.
Robinson, I. K., R. Pindak, R. M. Flemimg, S. B. Dierker, K. Ploog, G. Grübel, D. L. Abernathy, and J. Als-Nielsen, 1995, Phys. Rev. B **52**, 9917.
Romanov, V. P., and A. N. Shalaginov, 1992, Sov. Phys. JETP **75**, 483.
Romanov, V. P., and S. V. Ul'yanov, 2001, Phys. Rev. E **63**, 031706.
Rosenblatt, C., and N. Amer, 1980, Appl. Phys. Lett. **36**, 432.
Rosenblatt, C., R. Pindak, N. A. Clark, and R. B. Meyer, 1979, Phys. Rev. Lett. **42**, 1220.
Roux, D., and C. R. Safinya, 1988, J. Phys. (Paris) **49**, 307.
Rowlinson, J. S., and B. Widom, 1982, *Molecular Theory of Capillarity* (Clarendon, Oxford).
Russell, T. P., 1990, Mater. Sci. Rep. **5**, 171.
Safinya, C. R., D. Roux, G. S. Smith, S. K. Sinha, P. Dimon, N. A. Clark, and A. M. Belloq, 1986, Phys. Rev. Lett. **57**, 2718.
Safinya, C. R., E. B. Sirota, D. Roux, and G. S. Smith, 1989, Phys. Rev. Lett. **62**, 1134.
Safran, S. A., 1994, *Statistical Thermodynamics of Surfaces, Interfaces, and Membranes* (Addison-Wesley, Reading, MA).
Salditt, T., I. Koltover, J. O. Rädler, and C. R. Safinya, 1997, Phys. Rev. Lett. **79**, 2582.
Samoilenko, I. I., O. V. Konovalov, L. A. Feigin, B. M. Shchedrin, and L. G. Yanusova, 1999, Crystallogr. Rep. **44**, 310.
Samoilenko, I. I., B. M. Shchedrin, and L. A. Feigin, 1996, Physica B **221**, 542.
Sanyal, M. K., S. K. Sinha, K. G. Huang, and B. M. Ocko, 1991, Phys. Rev. Lett. **66**, 628.
Schick, M., 1990, in *Liquids at Interfaces*, edited by J. Charvolin, J. F. Joanny, and J. Zinn-Justin (Elsevier, Amsterdam), p. 417.
Selinger, J. V., 1988, J. Phys. (Paris) **49**, 1387.
Selinger, J. V., and D. R. Nelson, 1989, Phys. Rev. A **39**, 3135.
Sentenac, D., and J. Benattar, 1998, Phys. Rev. Lett. **81**, 160.
Sentenac, D., A. Fera, R. Opitz, B. I. Ostrovskii, O. Bunk, and W. H. de Jeu, 2000, Physica B **283**, 232.
Sentenac, D., A. N. Shalaginov, A. Fera, and W. H. de Jeu, 2000, J. Appl. Crystallogr. **33**, 130.
Seydel, T., A. Madsen, M. Tolan, G. Grübel, and W. Press, 2001, Phys. Rev. B **63**, 073409.
Shalaginov, A. N., and V. P. Romanov, 1993, Phys. Rev. E **48**, 1073.
Shalaginov, A. N., and D. E. Sullivan, 2000, Phys. Rev. E **62**, 699.
Shalaginov, A. N., and D. E. Sullivan, 2001, Phys. Rev. E **63**, 031704.
Shi, Y., B. Cull, and S. Kumar, 1993, Phys. Rev. Lett. **71**, 2773.
Shindler, J. D., E. A. L. Mol, A. N. Shalaginov, and W. H. de Jeu, 1995, Phys. Rev. Lett. **74**, 722.
Sikharulidze, I., I. D. Dolbnya, A. Fera, A. Madsen, B. I. Ostrovskii, and W. H. de Jeu, 2002, Phys. Rev. Lett. **88**, 115503.
Sinha, S. K., 1991, Physica B **173**, 25.
Sinha, S. K., E. B. Sirota, S. Garoff, and H. B. Stanley, 1988, Phys. Rev. B **38**, 2297.
Sirota, E. B., P. S. Pershan, S. Amador, and L. B. Sorensen, 1987a, Phys. Rev. A **35**, 2283.
Sirota, E. B., P. S. Pershan, L. B. Sorensen, and J. Collett, 1985, Phys. Rev. Lett. **55**, 2039.
Sirota, E. B., P. S. Pershan, L. B. Sorensen, and J. Collett, 1987b, Phys. Rev. A **36**, 2890.
Smith, G. S., C. R. Safinya, D. Roux, and N. A. Clark, 1987, Mol. Cryst. Liq. Cryst. **144**, 235.
Smith, G. S., E. B. Sirota, C. R. Safinya, and N. A. Clark, 1988, Phys. Rev. Lett. **60**, 813.
Smith, G. S., E. B. Sirota, C. R. Safinya, R. J. Plocno, and N. A. Clark, 1990, J. Chem. Phys. **92**, 4519.
Sonin, A. A., 1998, *Freely Suspended Liquid Crystalline Films* (Wiley, Chichester).
Soto Bustamante, E. A., S. V. Yablonski, B. I. Ostrovskii, L. A. Beresnev, L. M. Blinov, and W. H. Haase, 1996, Chem. Phys. Lett. **260**, 447.
Sprunt, S., M. S. Spector, and J. D. Litster, 1992, Phys. Rev. A **45**, 7355.
Stanley, H., 1971, *Introduction to Phase Transitions and Critical Phenomena* (Oxford University, New York).
Stannarius, R., and C. Cremer, 1998, Europhys. Lett. **42**, 43.
Stoebe, T., R. Geer, C. C. Huang, and J. W. Goodby, 1992, Phys. Rev. Lett. **69**, 2090.

Stoebe, T., and C. C. Huang, 1995, Int. J. Mod. Phys. B **9**, 2285.
Stoebe, T., P. Mach, and C. C. Huang, 1994, Phys. Rev. Lett. **73**, 1384.
Strandburg, K. J., 1988, Rev. Mod. Phys. **60**, 161.
Strandburg, K. J., 1992, *Bond-orientational Order in Condensed Systems* (Springer, New York/Berlin).
Swanson, B. D., H. Stragier, D. J. Tweet, and L. B. Sorensen, 1989, Phys. Rev. Lett. **62**, 909.
Takanishi, Y., A. Ikeda, H. Takezoe, and A. Fukuda, 1995, Phys. Rev. E **51**, 400.
Tarczon, J. C., and K. Miyano, 1981, Phys. Rev. Lett. **46**, 119.
Thiriet, Y., and P. Martinoty, 1982, J. Phys. (Paris) Lett. **43**, 137.
Thurn-Albrecht, T., G. Meier, P. Müller-Buschbaum, A. Patkowski, W. Steffen, G. Grübel, D. L. Abernathy, O. Diat, M. Winter, M. G. Koch, and M. T. Reetz, 1999, Phys. Rev. E **59**, 642.
Thurtell, J. H., M. M. T. da Gama, and K. E. Gubbins, 1985, Mol. Phys. **54**, 321.
Tidswell, I. M., T. A. Rabedeau, P. S. Pershan, and S. D. Kosowsky, 1991, Phys. Rev. Lett. **66**, 2108.
Tjipto-Margo, B., A. K. Sen, L. Mederos, and D. E. Sullivan, 1989, Mol. Phys. **67**, 601.
Tolan, M., 1998, *X-ray Scattering from Soft-Matter Thin Films* (Springer, Berlin).
Tsui, O. K. C., and S. G. J. Mochrie, 1998, Phys. Rev. E **57**, 2030.
Tweet, D. J., R. Hołyst, B. D. Swanson, H. Stragier, and L. B. Sorensen, 1990, Phys. Rev. Lett. **65**, 2157.
Val'kov, A. Y., V. P. Romanov, and M. Romanov, 2001, Sov. Phys. JETP **93**, 344.
Vertogen, G., and W. H. de Jeu, 1988, *Thermotropic Liquid Crystals, Fundamentals* (Springer, Berlin).
Vlieg, E., S. A. de Vries, J. Alvarez, and S. Ferrer, 1997, J. Synchrotron Radiat. **4**, 210.
Wack, D. C., and W. W. Webb, 1989, Phys. Rev. A **40**, 1627.
Wong, G. L., Y. L. Koltover, and C. R. Safinya, 1998, Appl. Phys. Lett. **73**, 2042.
Yoneda, Y., 1963, Phys. Rev. **131**, 2010.
Young, A. P., 1979, Phys. Rev. B **19**, 1855.
Young, C. Y., R. Pindak, N. A. Clark, and R. B. Meyer, 1978, Phys. Rev. Lett. **40**, 773.
Zabel, H., and I. K. Robinson, 1992, Eds., *Surface X-ray and Neutron Scattering*, Springer Proceedings in Physics No. 61 (Springer, Berlin).
Zakri, C., A. Renault, J.-P. Rieu, M. Vallade, B. Berge, J. Legrand, G. Vignault, and G. Grübel, 1997, Phys. Rev. B **55**, 14 163.
Zisman, A. N., D. V. Nikiforov, B. I. Ostrovskii, and E. M. Terentjev, 1987, JETP Lett. **45**, 238.